

Characterization of native FGF23 protein and mutant forms
causing autosomal dominant hypophosphatemic rickets and
familial tumoral calcinosis

Dissertation
zur Erlangung des Doktorgrades der Naturwissenschaften
(Dr. rer. nat.)
der Fakultät für Biologie der Ludwig-Maximilians-Universität München



vorgelegt von
Anna Benet Pagès

April 2005

eingereicht am: 09. Juni 2005
1. Gutachter: Prof. Dr. Thomas Cremer
2. Gutachter: Prof. Dr. Heinrich Leonhardt
Sondergutachter: PD Dr. Tim-Matthias Strom
Tag der mündlichen Prüfung: 23. Februar 2006

TABLE OF CONTENTS

TABLE OF CONTENTS	1
ABREVIATIONS	5
SUMMARY	8
A. INTRODUCTION	
1. PHOSPHATE HOMEOSTASIS	10
1.1 Phosphorus	10
1.2 Phosphate transport	11
1.3 Cellular mechanisms of renal phosphate transport	12
1.4 Hormonal regulation	12
2. DISORDERS OF PHOSPHATE METABOLISM: Hypophosphatemias	14
2.1 X-linked hypophosphatemia	15
2.1.1 <i>Hyp</i> and <i>Gy</i> mice models	16
2.1.2 Mutations in the <i>PHEX</i> gene cause XLH	17
2.1.3 The PHEX protein	17
2.1.4 Relevance of PHEX in the pathophysiology of XLH	18
2.2 Autosomal dominant hypophosphatemic rickets	19
2.2.1 Mutations in the <i>FGF23</i> gene cause ADHR	19
2.2.2 FGF23 belongs to the fibroblast growth factor family	20
2.3 Tumor induced osteomalacia	21
2.3.1 Characterization of “phosphatonins” from TIO tumors	22
3. DISORDERS OF PHOSPHATE METABOLISM: Hyperphosphatemias	23
3.1 Familial tumoral calcinosis	23
4. FUNCTION OF PHEX AND FGF23: a unifying hypothesis	25
5. AIMS OF THE INVESTIGATION	26
B. MATERIALS AND METHODS	
1. MATERIALS	28
1.1 DNA-Resources	28
1.1.1 Patients	28
1.1.2 cDNAs	28
1.1.3 Plasmids	28
1.2 Enzymes, chemicals and other materials	29
1.2.1 Enzymes and chemicals	29
1.2.2 Kits	29
1.2.3 Oligonucleotides	29
1.2.4 Antibodies	31
1.2.5 Cell lines	32

2. METHODS	32
2.1 DNA- and RNA-preparations	32
2.1.1 DNA extraction from blood	32
2.1.2 RNA extraction from cells	33
2.2 Reverse transcription	33
2.3 Polymerase chain reaction (PCR)	34
2.3.1 Standard PCR	34
2.3.2 RT-PCR and RT-”nested”-PCR	34
2.3.3 Multiplex RT-PCR	35
2.4 Site-Directed mutagenesis	35
2.5 DNA sequencing	35
2.6 Electrophoresis	36
2.6.1 Agarose gel electrophoresis	36
2.6.2 Polyacrylamide Gel Electrophoresis	36
2.6.2.1 Preparation of the mini gels	37
2.6.2.2 Electrophoresis	37
2.6.2.3 Drying SDS-polyacrylamide gels	38
2.6.3 Western blot	38
2.7 DNA cloning	38
2.7.1 DNA digestion	39
2.7.2 DNA ligation	39
2.7.3 Preparation of competent <i>E. coli</i> using the CaCl ₂ method	39
2.7.4 DNA transformation	40
2.7.5 Preparation of recombinant plasmid-DNA	40
2.8 Protein expression	40
2.8.1 Expression in a prokaryotic system	40
2.8.2 Expression in an eukaryotic system	41
2.9 Cell culture	42
2.9.1 Preparation of conditioned medium	42
2.9.2 Preparation of cells	42
2.9.3 Treatment with inhibitors	42
2.9.3.1 Inhibition of SPCs activity	42
2.9.3.2 Inhibition of secPHEX activity	43
2.9.4 Treatment with glycosidases	43
2.9.4.1 N-glycosylation assay	43
2.9.4.2 O-glycosylation assay	43
2.10 Protein purification	44
2.10.1 FGF23/His purification	44
2.11 Protein quantification	44
2.11.1 Agilent protein assay	44

2.11.2 Bradford method	44
2.12 Protein staining.....	45
2.12.1 Coomassie staining	45
2.12.2 Silver staining	45
2.12.3 Ponceau S staining	46
2.13 Protein detection	46
2.13.1 Immunoblot	46
2.13.2 Immunocytochemistry	47
2.13.3 Enzyme-Linked Immunosorbent Assay (ELISA)	47
3. DATABASES AND COMPUTER PROGRAMS	48
3.1 Databases	48
3.2 Analysis tools and software packages	48
C. RESULTS	
1. CHACTERIZATION OF THE NATIVE FGF23 PROTEIN	49
1.1 Description of the FGF23 amino acid sequence	49
1.1.1 Expression analysis of FGF23 in human and mouse tissues	51
1.2 FGF23 expression in <i>E.coli</i>	52
1.2.1 Generation of a FGF23 prokaryotic expression construct	52
1.2.2 Expression and purification	53
1.3 Expression in mammalian cells	55
1.3.1 Generation of recombinant tagged and untagged FGF23 constructs	55
1.3.2 Expression of tagged and untagged FGF23 by mammalian cells and polyclonal antibody assessment	56
1.3.3 Quantification of the FGF23 fraction in the conditioned medium ...	58
1.4 Protein characterization	59
1.4.1 Stability of native FGF23	59
1.4.2 Intracellular versus extracellular cleavage	60
1.4.3 Glycosylation of native FGF23	60
1.4.4 Purification of FGF23/His and mass spectrometry analysis	62
2. CHARACTERIZATION OF FGF23 MUTANT PROTEINS	63
2.1 Mutation analysis in FTC	63
2.2 FGF23 mutant proteins and expression in mammalian cells	65
2.2.1 Analysis of the ADHR FGF23-R176Q and -R179Q mutant proteins	66
2.2.1.1 Inhibition of FGF23 processing at the RHTR site	67
2.2.1.2 Expression of SPC in HEK293 cells and in mice osteoblasts	68
2.2.2 Analysis of the FGF23-S71G mutant protein	69
2.2.2.1 Subcellular localization of the FGF23-S71G mutant protein	70
2.2.2.2 Quantification of plasma FGF23 levels	71
3. FGF23 A SUBSTRATE OF THE PHEX ENDOPEPTIDASE.....	72

3.1. Expression of secPHEX in HEK293 cells	72
3.1.1 Generation of recombinant PHEX constructs	72
3.1.2 Expression of PHEX and secPHEX in HEK293 cells	73
3.1.3 Quantification of secPHEX fraction in the conditioned medium ...	74
3.2 Endopeptidase activity of secPHEX	75
3.2.1 Analysis of the secPHEX activity	75
3.2.2 Inhibition of secPHEX activity	75
3.3 sec PHEX co-incubation with FGF23	76
D. DISCUSSION	
1. NATIVE FGF23	79
1.1 Overview of the FGF23 sequence	79
1.2 FGF23 is a secreted protein	81
1.3 Analysis of the FGF23 cleavage	82
1.4 FGF23 glycosylation	83
1.5 FGF23 expression in human and mouse tissues	84
1.5.1 FGF23 expression in bone	85
2. AUTOSOMAL DOMINANT HYPOPHOSPHATEMIC RICKETS	86
2.1 FGF23-R176Q and –R179Q mutant proteins are resistant to cleavage	86
2.2 ADHR mutations causes gain of protein function	86
2.3 Searching for the FGF23 receptor	87
3. FAMILIAL TUMORAL CALCINOSIS WITH HYPERPHOSPHATEMIA	87
3.1 FGF23 in familial tumoral calcinosis	87
3.1.1 FGF23-S71G mutant protein is not secreted	87
3.1.2 FTC mutation causes reduction of protein function	88
3.2 GALNT3 in familiar tumoral calcinosis	89
4. FGF23 IN X-LINKED HYPOPHOSPHATEMIC RICKETS	90
4.1 Does PHEX function as an endopeptidase?	90
4.2 Co-incubation of FGF23 and PHEX in an optimized assay	92
4.3 PHEX proteolytic function remains unclear	92
5. A MORE COMPLEX MODEL TO EXPLAIN PHOSPHATE REGULATION	93
REFERENCES	95
ANNEX	105
Acknowledgements	105
Curriculum Vitae	106
Scientific publications	107

ABBREVIATIONS

1,25(OH) ₂ D ₃	1,25-dihydroxyvitamin D ₃
25(OH)D ₃	25-dihydroxyvitamin D ₃
1α(OH)ase	1α-hydroxylase
A	absorbance
ADHR	autosomal dominant hypophosphatemic rickets
a.m.	after midday
APS	ammonium peroxydisulfate
ATP	adenosine triphosphate
ATPase	adenosine triphosphatase
bp	base pare
BSA	bovine serum albumin
c.	cDNA sequence position
°C	centigrade
cAMP	cyclic adenosine monophosphate
cDNA	complementing DNA
cm ²	square centimetre
C-term	carboxyl terminal
Dec-RVKR-CMK	decanoyl-Arg-Val-Lys-Arg-chloromethyl ketone
DEPC	diethylpyrocarbonat
dH ₂ O	deionized water
DHPLC-H ₂ O	denaturing high-performance liquid chromatography water
dl	decilitre
DMP1	dentin matrix protein 1
DNA	desoxyribonucleic acid
dNTP	desoxynucleotide
DTT	dithiothreiol
ECF	extracellular fluid
EDTA	ethylenediaminetetraacetic acid
<i>et al.</i>	<i>et alii</i>
f	female
FCS	foetal calf serum
<i>FGF23</i>	fibroblast growth factor 23 gene
FGF23	fibroblast growth factor 23 protein
<i>Fgf23</i>	fibroblast growth factor 23 mouse orthologe gene
Fgf23	fibroblast growth factor 23 mouse orthologe protein
FGFR	fibroblast growth factor receptor protein
Fig.	figure
FRP4	frizzled-related protein 4
FTC	familial tumoral calcinosis

g	gram
Gal	galactose
GalNAc	N-acetylgalactosamine
GALNT3	N-acetylgalactosaminyltransferase
GAPDH	glyceraldehyde-3-phosphate dehydrogenase
GFR	glomerular filtration rate
h	hours
HEK293	human embryonic kidney cells
HPO ₄ ⁻	hydrogen monophosphate
H ₂ PO ₄ ⁻	hydrogen diphosphate
HRP	horse-radish peroxidase
<i>i.e.</i>	<i>id est</i>
IgG	immunoglobulin G
IPTG	isopropyl-1-thio-β-D-Galactopyranoside
kb	kilo base
kDa	kilo Dalton
l	litre
m	male
M	molar
mA	milliamper
MBP	maltose-binding protein
MEPE	matrix extracellular phosphoglycoprotein
mg	milligram
μg	microgram
min	minutes
ml	millilitres
μl	microlitre
mm	millimeter
mm ²	square millimeters
mM	millimolar
MOPS	3-(N-Morpholino)propanesulfonic acid
mRNA	messenger ribonucleic acid
mU	milliunits
<i>neo</i>	neomycin gene
NEP	neprilysin
NeuAc	N-acetylneuraminic acid, sialic acid
ng	nanogram
nm	nanometer
NPT	sodium phosphate cotransporter protein
Npt	sodium phosphate cotransporter mouse ortholog protein
OD	optical density
ORF	open reading frame

p.	protein sequence position
PAGE	polyacrylamide gel electrophoresis
PBS	phosphate buffer saline
PCR	polymerase chain reaction
<i>PHEX</i>	phosphate regulating gene with homologies to endopeptidases on the X-chromosome
PHEX	phosphate regulating gene with homologies to endopeptidases on the X-chromosome protein
<i>Phex</i>	PHEX mouse ortholog gene
Phex	PHEX mouse ortholog protein
Pi	phosphate
pmol	picomols
PTH	parathyroid hormone
PVDF	polyvinylidene fluoride
RNA	ribonucleic acid
RNase	ribonuclease
RT	room temperature
RT-PCR	retro-transcriptase polymerase chain reaction
SDS	sodium dodecyl sulphate
sec	seconds
secPHEX	secreted PHEX protein
SPC	subtilisin-like proprotein convertase
Spc	subtilisin-like proprotein convertase mouse ortholog
Tab.	Table
TBE	tris-borat-EDTA
TEMED	N,N,N',N'-Tetramethyldiamine
TIO	tumour induced osteomalacia
TmP	phosphate maximal tubular reabsorption
Tris	2-amino-2(hydroxymethyl)-1,3-propandiol
U	unit
UV	ultraviolet
V	volt
XLH	X-linked hypophosphatemia

SUMMARY

The regulation of phosphate metabolism is a complex process that is still only partly understood. At the end of the eighties, studies in a mouse model for hypophosphatemic rickets provided evidence that phosphate wasting could not be explained by a primary defect of the kidney but rather by an unknown circulating factor with phosphaturic properties. X-linked hypophosphatemia (XLH), autosomal dominant hypophosphatemic rickets (ADHR), and tumor induced osteomalacia (TIO) are three well defined human disorders of isolated renal phosphate wasting. XLH and ADHR are mendelian diseases while TIO is caused by rare, mostly benign tumors. The opposite phenotype, hyperphosphatemia due to increased renal phosphate reabsorption is associated to the recessive disorder familial tumoral calcinosis (FTC).

At the beginning of this work the genes mutated in XLH and ADHR were cloned. One gene codes for the endopeptidase PHEX, the other for the fibroblast growth factor FGF23. Both proteins are probably involved in a novel common pathway of the regulation of phosphate homeostasis. Missense mutations in FGF23 causing phosphate wasting in patients with ADHR, overexpression of FGF23 in tumors from patients with TIO, and the observation that FGF23 plasma levels are elevated in most patients with XLH provided strong evidence that FGF23 is a hormone with phosphaturic activity. However, the function of FGF23 in the regulation of phosphate metabolism is far from understood.

The intention of this study was to investigate the molecular properties of native FGF23 and its mutant forms. I conducted protein expression experiments in HEK293 cells which showed that native FGF23 is a secreted protein partially processed into an N-terminal fragment and a C-terminal fragment. I provided evidence that this cleavage occurs during protein secretion and it is performed by subtilisin like-protein convertases (SPCs). In addition, I determined that native FGF23 undergoes O-linked glycosylation before secretion by using a deglycosylation assay. Further, RT-PCR analysis of human tissues showed FGF23 expression in whole fetus, heart, liver, thyroid/parathyroid, small intestine, testis, skeletal muscle, differentiated chondrocytes and TIO tumor tissue. In mouse, FGF23 was expressed in day 17 embryo and spleen.

The FGF23 ADHR mutations replace arginine residues at the SPC cleavage site (RXXX motif). By expression of the FGF23-R176Q and -R179Q mutant proteins in HEK293 cells

I showed that ADHR mutations prevent cleavage at the RXXR site and stabilize FGF23. This alteration in the FGF23 cleavage enhances FGF23 phosphaturic activity in ADHR.

Familial tumoral calcinosis (FTC) with hyperphosphatemia is a disease considered the mirror image of the hypophosphatemic condition. It is known that FTC is caused by mutations in the *GALNT3* gene. By performing mutation analysis in two families with FTC, I could show that FTC can also be caused by inactivating mutations in the *FGF23* gene. To characterize the FGF23-S71G mutant protein I conducted *in vitro* expression assays, immunocytochemistry and ELISA to measure the FGF23 plasma levels in the patient with FTC. Taken together the results of these experiments showed that intact FGF23-S71G mutant protein remained inside the cells and only the C-terminal FGF23 fragment was secreted. These investigations demonstrate that FGF23 mutations in ADHR and FTC have opposite effects on phosphate homeostasis.

There is evidence that the endopeptidase PHEX which is mutated in patients with XLH and FGF23 act in the same pathway. PHEX function resides upstream of FGF23 and may be involved in the degradation of FGF23 thereby regulating its phosphaturic activity. I designed an assay with a recombinant secreted form of PHEX (secPHEX) to prove whether FGF23 is a substrate of PHEX. Although secPHEX activity could be demonstrated by degradation of PTHrP₁₀₇₋₁₃₉, secPHEX failed to degrade FGF23 in this assay. These results provided evidence against a direct interaction of PHEX and FGF23.

A. INTRODUCTION

In adult vertebrates, 10% of the skeletal bone mass is replaced every year, amounting to a complete structural overhaul every decade (Adelman and Solhaug 2000). This constant remodelling allows bone to carry out its many functions: to support the body and allow movement, to incubate developing immune cells, and to act as reserve of inorganic minerals, especially phosphorus and calcium. Phosphorus is one of the body's most important and abundant ions and the homeostasis of the plasma phosphate level is essential for many biological processes. However, the regulation of serum phosphorus concentrations is a complex process and our current models are far from complete.

1. PHOSPHATE HOMEOSTASIS

The major determinants of phosphate homeostasis are dietary phosphate intake, intestinal absorption, exchange with intracellular and bone storage pools, and renal reabsorption. The serum phosphate level is maintained within a narrow range through elaborate controls developed to keep phosphate from precipitating in tissues and to allow the controlled deposition of phosphate and calcium as hydroxyapatite ($\text{Ca}_5(\text{PO}_4)_3\text{OH}$) in bone. The movement of phosphate into and out of bone mineral is mainly regulated by parathyroid hormone (PTH) and 1,25-dihydroxyvitamin D₃ [$1,25(\text{OH})_2\text{D}_3$] (for review see Tenenhouse and Econs 2001).

1.1 Phosphorus

Phosphorus exists in our body in an inorganic form and an organic form. Organic phosphorus is found inside the cells where it has a structural role in phospholipids and nucleic acids, forms high-energy ester bonds (e.g., in ATP and cAMP) and participates in cellular signalling through covalent phosphorylation of proteins and lipids (Tenenhouse and Econs 2001). Outside the cells, inorganic phosphate is the principal urinary buffer and plays a critical function in the regulation of free hydrogen ions. Approximately 12% of the plasma inorganic phosphorus is protein bound, and the remainder circulates as free monovalent (H_2PO_4^-) or divalent (HPO_4^{2-}) orthophosphate ions (Hopkins *et al.* 1952). In animals with bones, most extracellular phosphate is found in bone mineral. The human

body contains around 700 g phosphorus whereof 600 g is bound in bones and teeth in the form of hydroxyapatite (Strom and Lorenz-Depiereux 2001).

The plasma phosphate concentration varies as a function of age in humans: in the range of 3.8-5.5 mg/dl in children and 2.7-4.5 mg/dl in adults (Greenberg *et al.* 1996). Although long term changes in plasma phosphate concentration clearly depend on the balance between intestinal absorption and renal excretion, short-term changes are affected by the continuous exchange of phosphate between the extracellular fluid (ECF) and either bone or cell constituents. ECF phosphate represents less than 1% of total body phosphate (Tenenhouse and Econs 2001).

Plasma phosphate concentration shows a circadian rhythm with a minimum at 9:30-10:00 a.m. and a peak at 4:00 a.m. The variation from nadir to peak may be as much as 1 mg/dl; *i.e.* 25-35% change in concentration (Markowitz *et al.* 1981). The factors determining this diurnal variation are not known.

1.2 Phosphate transport

The principal sources of dietary phosphorus are milk, milk products and meat. The daily intake of phosphorus is normally between 0.8 and 1.5 g (Walling 1977). About 70 % of ingested phosphate is absorbed in the small intestine, and enters the blood circulation through a sodium-dependent specific phosphate uptake cotransporter while the rest is excreted in the faeces. Intestinal phosphate absorption increases in proportion to the phosphate content of the diet and $1,25(\text{OH})_2\text{D}_3$ stimulates the reabsorption when phosphate intake is significantly reduced (Lee *et al.* 1986, Rizzoli *et al.* 1977).

Even though phosphate is actively transported across the bowel wall, the kidney plays the major role in regulating body phosphate. Approximately 90% of the phosphate in plasma is filtered through the glomerulus, and 80-90% of this filtered load is reabsorbed in the proximal tubule. The rest is excreted in the urine (Harris *et al.* 1977, Pastoriza-Munoz *et al.* 1978). Only a small percentage of absorbed phosphate is incorporated into organic forms in proliferation cells, or deposited as a component of bone mineral (Tenenhouse and Econs 2001).

The transcellular transport of phosphate is a carrier-mediated, saturable process and a maximal rate for tubular reabsorption of phosphorus (TmP), can be determined. The

balance between the rates of glomerular filtration (GFR) and maximal tubular reabsorption (TmP/GFR) determines the renal excretion of phosphate (Tenenhouse and Econs 2001).

1.3 Cellular mechanisms of renal phosphate transport

Phosphate travels across the brush-border membrane into the proximal tubular epithelial cell against an electrochemical gradient mediated by a sodium (Na^+) phosphate (Pi) cotransporter (NPT) (Bonjour and Caverzasio 1984, Murer *et al.* 1991).

Three types of Na^+ /Pi cotransporters have been identified (NPT-I, NPT-II, and NPT-III) but the main determinant of phosphate balance is the relative abundance of the type 2a cotransporter (NPT-IIa) localized in the apical brush-border membrane of the renal proximal tubular cells (Tenenhouse *et al.* 1998). Increased abundance of the NPT-IIa protein confers increased TmP/GFR and consequently raises serum Pi levels. NPT-IIa brush-border membrane abundance is determined by both transcriptional and post-transcriptional events such as membrane retrieval/internalization and membrane insertion (Murer and Biber 1996).

1.4 Hormonal regulation

The homeostasis of phosphate as well as calcium is known to be modulated by vitamin D. Vitamin D receptor null mice (*vdr* $^{-/-}$) are characterized by hypocalcemia and hypophosphatemic rickets (Yoshizawa *et al.* 1997). Vitamin D synthesis results from the photolytic cleavage of the B rings of ergosterol and 7-dehydrocholesterol which are obtained from the diet. Vitamin D is activated to 25-hydroxyvitamin D₃ [25(OH)D₃] in the liver. Further hydroxylation to 1,25-dihydroxyvitamin D₃ [1,25(OH)₂D₃] is mediated by 25(OH)D₃ 1 α -hydroxylase [1 α (OH)ase] in the proximal tubule of the kidney (DeLuca 1982). 1,25(OH)₂D₃ (calcitriol) is known to play an important role in the maintenance of phosphate levels in serum. Renal production of 1,25(OH)₂D₃ is stimulated by PTH and hypophosphatemia (Garabedian *et al.* 1972), and inhibited by 1,25(OH)₂D₃ itself and hypercalcemia (Tanaka and DeLuca 1972).

PTH is the best-characterized physiological regulator of phosphate reabsorption, but its principal function is to maintain calcium homeostasis. Hypocalcemia increases serum 1,25(OH)₂D₃ levels by stimulating 1 α (OH)ase activity through a PTH-dependent

mechanism (Omdahl *et al.* 1972). These effects are exerted directly on the renal proximal tubular cells and are mediated by cAMP (Rost *et al.* 1981).

Hypophosphatemia stimulates $1,25(\text{OH})_2\text{D}_3$ synthesis via the $1\alpha(\text{OH})\text{ase}$ in the kidney, leading to increased calcium and phosphate absorption in the intestine and enhanced mobilization of calcium and phosphorus from bone. In addition, hypophosphatemia stimulates the maximal tubular reabsorption of phosphate (TmP/GFR) in the kidney. The resultant increased serum calcium inhibits PTH secretion with a subsequent increase in urinary calcium excretion and tubular reabsorption of phosphate (Fig. 1). Thus, normal serum calcium levels are maintained and serum phosphorus levels are returned to normal (Tanaka and DeLuca 1973, Kawashima and Kurokawa 1986).

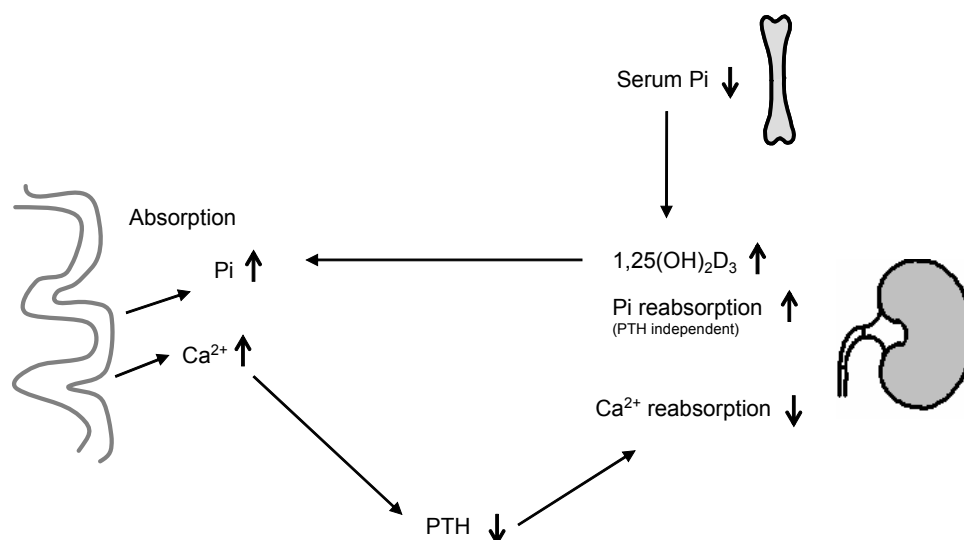


Fig. 1. Role of $1,25(\text{OH})_2\text{D}_3$ in phosphate homeostasis. A decrease of the phosphate concentration in plasma leads to a PTH-independent rise of phosphate reabsorption and $1,25(\text{OH})_2\text{D}_3$ synthesis. The increase of $1,25(\text{OH})_2\text{D}_3$ plasma concentration activates intestinal absorption of phosphate (Pi) and calcium (Ca) and thus, rises the bone resorption. Further, PTH secretion is inhibited reducing the renal tubular calcium reabsorption.

The mechanism by which restriction of phosphorus increases the $1\alpha(\text{OH})\text{ase}$ activity occurs at the level of mRNA and seem to be independent of PTH and changes in serum calcium (Bushinsky *et al.* 1985, Shinki *et al.* 1997). Further evidence for a PTH-independent regulation of $1,25(\text{OH})_2\text{D}_3$ was provided by Hughes *et al.* Dietary phosphate restriction in rats enhanced circulating $1,25(\text{OH})_2\text{D}_3$ and $1\alpha(\text{OH})\text{ase}$ concentrations independently on the presence or absence of the parathyroid or thyroid glands (or both) (Hughes *et al.* 1975).

2. DISORDERS OF PHOSPHATE METABOLISM: HYPOPHOSPHATEMIAS

In industrialized nations where vitamin D deficiency is relatively uncommon, inherited renal phosphate-wasting disorders are the most common cause of osteomalacia and rickets. Several hereditary disorders of isolated phosphate wasting have been described. These include X-linked hypophosphatemia (XLH), autosomal dominant hypophosphatemic rickets (ADHR), hypophosphatemic bone disease (HBD), and hereditary hypophosphatemic rickets with hypercalciuria (HHRH). In addition, tumor induced osteomalacia (TIO) also termed oncogenic hypophosphatemic osteomalacia (OHO) is an acquired disorder of renal phosphate wasting (Econs and Strom 1999). Hypophosphatemia due to impaired renal function is also a prominent feature of several syndromes of hereditary hypercalciuric nephrolithiasis (kidney stones) associated to mutations in the chloride channel 5 (CLCN-5). These include X-linked recessive nephrolithiasis (XRN), X-linked recessive hypophosphatemic rickets (XLRH), Japanese idiopathic low molecular weight proteinuria (JILMWP) and Dents disease (Rajesh 2000).

Tab. 1. Characteristics of the phosphate syndromes.

	HYPOPHOSPHATEMIA			HYPERPHOSPHATEMIA
	XLH	ADHR	TIO	FTC
Serum phosphorus	low	low	low	high
Serum calcium	normal	normal	normal	normal
1,25(OH)₂D₃	normal/low	normal/low	normal/low	high
PTH	normal/high	normal	normal/high	normal/high
TmP/GFR	decreased	decreased	decreased	increased
Urine calcium	normal	normal	normal	normal
Dental defect	dentin defects, dental abscesses	dental abscesses	none	pulp stones
Muscle weakness	minimal	present	prominent	none
Inheritance	X-linked dominant	autosomal dominant	tumor associated	autosomal recessive
Chromosome	Xp22.1	12p13	acquired	2q24
Gene defect	<i>PHEX</i>	<i>FGF23</i>	excess FGF23 (and other phosphaturic proteins?)	<i>GALNT3</i>

XLH: X-linked hypophosphatemia, ADHR: autosomal dominant hypophosphatemic rickets, TIO: tumor induced osteomalacia, FTC: familial tumoral calcinosis, 1,25(OH)₂D₃: 1,25-dihydroxyvitamin D₃, PTH: parathyroid hormone, TmP: maximal phosphate transport, GFR: rate of glomerular filtration, PHEX: phosphate regulating gene with homologies to endopeptidases on the X-chromosome, FGF23: fibroblast growth factor 23, GALNT3: N-acetylgalactosaminyltransferase. Adapted from Jan de Beur and Levine 2002.

The characteristic symptoms of hypophosphatemic rickets are normal PTH levels in serum, but low serum phosphate and reduced TmP/GFR. Hypophosphatemia usually stimulates renal 1 α (OH)ase and increases serum 1,25(OH)₂D₃ levels as a part of the homeostatic

mechanism. In contrast, patients with XLH, ADHR, and TIO show inappropriately normal or low serum $1,25(\text{OH})_2\text{D}_3$ levels. Table 1 summarizes some clinical manifestations of these syndromes. Therefore, regulatory mechanisms for both tubular reabsorption of Pi and vitamin D metabolism are deranged in these hypophosphatemic diseases.

2.1 X-linked hypophosphatemia

XLH (Online Mendelian Inheritance in Man [OMIM] 307800) is the most common cause of rickets, with a prevalence of 1 in 20,000. The disease is inherited in an X-linked dominant manner and is highly penetrant, but the severity and specific clinical manifestations are variable, even among members of the same family (Econs and Strom 1999).

Manifestations of XLH include short stature, bone pain, tooth abscesses and lower-extremity deformities. Progressive enthesopathy (calcification of tendon insertions, ligaments, and joint capsules) can occur, with pain and limitation of motion (Polisson *et al.* 1985). Patients with XLH present hypophosphatemia secondary to renal phosphate wasting with inappropriately normal or low serum $1,25(\text{OH})_2\text{D}_3$ concentrations. Other laboratory manifestations are outlined in table 1. Radiographic changes of rickets, which include widening and cupping of the metaphyseal ends of long bones (Fig. 2), are often but not always present in children (Econs *et al.* 1991). Adults present osteomalacia (Reid *et al.* 1989) and can have a variety of radiographic findings depending on disease severity, including pseudofractures, osteoarthritis, and enthesopathic changes (Polisson *et al.* 1985, Hardy *et al.* 1989).



Fig. 2. Radiography from a 2 ½ years old boy with XLH. Typical radiographic findings of XLH showing bowing of the long bones with cupping of the metaphyseal ends of the bones (from Dr. K. L. Mohnike, Magdeburg).

The most effective treatment of XLH consists of a combination of oral phosphate and vitamin D (1,25(OH)₂D₃) (Lyles and Drezner 1982). However, this form of therapy is less than ideal and has potentially serious long term side effects including hypercalcemia, hypercalciuria and nephrocalcinosis.

2.1.1 *Hyp* and *Gy* mice models

The *Hyp* and *Gy* mice, murine homologs of XLH, have provided useful models to study the basis for hypophosphatemia in this disorder. Early studies of parabiotic union of *Hyp* and normal mice showed development of hypophosphatemia and phosphaturia in the normal mouse rather than correction of the phosphaturic defect in the *Hyp* mouse (Meyer *et al.* 1989) and provided the initial evidence of a humoral factor as the cause of renal phosphate wasting. Subsequent work using renal cross-transplantation between normal and *Hyp* mice showed that the mutant phenotype was not transferred by transplantation of *Hyp* kidneys into normal mice, nor was the *Hyp* defect corrected by transplantation of normal kidneys into *Hyp* mice (Nesbitt *et al.* 1992).

These studies confirmed earlier suggestions that *Hyp* mice produce a circulating factor that inhibits the Npt2 cotransporter which is not inactivated by circulation through a normal mouse (Tenenhouse 1994). The humoral factor in the *Hyp* mouse was further characterized in studies that demonstrated that *Hyp* mouse serum could inhibit phosphate uptake in primary cultures of mouse proximal renal tubular cells in a dose-dependent manner (Lajeunesse *et al.* 1996). A similar pathogenetic mechanism appears operative in XLH, because transplantation of an unaffected sister's kidney into a brother with XLH led to renal phosphate wasting by the normal kidney (Morgan *et al.* 1974). The source of the circulating factor is unknown, but the factor may be produced by osteoblasts since transplantation of *Hyp* bone nodules into normal mice failed to correct completely the mineralization defect (Ecarot-Charrier *et al.* 1988).

2.1.2 Mutations in the *PHEX* gene cause XLH

The HYP consortium identified the gene responsible for XLH in 1995 by a positional cloning approach (The HYP consortium 1995). The gene is called *PHEX*, for phosphate regulating gene with homologies to endopeptidases on the X-chromosome. To date, there are more than 176 known mutations (www.phexdb.mcgill.ca) scattered throughout the *PHEX* gene including deletions, splice site and frameshift mutations, duplications, insertion, deletional insertions and missense mutations, all of which lead to loss of protein function. Mutations in the *Phex* murine homolog were also identified in the *Hyp* and *Gy* mouse models of XLH (Strom *et al.* 1997, Lorenz *et al.* 1998).

2.1.3 The *PHEX* protein

PHEX codes for a 749-amino acid protein (Fig. 3) with homology to the M13 family of zinc metallopeptidases, which includes neprilysin (NEP), endothelin-converting enzymes 1 and 2 (ECE-1 and ECE-2), the Kell blood-group protein, damage induced neuronal endopeptidase/X-converting enzyme (DINE/X-CE), and soluble endopeptidases/NEP-like enzyme 1 (SEP/NL1) (for review see Turner *et al.* 2001, Valdenaire *et al.* 1999, Ghaddar *et al.* 2000). The members of this family are involved in the degradation or activation of several bioactive peptides (Roques *et al.* 1993, Turner and Tanzawa 1997). Sequence similarity of *PHEX* to members of this family suggests also a role in regulating the activity of bioactive peptides. Indeed, experiments with internally quenched fluorogenic peptide substrates revealed that a secreted recombinant form of *PHEX* has endopeptidase activity (Campos *et al.* 2003), whereas mutated *PHEX* does not (Sabbagh *et al.* 2003).

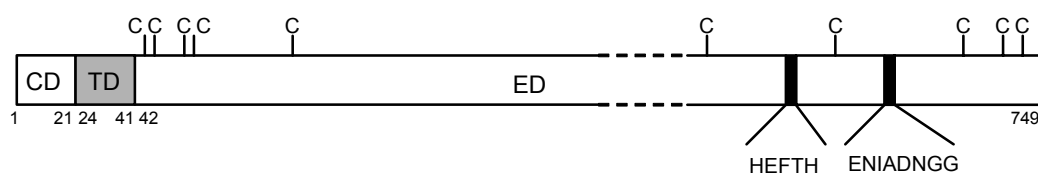


Fig. 3. Schematic representation of *PHEX*. Boxes represent the different domains of the *PHEX* protein: cytoplasmic domain (CD), transmembrane domain (TD) and extracellular domain (ED). Numbers down the boxes indicate amino acid positions. The zinc-binding motifs (HEXXH and ENXADXGG) are shown in black. C, Cystein residue.

PHEX is a type II integral membrane glycoprotein with a short cytoplasmic N-terminal region, a single transmembrane domain, and a long extracytoplasmic domain, which

contains the active site of the enzyme (Crine *et al.* 1997) (Fig. 3). PHEX is a glycoprotein with 8 potential N-glycosylation sites and 10 conserved cysteines, all involved in disulfide bridges, important for the maintenance of the three-dimensional protein structure (Oefner *et al.* 2000). The binding of Zn^{2+} ions is characteristic for this family of metallopeptidases. PHEX contains two conserved zinc-binding motifs, HEXXH and ENXADXGG, which are situated between the amino acids 580-584 (HEFTH) and 642-649 (ENIADNGG) respectively (Fig. 3). These residues are essential for zinc coordination and formation of the catalytic site (Holden *et al.* 1987).

2.1.4 Relevance of PHEX in the pathophysiology of XLH

The finding that PHEX is a membrane-bound protein with predicted enzymatic activity, and not a secreted protein, in addition to lack of PHEX expression in kidney clearly ruled out PHEX as the putative phosphaturic factor. Instead, it was hypothesized that PHEX, directly or indirectly, is involved in the processing of a peptide hormone, which plays an essential role in the regulation of bone mineralization, renal phosphate handling and vitamin D metabolism (The HYP Consortium 1995, Rowe 1997).

PHEX is mainly expressed in bone and teeth (Ruchon *et al.* 1998), but also at lower levels in lung, brain, muscle, and gonads. A primary osteoblast defect was also postulated to contribute to the bone disease in XLH since the observation that conditioned media from *Hyp* osteoblasts, but not normal osteoblasts, inhibited phosphate transport in primary mouse proximal tubule cells cultures (Lajeunesse *et al.* 1996). Other experiments showed that explants from *Hyp* mouse calvaria failed to mineralize appropriately even in physiologically normal environments and the mineralization effect was transferable to normal cells in co-culture experiments (Xiao *et al.* 1998). New experiments showed that the restoration of Phex function in *Hyp* mice by overexpression of Phex in osteoblasts failed to rescue the hypophosphatemia but resulted in partial correction of the skeletal phenotype (Bai *et al.* 2002, Liu *et al.* 2002). These findings implicate osteoblasts in the production of phosphate regulating hormones and suggest that PHEX has a double function in regulating phosphaturic hormones and a local effect in osteoblastic mineralization.

2.2 Autosomal dominant hypophosphatemic rickets

ADHR (OMIM 193100) is a very uncommon disorder; only four cases have been reported. ADHR has a phenotype similar to that of XLH, although the clinical presentation tends to be variable because of incomplete penetrance and variable age of onset.

Renal phosphate wasting and inappropriately normal $1,25(\text{OH})_2\text{D}_3$ concentrations are the predominant laboratory findings in ADHR (Tab. 1). Clinical and laboratory manifestations of ADHR are variable even within families and are characterized by short stature and bone mineralization defects that result in rickets, osteomalacia, and lower extremity deformities. Dental abscesses are a prominent feature of the syndrome. Those with childhood onset look phenotypically like XLH. Adults typically complain of bone pain, fatigue, and/or weakness and some have evidence of pseudofractures (Brame *et al.* 2004). Patients with ADHR patients are treated as those with XLH, i.e. oral substitution of phosphate and calcitriol.

2.2.1 Mutations in the *FGF23* gene cause ADHR

Linkage studies of one large ADHR kindred demonstrated linkage of the ADHR trait to chromosome 12p13 (Econs *et al.* 1997). Subsequent mutation screening from index patients of 4 unrelated families that had a male-to-male transmission and clinical features compatible with ADHR identified specific mutations in the *FGF23* gene (The ADHR Consortium 2000). *FGF23* is composed of a 11 kb genomic sequence, three exons, and a 3.0 kb cDNA that encodes a novel fibroblast growth factor (FGF23). Missense mutations affect one of two arginine residues at positions p.176 or p.179 leading to a glutamate or tryptophan substitution (R176Q, R179Q and R179W).

Interestingly, the mutated arginine residues disrupt a subtilisin-like proprotein convertase (SPC) consensus proteolytic cleavage motif (RXXR). Most secreted and membrane-bound proteins undergo post-translational modifications before expression of the mature polypeptide. The SPCs are a seven-member family of serine proteases responsible for the processing of peptide hormones, neuropeptides, adhesion molecules, receptors, growth factors, cell surface glycoproteins, and enzymes. The substrates are cleaved C-terminal of the R-(X)*n*-R consensus site where *n* is 0, 2, 4, or 6, and X is any amino acid except

cystein. These enzymes are widely expressed in the trans-Golgi network, and possess similar, but not the same substrate specificities (for review see Seidah and Chretien 1999).

2.2.2 FGF23 belongs to the fibroblast growth factor family

FGFs are a family of polypeptide growth factors that are found in animals from *Caenorhabditis elegans* to vertebrates, as well as in some arthropod viruses. The human FGF family is divided into seven subfamilies. Members of each subfamily share increased sequence similarity, and biochemical and developmental properties (Ornitz and Itoh 2001). FGF signaling has been implicated in cell proliferation, differentiation, survival, and migration and is required for both development and maintenance of vertebrates (Coulier *et al.* 1997).

There are 22 human FGF paralogues, ranging in size from 17 to 34 kDa. These proteins share a common core of around 140 amino acids, which consists of 12 antiparallel β -strands and has homology to the interleukin 1 β (IL-1 β) family of growth factors. Crystal structures have been solved for 6 of the 22 FGFs (FGF1, FGF2, FGF4, FGF7, FGF9, FGF10 and FGF19) (Harmer *et al.* 2003). These proteins all form a β -trefoil structure with a pseudo-3-fold axis of symmetry (Fig. 4).

FGFs bind to two types of molecules on the cell surface (Fig. 4). On one face of the FGF, they form a low-affinity interaction with heparin sulfate (HS). On a second face, they bind to and activate cell surface tyrosine kinase FGF receptors (FGFRs) that is required to mediate their biological responses. In mammals, there are five homologues (FGFR1-5) (Itoh and Ornitz 2004). Mutations in FGFRs are responsible for a diverse group of skeletal disorders involving craniosynostosis and dwarfing syndromes (Wilkie *et al.* 2002). In contrast, only two members of the fibroblast growth factor family are associated with a human disease. FGF23 was first reported causing ADHR (The ADHR consortium 2000) and recently, mutations in FGF10 have been associated with aplasia of lacrimal and salivary glands (Entesarian *et al.* 2005).

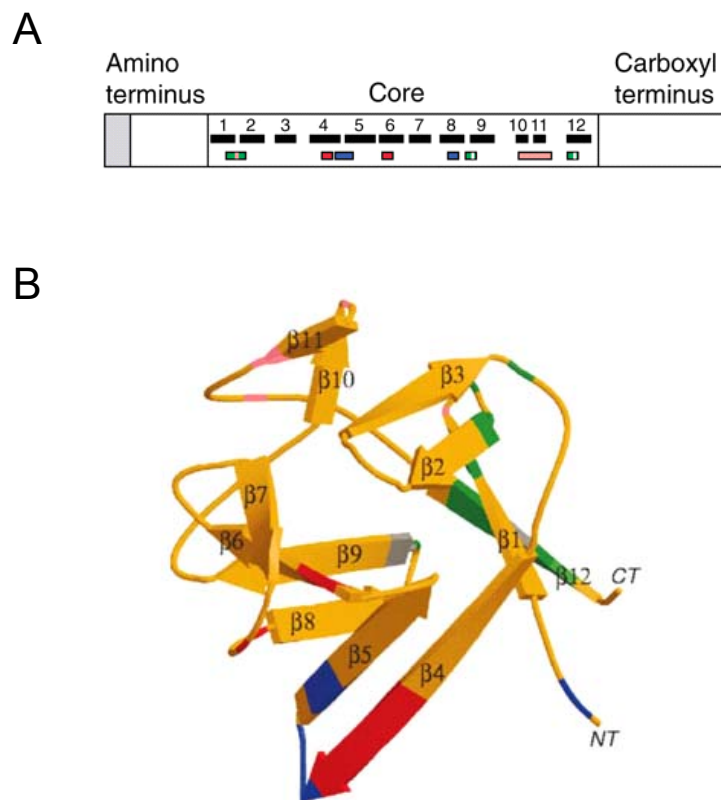


Fig. 4. Structural characterization of the FGF polypeptide. (A) Structural features of the FGF polypeptide: The amino terminus of some FGFs contains a signal sequence (shaded). All FGFs share a core region that contains conserved amino acid residues and conserved structural motifs. The locations of the β strands within the core region are numbered and shown as black boxes. The heparin-binding region is indicated in pink. Residues that contact the FGF receptor are shown in green, blue and red. (B) Three-dimensional structure of FGF2: a ribbon diagram is shown; β strands are labeled 1-12 and regions of contact with the FGF receptor and heparin are color coded as in A (Ornitz and Itoh 2001).

2.3 Tumor induced osteomalacia

TIO, also termed oncogenic hypophosphatemic osteomalacia (OHO), is an acquired disorder of renal phosphate wasting. There are no accurate prevalence numbers as it is an uncommon, but probably underdiagnosed, disorder. There are 120 cases described in the literature.

Laboratory abnormalities are similar to those in XLH and ADHR (Tab. 1). Clinical symptoms include gradual onset of muscular weakness, bone pain, and fatigue that may be present from a few months to many years before diagnosis. Children have the lower-extremity disorders characteristic of rickets, whereas adults develop fractures and pseudofractures (Drezner 2003, Brame *et al.* 2004).

TIO is caused by a variety of mostly benign mesenchymal tumors that secrete a factor or factors, collectively termed “phosphatonins” (Drezner 2000, Kumar 2002) which can inhibit proximal renal tubular Pi reabsorption and impair synthesis of 1,25(OH)₂D₃. Tumor extracts and conditioned media from cultured tumors can inhibit phosphate transport in renal cell lines *in vitro* (Cai *et al.* 1994), and can induce phosphaturia and hypophosphatemia when administered *in vivo* into mice (Popovtzer 1981). The tumors are often located in the skeleton but can be quite difficult to localize. Surgical removal of the tumor relieves all symptoms.

2.3.1 Characterization of “phosphatonins” from TIO tumors

In light of the clinical similarity between ADHR and TIO, White *et al.* examined FGF23 expression in TIO tumor tissue and found significantly higher levels of expression of FGF23 messenger RNA and protein than that of normal tissues (White *et al.* 2001). Other groups independently confirmed these findings by obtaining complementary DNA clones abundantly expressed in a tumor causing TIO. They identified several candidate molecules for the phosphaturic substance including fibroblast growth factor 23 (FGF23), frizzled-related protein 4 (FRP4), matrix extracellular phosphoglycoprotein (MEPE), dentin matrix protein 1 (DMP1), heat shock protein-90, and osteopontin (Rowe *et al.* 2000, Shimada *et al.* 2001, Jan de Beur *et al.* 2002).

Nude mice transfected with FGF23 tumor cells developed hypophosphatemia, renal phosphate wasting, and inappropriately low calcitriol levels with decreased expression of 1 α (OH)ase activity compared with control mice (Shimada *et al.* 2001). They also showed growth retardation and osteomalacia. Although FGF23 has been the best characterized tumor protein associated with TIO, it is not the only one. Phosphaturic activity of MEPE (Rowe *et al.* 2004) and FRP4 (Berndt *et al.* 2003) has also been described in *in vivo* and *in vitro* experiments. Thus, it is elusive whether only one or multiple secreted factors are involved in the pathogenesis of this syndrome.

3. DISORDERS OF PHOSPHATE METABOLISM: HYPERPHOSPHATEMIAS

Hyperphosphatemia usually occurs in the setting of impaired renal function, hypoparathyroidism, increased flux of phosphate into the extracellular fluid, or a combination of these factors. The most common cause of hyperphosphatemia is acute or

chronic renal failure (Avioli *et al.* 1968). Hyperphosphatemia may also result from the excessive administration of phosphate using cytotoxic drugs to treat malignancies, especially lymphomas or leukaemia. Other circumstances, in which renal tubular phosphate excretion is decreased, include acromegaly, and chronic therapy with etidronate or heparin (Wilber and Slatopolsky 1968, Bringhurst *et al.* 1999). The only hereditary disorder associated with hyperphosphatemia which has been described is familial tumoral calcinosis (FTC).

3.1 Familial tumoral calcinosis

Inclan *et al.* (Inclan *et al.* 1943) gave the name “tumoral calcinosis” to a condition characterized by ectopic calcifications, although the same disorder was originally described by Duret in 1899 (Duret *et al.* 1899). Familial tumoral calcinosis (OMIM 211900) seems to represent the metabolic mirror image of hypophosphatemic conditions (Tab. 1). FTC is a rare disease, inherited in an autosomal recessive mode. The disease most commonly occurs in black African populations and usually appears before the second decade of life (Palmer *et al.* 1966, Martinez 2002).

FTC is characterized by periarticular calcified masses often localized in the hip, elbow or shoulder. They start as small, discrete, calcified nodules and progress to large and more definite lobulated tumors with a calcifying progress and final ossification (Fig. 5 A). Since vascularity is observed in the more active lesions, it seems that FTC represents a disordered reparative process (Thomson 1966). These masses are usually asymptomatic but can cause discomfort or pain when they compress the adjacent muscles and impinge on nerves and vessels. Diaphyseal hyperostosis (Clarke *et al.* 1984) and developmental abnormalities of the dentine and pulp are often associated to this condition (Fig. 5 C). Calcification of other tissues including skin, cartilage, cerebral vessels, retina, and vascular calcification causing severe complications may be seen in FTC (Martinez 2002).

FTC is associated with hyperphosphatemia and increased proximal tubular phosphate reabsorption despite normal serum levels of calcium and PTH (Lufkin *et al.* 1983 and 1980, Mitnick *et al.* 1980). Serum levels of $1,25(\text{OH})_2\text{D}_3$ may be normal or elevated in these patients (Slavin *et al.* 1993). Despite this conflicting data, the presence of inappropriately normal to slightly elevated concentrations of $1,25(\text{OH})_2\text{D}_3$ in the presence

of pronounced hyperphosphatemia, suggests that these patients also have a defect in the regulation of the renal $1\alpha(\text{OH})\text{ase}$ (Tab. 1).

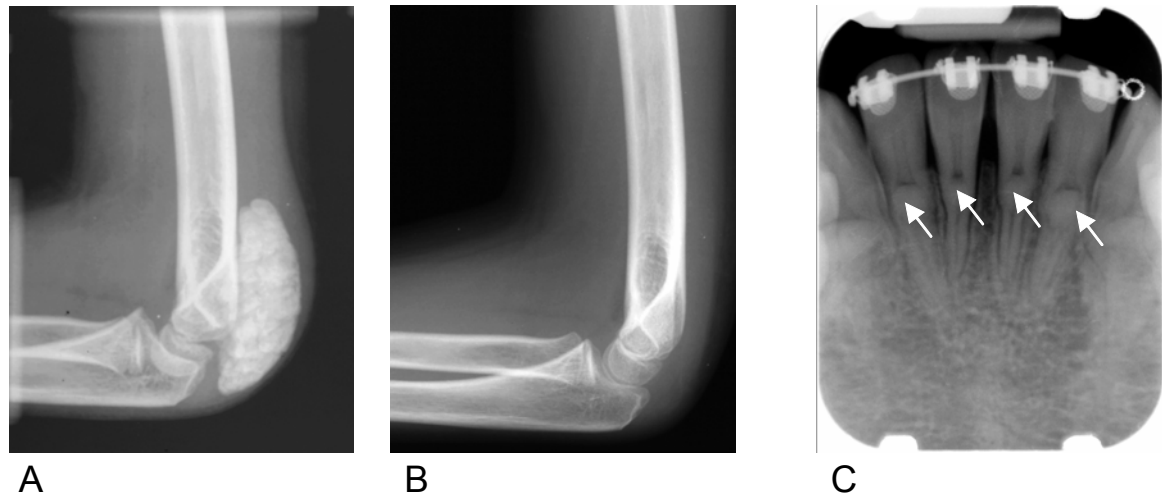


Fig. 5. Characteristic findings of FTC in a 12 years old boy. Radiographs show the left elbow (A) before and (B) after resection of a discoid lobulated calcified tumoral mass in the soft tissue of the extensor site of the left distal humerus. Radiograph of the lower incisors (C) shows round calcareous deposits (arrows) within the pulp chambers so-called pulp stones (Benet-Pagès *et al.* 2005).

Recently, biallelic mutations in the UDP-N-acetyl-alpha-D-galactosamine:polypeptide N-acetylgalactosaminyltransferase 3 (*GALNT3*) gene have been identified in two large families as a cause of FTC (Topaz *et al.* 2004). *GALNT3* encodes a glycosyltransferase that belongs to a large family of Golgi-associated biosynthetic enzymes that are responsible for initiating mucin-type O-glycosylation. This finding suggests that a defective post-translational modification underlies this disorder. Furthermore, evidence for heterogeneity was provided.

4. FUNCTION OF PHEX AND FGF23: AN UNIFYING HYPOTHESIS

The striking biochemical and clinical similarities between TIO, XLH, and ADHR have led to the speculation that a common circulating factor plays a pathogenic role in these disorders. The observation of high FGF23 concentrations in serum of patients with TIO (Yamazaki *et al.* 2002) and in most but not all patients with XLH (Jonsson *et al.* 2003) as well as in serum of *Hyp* mice (Aono *et al.* 2003), together with the finding that mutations in FGF23 were the cause for ADHR, suggested FGF23 as the phosphaturic candidate.

The discovery of PHEX in XLH and its homologies to other endopeptidases, has invited speculations concerning potential interactions between the PHEX metallopeptidase and the circulating factor causing phosphaturia. Whether or not FGF23 is a substrate of PHEX is controversial. It was initially reported that PHEX degraded FGF23 in an *in vitro* translation system (Bowe *et al.* 2001), but subsequent experiments were unable to show cleavage of an FGF23 peptide that encompassed arginines p.176 and p.179 by PHEX (Guo *et al.* 2001).

Most likely, FGF23 plays a central role in the pathophysiology of these disorders. Thus, a model explaining the link of FGF23 to all three phosphate wasting disorders was proposed (Strewler 2001): in XLH and *Hyp* mice, loss of function of PHEX may lead to higher concentrations of FGF23, which subsequently causes renal phosphate wasting. In ADHR, missense mutations replace key amino acids in FGF23 and render the protein resistant to proteolysis, thereby leading to enhanced FGF23 activity. Similarly, excess of FGF23 synthesis by TIO tumors leads to extremely increased FGF23 plasma levels that cause phosphaturia. This model is summarized in figure 6.

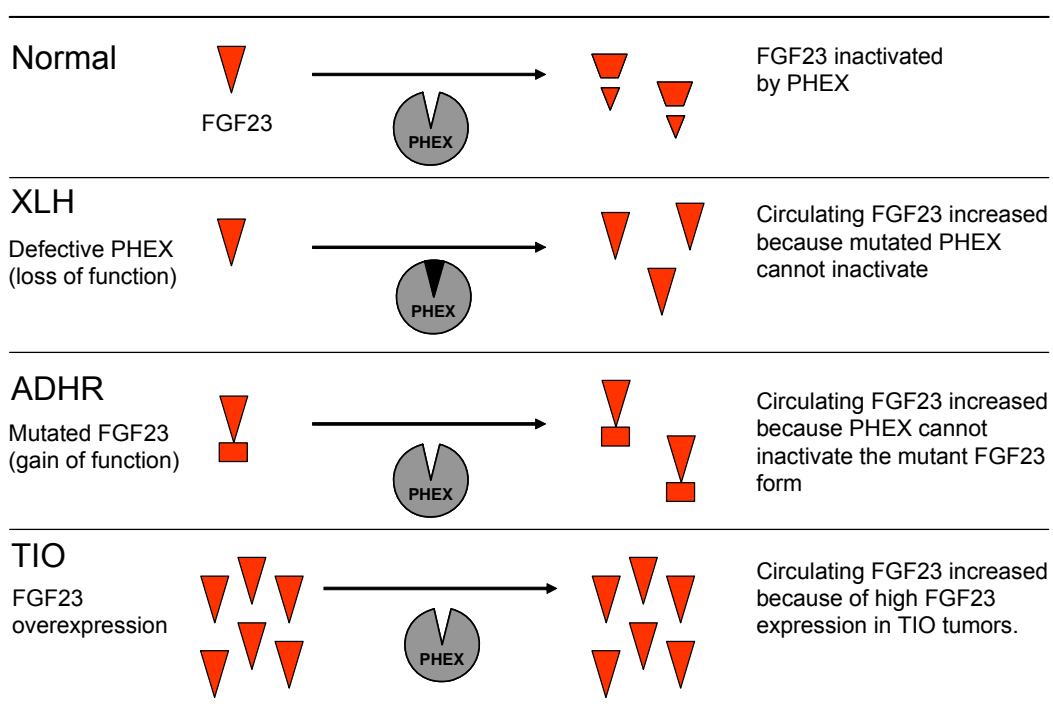


Fig. 6. Hypothesis of the FGF23 role in phosphate wasting conditions. Under normal conditions, FGF23 activity may be negatively regulated by PHEX. In XLH and *Hyp* mice, the defective PHEX is unable to cleave and inactivate FGF23. Specific mutations render FGF23 resistant to PHEX processing within individuals with ADHR. In TIO, FGF23 is produced in such excess that FGF23 levels and activity cannot be modulated.

5. AIMS OF THE INVESTIGATION

In the year 1995, the HYP consortium identified loss of function mutations in the PHEX metalloproteinase in patients with X-linked hypophosphatemic rickets (The HYP Consortium 1995). Five years later, mutations in a novel fibroblast growth factor (FGF23) have been identified as the cause of autosomal dominant hypophosphatemic rickets (ADHR) by positional cloning (The ADHR Consortium 2000). The phenotypic similarity between XLH and ADHR suggested that a common mechanism is involved in the pathogenesis of both disorders and an interaction between PHEX and FGF23 was proposed (Strewler 2001). The finding that FGF23 was overexpressed in tumours from patients with oncogenic hypophosphatemic osteomalacia provided further evidence that FGF23 is involved in the regulation of renal phosphate reabsorption (White *et al.* 2001, Shimada *et al.* 2001).

However, the molecular and physiological mechanisms by which the mutations in FGF23 lead to misregulation of renal phosphate handling in ADHR are currently unknown. To understand how FGF23 is involved in regulating renal phosphate wasting, it is particularly important to know more about the properties of this new hormone. To achieve this goal, I conducted the following studies in the present work:

- Molecular characterization of the FGF23 protein. For this purpose antibodies against FGF23, which can be used for western blot and immunocytological assays, should be established. It should be proven whether FGF23 is a secreted protein and whether it is glycosylated.
- ADHR is inherited in an autosomal mode and caused by missense mutations which could be explained by a gain of protein function. The mutations replace arginine residues within a subtilisin-like proprotein convertase cleavage site. It should be determined if the ADHR mutations lead to protease resistance of FGF23.
- DNA from three patients with familial tumoral calcinosis was collected. Since FTC is considered the mirror image of the hypophosphatemic rickets, it should be investigated whether FTC can be caused by FGF23 mutations and whether the functional characterization of the mutant protein could explain this phenotype.

- Establishment of an assay to demonstrate possible substrates of the PHEX endopeptidase with the goal to determine whether there is an interaction between FGF23 and PHEX. This was based on the hypothesis that PHEX could regulate physiologically the amounts of FGF23.

B. MATERIALS AND METHODS

1. MATERIALS

1.1 DNA-Resources

1.1.1 Patients

Mutation screening was performed in members of two families from Austrian (family 1), and Spanish (family 2) origin that presented familial tumoral calcinosis (FTC) with hyperphosphatemia (Tab. 2). Blood samples from the members of the whole family were provided by Dr. Peter Orlik from the “Universitätsklinik für Kinder- und Jugendheilkunde”, Innsbruck, Austria, and Dr. Pilar Blay from the “Hospital central de Asturias”, Oviedo, Spain.

Tab. 2. Mutation screening in families with FTC

Family	Patient	Gender	Affected	Diagnose
1	23198	m	no	
1	23199	f	no	
1	23200	f	no	
1	23201	f	no	
1	23202	m	yes	FTC
2	23293	f	yes	FTC
2	23294	m	no	
2	23295	f	no	
2	23296	m	yes	FTC

m: male, f: female, FTC: familial tumoral calcinosis

1.1.2 cDNAs

Human RACE-cDNAs: whole fetus, fetal brain, fetal kidney, brain, heart, small intestine, kidney, liver, testis, lung, skeletal muscle, and thyroid/parathyroid Marathon-Ready™ cDNAs were provided by Clontech. Mouse RACE-cDNAs: embryo 12.5 days, embryo 17 days, and spleen Marathon-Ready™ cDNAs were provided by Clontech.

1.1.3 Plasmids

Full-length *FGF23* and *PHEX* cDNAs were previously cloned in pBluescriptII SK +/- vector (Stratagene). Subsequent directional cloning for expression analysis was done in pMAL-c2 (New England Biolabs) or in pcDNA3.1/*myc*-His version B (Invitrogen).

1.2 Enzymes, chemicals and other materials

1.2.1 Enzymes and chemicals

The companies New England Biolabs and MBI Fermentas provided restriction enzymes. MBI Fermentas provided Taq- and Vent-polymerases used for PCR amplification. T4 DNA-ligase and the 1 kb DNA ladder (0.075-12.216 kb) were obtained from Gibco BRL. PNGase F and Endo H glycosidases were provided by New England BioLabs, O-glycosidase from *Diplococcus pneumoniae* by Roche and Neuraminidase X from *Clostridium perfringens* by Sigma.

All chemicals used in this work had a degree of purity suitable *pro analyse* and were provided by Merck or Sigma. Other chemicals, buffers, and additional materials are described under the corresponding methods.

1.2.2 Kits

Advantage cDNA PCR Kit	Clontech
Big Dye Terminator v3.1 Cycle Sequencing Kit	Applied Biosystems
First-Strand cDNA-Synthesis Kit	Pharmacia
QIAquick Gel Extraction Kit	Qiagen
QIAquick PCR purification Kit	Qiagen
QIAprep Spin Plasmid Miniprep Kit	Qiagen
QIAGEN Plasmid Midi Kit	Qiagen
Ni-NTA Spin Kit	Qiagen
QuikChangeXL Site-Directed mutagenesis Kit	Stratagene
PCR Master Mix Kit	Promega
Human FGF-23 (C-Term) ELISA Kit	Immutopics

1.2.3 Oligonucleotides

All oligonucleotides used in the PCR reactions were synthesised by the manufacturer Metabion. Table 3 shows primer pairs used for the directional cloning of the *FGF23*- (1) and *PHEX*-cDNA (2) sequences into the corresponding expression vectors (restriction sites are underlined). Primers used for *FGF23* cloning into pMAL-c2 (1a), pcDNA3.1/myc-His with His tag (1b) and cloning of *FGF23*-cDNA fragment corresponding to amino acids 1-178 in pcDNA3.1/myc-His (1c). Primers used for *PHEX* cloning in pcDNA3.1/myc-His (2a) and in pcDNA3.1/myc-His with His tag (2b).

Tab. 3. Cloning primers

	Forward primer (5' → 3')	Reverse Primer (5' → 3')	°C
1a	CGGAATTCATCCCAATGCCTCCCCTG	CGGGATCCCTAGATGAACTTGGCGAAGGG	58
1b	CGGAATTCACAGGCACGATTTGGGGGC	GCTCTAGACTGATGAACTTGGCGAAGGGGCG	58
1c	CGGAATTCACAGGCACGATTTGGGGGC	GCTCTAGACTAGGTGTGCCGCCGTGGTATG	58
2a	ATAAGAATGCGGCCGCACATGGAAGCAGAAACAGGGAGC	GCTCTAGACTACCAGAGTCGGAGGA	58
2b	ATAAGAATGCGGCCGCACATGGAAGCAGAAACAGGGAGC	TGCTCTAGATACCAGAGTCGGCGGAGTC	58

Primer pairs designed to introduce the p.R176Q, p.R179Q and p.S71G mutations into the *FGF23*-cDNA sequence and to create a secPHEX construct by site-directed mutagenesis PCR (Tab. 4).

Tab. 4. Site-directed mutagenesis primers

Name	Forward primer (5' → 3')	Name	Reverse Primer (5' → 3')	°C
FGF23 _{R176Q}	CCATACCACGGCAGCACACCCGGAG	FGF23 _{R176Q}	CTCCGGGTGTGCTGCCGTGGTATGG	60
FGF23 _{R179Q}	GCGGCACACCCAGAGCGCCGAGG	FGF23 _{R179Q}	CCTCGGCGCTCTGGGTGTGCCGC	60
FGF23 _{S71G}	CATCAGACCATCTACGGTGCCTGATGATC	FGF23 _{S71G}	GATCATCAGGGCACCGTAGATGGTCTGATG	60
PHEX ₂₈₋₂₉	GTCGTGTTTGTCTTACCACCCTAGTTCTG	PHEX ₂₈₋₂₉	CAGAACTAGGGTGGTAAGGACAAACACGAC	60
PHEX _{del}	GTTCTGGGCACGACCAGTCAAGGTCTC	PHEX _{del}	GAGACCTTGACTGGTCTGCTGCCAGAAC	60
PHEX ₃₀₋₃₂	TTTGTCTTACCGTCATAGCTCTGGGCACGAT	PHEX ₃₀₋₃₂	GATCGTGCCAGAGCTATGACGGTAAGGACA	60
PHEX ₃₃₋₃₄	CCGCATAGCTCAGCAGACGATCCTCTTTC	PHEX ₃₃₋₃₄	GAAAGAGGATCGTCTGCTGAGCTATGACGG	60
PHEX ₃₆	GCTCAGCAGACGACCTCTTTCTAGTG	PHEX ₃₆	CACTAGAAAGAGGGTCTGCTGCTGAGC	60
PHEX ₃₇₋₄₀	GCTCAGCAGACGACCAGTCAAGGTCTCTTAA	PHEX ₃₇₋₄₀	CTTAAGAGACCTTGACTGGTCTGCTGCTGAGC	60

Mutation analysis of the *FGF23* and *GALNT3* genes was performed with intronic primer pairs to amplify each exon separately (Tab. 5). All primers were used at an annealing temperature of 60°C.

Tab. 5. FGF23 and GALNT3 amplification primers

Exon	Name	Forward primer (5' → 3')	Name	Reverse primer (5' → 3')	bp
1	FGF23e1F	AATCTCAGCACCAGCCACTC	FGF23e1R	GATGGACAACAAGGGTGCTC	294
2	FGF23e2F	TTTCAGGAGGTGCTTGAAGG	FGF23e2R	TTGCAAATGGTGACCAACAC	208
3	FGF23e3F	CTTCACGTGGTTCGCTCTTG	FGF23e3R	TGCTGAGGGATGGGTTAAAG	510
1.1	GALNT3e1.1F	CTACCATTAAAGATACCTTCTCTCAG	GALNT3e1.1R	AGGACAGGCTTCAATTCTGC	257
1.2	GALNT3e1.2F	GATGTTGGATTTAATGCTAGAAGC	GALNT3e1.2R	CTCCCTGCAAAGCCTG	257
2	GALNT3e2F	TCTCTGGGTGAGTGATTTGC	GALNT3e2R	TGAATATGTCCATCCTTGGATTC	173
3	GALNT3e3F	TTTGAAGGATCATTGCTCTG	GALNT3e3R	CCTTTTAAATTAGAGGGAGAGGG	150
4	GALNT3e4F	TCAAACACAAATTGACTCTGTTATTC	GALNT3e4R	GCAAGTACACAAATGAATGACTTTTAG	235
5	GALNT3e5F	CAAAAATCTTGACTTTGAAGATAGC	GALNT3e5R	TCTGTAATCATATGTACCAGCCG	118
6	GALNT3e6F	GGTGAACCTAAAAGCAACTTTG	GALNT3e6R	ACGCAAAAAGGACGTGTGAAC	201
7-8	GALNT3e7/8F	GCCTCTTGAATTTTAGCATGG	GALNT3e7/8R	AGGCAACATCTCACTTGTGC	437
9	GALNT3e9F	TTTTGCAACTGAGCACATGG	GALNT3e9R	CATGTTCCACTCATTTTCCC	153
10	GALNT3e10F	TGGCTCACCTAGAAAGATTTG	GALNT3e10R	TTTTCAAAAACACTACAGTGTATGCC	123

Primer pairs used for semiquantitative multiplex-PCR of the seven human and mouse SPCs (Tab. 6). Due to high homology between the human and the mouse *SPC* sequences, only specific primers for the amplification of mouse *Spc3*, *Spc6* and *Spc7* were required.

Tab. 6. Multiplex-PCR primers

Name	Forward primer (5' → 3')	Name	Reverse primer (5' → 3')	bp	°C
SPC1F	CTGGCGAGTGGGTCCTAGAG	SPC1R	CAAGTCTGCTCCACAGGGTC	394	59
SPC2F	ACATGCAGCATCTGACTGTG	SPC2R	TCAGCAAATGGACTTGGTG	387	59
SPC3F	GGTACTTGGACTTTGAGAATTACGAC	SPC3R	AAGTTTTCATAAGGGATGTTGAGC	407	59
SPC4F	CGCGGGTCATAAAGTTAGCC	SPC4R	CTCAGCCTTTTCTCCCAG	398	59
SPC5F	GACCTGGAGATCTCGCTCAC	SPC5R	GCAGGTGTAGCAGGAGGC	340	59
SPC6F	GGTATTTCAACGGCCAGGAC	SPC6R	GGCACAGATTGTTCTTTTTCAC	366	59
SPC7F	CCTACAGGCTTGTATCAGG	SPC7R	TCTAGCTCTGTCCCTTCCTCC	403	59
Spc3F	TACAGACATGTCTGGAAGAATGC	Spc3R	TTCAGAGCCTTCAAGCTTGGAG	407	59
Spc6F	GTCTACACCAACCACTGGGCA	Spc6R	GGCTCCTTCGATATCATGTCA	366	59
Spc7F	GCAGAAAGTCCCACTTGGA	Spc7R	CCTCTCAGCAGCGTTTGCTC	403	59

First (1) and second (2) round primers used for the analysis of *FGF23* expression in human and mouse tissues by RT-PCR (Tab. 7).

Tab. 7. RT-PCR primers

Name	Forward primer (5' → 3')	Name	Reverse Primer (5' → 3')	°bp	°C
FGF23F1	TCAGAGGATGCTGGCTTTGTGGTG	FGF23R1	TGCGTGTTCACTCGACCGCC	480	58
FGF23F2	CCTCTGCATGGATTTAGAGGCAAC	FGF23R2	ATGGGTCCTGCGCCATCGGG	396	58
Fgf23F1	AGCCTGTCTGGGAGTGTGAC	Fgf23R1	ATTCTGAATAGCGGTGCTG	610	58
Fgf23F2	TCAAACCTCAGCATTAGCCACTC	Fgf23R2	TTCCTCTACGTGGGCTGAAC	510	58

1.2.4 Antibodies

Anti-MBP monoclonal antibody	New England BioLabs
Anti-His (C-term)-HRP antibody	Invitrogen TM
Anti-Flag M2-HRP antibody	Sigma
Anti-calnexin [AF18] antibody	Abcam
Anti-Lamp1 [LY1C6] antibody	Abcam
Monoclonal antibody against human mitochondria	Chemicon
Wheat germ agglutinin (WGA) antibody	Molecular Probes
Goat anti-rabbit IgG (H+L)-HRP conjugate	Bio Rad
Alexa Fluor 594 conjugate	Molecular Probes

The company Eurogentec provided the production and purification of polyclonal antibodies against human FGF23 and PHEX proteins. Immunizations were performed in

rabbits. Antigens were designed against peptides detailed in table 8.

Tab. 8. Antibodies

Protein	Fragment	Name	Peptide	Concentration
FGF23	N-terminal	FGF23 ₄₈₋₆₇	₄₈ RNSYHLQIHKNGHVDGAPHQ ₆₇ +C	0.75 mg/ml
FGF23	N-terminal	FGF23 ₁₄₈₋₁₆₃	₁₄₈ GMNPPYSQFLSRRNE ₁₆₃ +C	0.59 mg/ml
FGF23	C-terminal	FGF23 ₁₇₃₋₁₈₇	₁₇₃ IPRRHTRSAEDDSER ₁₈₇ +C	0.37 mg/ml
FGF23	C-terminal	FGF23 ₂₀₇₋₂₂₂	₂₀₇ SQELPSAEDNSPMASD ₂₂₂ +C	0.33 mg/ml
PHEX		PHEX ₁₇₁₋₁₈₅	₁₇₁ ESNIGPEGVWSERKF ₁₈₅ +C	1.2 mg/ml

1.2.5 Cell lines

Human embryonic kidney cells (HEK293) were provided by the “Deutsches Krebsforschungszentrum” (DKFZ). Human prostate cancer cells (PC3), osteosarcoma cells (SaOS), chondrocytes, human microvascular endothelial cells (HMEC-1), and mouse osteoblastic cell line (MC3T3) were a gift from Dr. Beate Lanske, Harvard Medical School, Boston.

2. METHODS

2.1 DNA- and RNA- preparation

2.1.1 DNA extraction from blood

DNA was extracted from (EDTA)-whole blood following a modified protocol from Miller *et al.* from peripheral blood leukocytes (Miller *et al.* 1988). (EDTA)-Whole blood (5-10 ml) was mixed with 40-45 ml lysis buffer. Erythrocytes were lysed and separated from the leukocytes after a centrifugation step (300 x g, 10 min, 10°C). Overnight incubation at 37°C with 5 ml SE-buffer, 25 µl pronase E (20 mg/ml) and 250 ml 20% SDS, dissociated nucleate cells. Following addition of 2-3 ml 5 M NaCl, intensive vortex and centrifugation at 1300 x g for 10 min at RT, achieved protein precipitation. The DNA-containing supernatant was transferred into a clean tube and two volumes of absolute ethanol were added for DNA precipitation. Precipitated DNA was washed once with 70% ethanol, dried and diluted in 100-1000 µl TE-buffer. DNA-concentrations were measured with the SYBR-green I method (Molecular Probes) in a GENios micro plate reader (Tecan).

Lysis buffer: 155 mM NH₄Cl, 10 mM KHCO₃, 0.1 mM EDTA up to 1 l dH₂O (pH 7.4)

SE-Puffer: 75 mM NaCl, 25 mM EDTA, pH 8 (NaOH)
TE-Puffer: 10 mM Tris-HCl (pH 8), 1 mM EDTA

2.1.2 RNA extraction from cells

RNA isolation was achieved by using the TRIZOL reagent (Gibco BRL) following the instructions supplied by the manufacturer. The reagent, a mono-phased solution of phenol and guanidine isothiocyanate, allows a single step isolation method developed by Chomezynski and Sacchi (Chomezynski and Sacchi 1987). Confluent cells growing in a small cell culture flask (25 cm²) were collected and mixed with 1 ml TRIZOL reagent.

Addition of chloroform (0.2 ml/1 ml TRIZOL) followed by centrifugation (12000 x g, 10 min, 4 °C), separates the solution into an aqueous phase and an organic phase. RNA remains exclusively in the aqueous phase. After transfer of the aqueous phase into a clean 1.5 ml reaction tube, the RNA was recovered by precipitation with isopropyl alcohol (0.5 ml/1 ml TRIZOL) and centrifugation at 12000 x g for 5 min at 4°C. RNA pellet was washed with 75% ethanol, centrifuged (7500 x g, 5 min, 4°C) and briefly dried. The prepared RNA can be stored in 75 % ethanol for one year or in DEPC-H₂O for 4 weeks at 20°C.

To prove RNA quality and quantity, an aliquot of isolated RNA (1-2 µl) was analysed by electrophoreses in a 0.7% agarose gel and viewed under a 300 nm UV light illuminator. RNA concentration was measured in a photometer under an absorbance of 260 (1 OD₂₆₀ = 40 µg RNA/ml). The degree of purity from the isolated RNA measured at A₂₆₀₋₂₈₀ should be between 1.6-1.8.

DEPC-H₂O: 0.01% (v/v) DEPC in dH₂O, shake for 12 h at RT and autoclave

All substances, dilutions and materials must be RNase free. General precautions for preventing RNase contamination are found in Sambrook *et al.* (Sambrook *et al.* 1989).

2.2 Reverse transcription

The synthesis of first-strand cDNA from isolated RNA was performed using the 1st Strand cDNA Synthesis Kit (Pharmacia). The cDNA was generated from 1-5 µg of total RNA. RNA was mixed with RNase-free water to 8 µl end volume, denatured at 65°C for 10 min and then chilled on ice for 10 min. For reverse transcription, 5 µl Bulk First-Strand cDNA

Reaction Mix, 1 µl DTT Solution, 1 µl NotI-d(T)₁₈ primer (1:25 dilution) were mixed with the heat-denatured RNA in a 1.5 ml reaction tube and incubated at 37°C for 1 h. The completed first-strand cDNA reaction product is ready for immediate second-strand cDNA synthesis or PCR amplification.

2.3 Polymerase chain reaction (PCR)

2.3.1 Standard PCR

PCR was established following the standard Saiki method (Saiki *et al.*, 1988). Amplification protocols and reaction mixture conditions were optimized depending on the original DNA template (genomic DNA, cDNA, recombinant plasmid). Oligonucleotide primer pairs are detailed in section 1.2.3. Negative controls were always used and positive controls if required. For 50-100 ng genomic DNA template or 10-50 ng cDNA template, the reaction mixture consists of 50 µl with 1x PCR-buffer, 200 mM dNTPs, 40 pmol oligonucleotide primer (sense and antisense) and 0.5 U Taq-Polymerase (New England Biolabs). PCR reaction was performed in a thermal cycler (MJ Research PTC-225) with the following basic amplification program:

1. 94°C 5 min
2. 94°C 30 sec
3. (*)°C 30 sec
4. 72°C (**)
sec
5. 72°C 5 min

The amplification stage comprises of 30 cycles from step 2 to 4. The annealing temperature of the primers (*) depends on the composition of them and the time required for primer extension (**) is directly related to the length of the desired PCR product.

PCR-Buffer 10x: 750 mM Tris-HCl (pH 9), 200 mM (NH₄)SO₄, 25 mM MgCl₂,
0.1% Tween 20

2.3.2 RT-PCR and RT-“nested”-PCR

The amplification of a specific cDNA resulted from performing RT-PCR using 10 ng of first strand cDNA obtained by reverse transcription of isolated RNA (see section 2.2) or from supplied cDNA (see section 1.1.2). Depending on the expression level of the gene, a second “nested”-PCR can be attached to the RT-PCR. The template for the second round is

the product obtained in the RT-PCR. The primer pairs for the “nested”-PCR are located within the first RT-PCR amplified cDNA sequence. Primer pairs are described in section 1.2.3. To avoid polymerase mistakes for later expression experiments, 0.2 U of a proofreading Vent-Polymerase were added to the standard PCR reaction mixture.

2.3.3 Multiplex RT-PCR

For semiquantitative analysis of the expression level of a certain gene in a tissue or cell line of interest, multiplex RT-PCR was performed using 10 ng of first cDNA obtained by reverse transcription from isolated RNA (see section 2.2) as template. Two pairs of primers were used in the same PCR reaction. One pair of primers was used for amplification of the gene of interest and a second pair was used for amplification of the *GAPDH* gene as an internal control. PCR Advantage Kit (Clontech) was used with the following amplification program: 95°C for 8 min, 95°C for 45 sec, (*)°C for 30 sec and 72°C for 30 sec during 35 cycles and 72°C for 10 min. Primers and annealing temperature are detailed in section 1.2.3. Two specific PCR products for every reaction are expected to be viewed in a 2% agarose gel after electrophoresis (see section 2.6.1).

2.4 Site-Directed mutagenesis

To construct expression vectors for the FGF23-R176Q, -R179Q, -S71G mutant proteins and the secreted form of the PHEX protein (secPHEX), *in vitro* site-directed mutagenesis was accomplished using the QuikChangeXL Site-Directed mutagenesis kit (Stratagene).

Full-length *FGF23* and *PHEX* plasmids previously cloned in pBluescript SK +/- (Stratagene) were used as templates for amplification with the mutagenesis oligonucleotide primers containing the desired mutation. Mutagenesis primers (see section 1.2.3) were designed considering the manufacturer's recommendations. PCR amplification was performed using *Pfu Turbo* DNA polymerase following the manufacturer's protocol and XL10-Gold Ultra competent cells were transformed.

2.5 DNA Sequencing

Automated DNA sequencing was performed in a capillary-based automated sequencer, (ABI Prism 3100 Genetic Analyser, Applied Biosystems), after a cycle-sequence reaction

using the BigDye-Terminator v3.1 Cycle Sequencing Kit (Applied Biosystems). The BigDye-Terminator sequencing conditions depend on the type of template. For a plasmid-DNA template, 100 ng of purified double-stranded DNA were mixed with 0,5 μ l BigDye-Terminator mix version 3.1, 1 μ l buffer, 1 μ l primer (0.20 pmol/ μ l) and dH₂O up to 5 μ l end volume reaction. The cycling program consists of 25 cycles: 10 sec 96°C, 5 sec 50°C, 4 min 60°C.

After the cycle-sequence reaction, the DNA was precipitated in 13 μ l 100% ethanol, incubated for 10 min and centrifuged (3000 x g, 30 min, RT). The pellet was washed in 20 μ l 70% ethanol in DHPLC-H₂O (LiChrosolv, Merck), vortexed for 1 min and centrifuged (2000 x g, 15 min, RT). The DNA pellet was dried at RT and dissolved in 50 μ l DHPLC-H₂O. Dissolved DNA (25 μ l) was transferred onto a microtiter plate, which was placed into the automated sequencer. The resulting data were collected and analysed using the Staden Package (see section 3.2).

2.6 Electrophoresis

2.6.1 Agarose gel electrophoresis

Electrophoresis through 0.7-1.5% horizontal agarose gels was used to separate, identify, and purify DNA fragments. The 6-7 mm thick gel consists of 1x TBE-agarose with 0.2 μ g/ml ethidium bromide in 1x TBE buffer. The concentration of agarose in the electrophoresis buffer must be appropriate to separate the particular size fragments under a migration rate of 1.5 V/cm for 30 min. A DNA, 1 kb-ladder standard (BRL *Gibco*) was used to interpret the results, viewed under a 300 nm UV light transilluminator.

10x TBE-buffer: 840 mM Tris, 900 mM boric acid, 20 mM EDTA, dH₂O up to 1 l (pH 8)
Ethidium bromide: 10 mg/ml stock
Gel-loading buffer: 0.05% (w/v) orange G or bromophenol blue in 25% (w/v) Ficoll

2.6.2 Polyacrylamide Gel Electrophoresis

Analytical electrophoresis for the separation of proteins was carried out in discontinuous sodium dodecyl sulfate polyacrylamide gels (SDS-PAGE). Denatured polypeptides bind SDS detergent in a ratio of 1:4 g SDS/g protein and become negatively charged because of the high negative density charge of SDS. As the amount of SDS bound is almost always

proportional to the molecular weight of the polypeptide and is independent of its sequence, SDS-polypeptide complexes separate by sieving through the gel according to size.

2.6.2.1 Preparation of the mini gels

Minigels with 0.75 mm of thickness were cast in the Mini-PROTEAN 3 Multi-Casting Chamber (Bio-Rad) following the instructions manual. The gel monomer solution was prepared with an Acrylamid/Bisacrylamid 30% v/w solution (SERVA Water-saturated isobutanol was used as overlaying solution. Polymerisation time was 30 min. Mini gels can be packed in a plastic foil and stored at 4°C for one week.

The analysis of small proteins and polypeptides requires a buffer system and acrylamide percentages especially suited to small molecules. Ready Gel precast 16.5% Tris-tricine gels (Bio-Rad) were used for the separation of peptides and small proteins with molecular weights as low as 1 kDa.

Tab. 9. Solutions for preparing tris-glycine SDS-PAGE resolving gels (7.5%, 10%, 12%, and 15%) and stacking gel (4%).

	7.5 %	10 %	12 %	15 %	4 %
Ultra pure H₂O	29 ml	24 ml	20 ml	14 ml	18.3 ml
1.5 M Tris/HCl pH 8.8	15 ml	15 ml	15 ml	15 ml	7.5 ml
PROTOGEL	15 ml	20 ml	24 ml	30 ml	4.0 ml
SDS (10%)	0.6 ml	0.6 ml	0.6 ml	0.6 ml	0.3 ml
TEMED	60 µl	60 µl	60 µl	60 µl	30 µl
APS (10%)	300 µl	300 µl	300 µl	300 µl	150 µl

2.6.2.2 Electrophoresis

Hand cast gels and Ready Gel precast gels were assembled in a Mini-PROTEAN 3 Cell running chamber and filled with running buffer following the manufacturer's instructions. Tris/glycine/SDS or Tris/tricine/SDS were used as running buffer systems. Protein samples were treated with Laemmli sample buffer or Tricine sample buffer in a 1:1 ratio, boiled at 95°C for 5 min and loaded into the wells of the gel. For the analysis of membrane proteins, protein samples were heated to 40°C for 5 min. The electrophoresis was run constant at 120 V until the bromophenol blue reached the edge of the gel. Kaleidoscope Prestained and Dual Color Prestained Precision Plus protein standards (Bio-Rad) were used for the determination of the molecular mass.

Tris/glycine/SDS buffer:	250 mM Tris, 1.92 M Glycine, 1% SDS, dH ₂ O up to 1 l
Tris/tricine/SDS buffer:	100 mM Tris, 100 mM Tricine, 0.1% SDS, dH ₂ O up to 1 l (pH 8.3)
Laemmli sample buffer:	4% SDS, 50 mM Tris/HCl pH 6.8, 10% β-mercaptoethanol, 20% glycerol, 0.2% bromophenol blue
Tricine sample buffer:	20% SDS, 50 mM Tris/HCl pH 6.8, 20% β-mercaptoethanol, 50% glycerol, 0.2% bromophenol blue

2.6.2.3 Drying SDS-PAGE

Mini-gels were dried using a mini gel drying system (Novex) following the manufacturer's instructions. Gels were immersed in drying solution for 20 min with gentle shaking and dried for 24 h at RT.

Gel drying solution: 20% methanol, 2% glycerol in dH₂O

2.6.3 Western blot

Electrophoretic transfer of proteins from polyacrylamide gels to a polyvinylidene fluoride (PVDF) membrane was performed using the mini Trans-Blot Electrophoretic Transfer Cell (Bio-Rad). PVDF membranes manifest a strong interfacial (hydrophobic) interaction with proteins with a capacity of 170 μg protein/cm². After gel electrophoresis, the gel was equilibrated for 15 min in pre-chilled transfer buffer. PVDF membrane (PALL Life Sciences) was moistened in methanol and soaked in transfer buffer together with two filter paper sheets and the fibre pads. Gel sandwich was prepared in the cassette following the instructions manual. Electrophoresis was performed at 100 mA for 1 h at 4°C. Upon completion of the run, the membrane was stained with Ponceau S (see section 2.12.3). The Detection of proteins in a PVDF membrane accomplished by using antibodies (see section 2.13.1).

Transfer buffer: 12 mM Tris, 96 mM glycine, 20% methanol in dH₂O

2.7 DNA cloning

Full-length *FGF23* and *PHEX* cDNAs, previously cloned in our laboratory into pBluescript SK +/-, were used as template for further directional cloning into different expression vector systems, depending on the purposes of the experiments. When needed,

insert DNA was amplified by PCR using pairs of oligonucleotide primers including cloning restriction sites to generate amplified segments of insert with cohesive ends. PCR products were enzymatically digested and directionally ligated into an expression vector system. pMAL-c2TM vector (New England BioLabs) was used for expression in a bacterial system and pcDNA3.1/*myc*-His version B (Invitrogen) vector was used for expression in eukaryotic cells.

2.7.1 DNA digestion

Target cDNA (1-10 µg), plasmid or plasmid-DNA was digested for 2 h with the appropriate restriction enzymes before cloning into the expression vector. The amount of endonuclease used depends on the µg of substrate to be digested; 1 U of restriction endonuclease digests 1 µg DNA in 1 h. The manufacturer specifies the reaction buffer and the optimum temperature for the digestion. At the end of the digestion, restricted DNA was viewed in an agarose gel and purified.

2.7.2 DNA ligation

For ligation of cohesive ends was used at a ratio of 3:1. Ligation mixture was set up in a 0.5 µl reaction tube: 1x T4-DNA ligation buffer and 5 U T4-DNA ligase were mixed with the corresponding amounts of insert and vector in a total volume of 10 µl. Samples were incubated overnight in a water bath at 15°C.

2.7.3 Preparation of competent *E. coli* using the CaCl₂ method

A single bacterial colony (*E. coli* XL1-Blue, Stratagene) for the competent bacterial line was transferred into a culture tube with 3 ml TYM/MgCl₂ medium and cultured overnight at 37°C. A part of this culture was diluted to 1:200 and incubated again for 3 to 4 hours at 37°C with vigorous agitation. The growth of the culture was monitored every 20 min until the OD₆₀₀ reached 0.9. The culture tube was chilled on ice for 10 min and the cells were recovered by centrifugation (3000 x g, 10 min, 4°C). Cell pellet was then resuspended by gentle vortex in 15 ml of chilled Tfb-I solution and centrifuged at 3000 x g for 8 min at 4°C. The cell pellet was again resuspended in 4 ml chilled Tfb-II solution, divided into 100 µl fractions and preserved at -70°C. The transformation efficiency of the competent cells can be controlled by transforming 1 µg circular plasmid-DNA which should yield 1x10⁶ to 1x10⁷ single colonies.

TYM /MgCl ₂ :	20 g tryptone, 10 g yeast extract, 5.88 g NaCl, dH ₂ O up to 1 l. Autoclave and add 1M MgCl ₂ to 10 mM end concentration.
Tfb-I solution:	30 mM K-Acetate, 50 mM MgCl ₂ , 100 mM KCl, 10 mM CaCl ₂ , 15% glycerol
Tfb-II solution:	10 mM Na-MOPS pH 7, 75 mM CaCl ₂ , 10 mM KCl, 15% glycerol

2.7.4 DNA transformation

For transformation, 100 µl *E. coli* XL1-blue competent cells were thawed on ice, mixed with 10 µl ligation reaction and incubated for 20 min on ice. Tubes were then transferred into a preheated 42°C circulating water bath for exactly 45 sec, and chilled on ice for 2 min. 900 µl TYM/MgCl₂ medium were added into each sample tube and incubated for 1 h at 37°C with vigorous agitation. Cells were recovered by centrifugation (1000 x g, 2 min, RT) and 5 - 50 µl of the bacterial suspension were plated onto LB/agar culture dishes with 50-100 µg ampicillin/ml. Cultured plates were incubated at 37°C in an incubator overnight.

LB-medium:	10 g tryptone, 5 g yeast extract, 10 g NaCl, dH ₂ O up to 1 l
LB/agar:	LB-medium with 1.5% agar
Ampicillin:	50 mg/ml stock solution

2.7.5 Preparation of recombinant plasmid-DNA

Single *E. coli* transformed colonies were transferred from the LB/agar cultured plates into 5 ml LB medium with antibiotic and incubated overnight at 37°C with vigorous agitation. After incubation, one aliquot of the bacterial culture was mixed with an equal volume of glycerol and stored at -70°C as bacterial stock. The rest of the cells were recovered by centrifugation (1000 x g, 10 min, RT). For the plasmid-DNA preparation the QIAprep Spin Plasmid Miniprep Kit (Qiagen) was used following the manufacturer's standard protocol.

2.8 Protein expression

2.8.1 Expression in a prokaryotic system

Expression of genes in *E. coli* was performed using the pMALTM Protein Fusion & Purification System (New England BioLabs) following the manufacturer's instructions. The gene of interest was cloned into a pMAL-c2 vector (see section 2.7) downstream from the malE gene, in frame with an encoded maltose-binding protein (MBP). This technique

uses an IPTG-inducible promoter and the translation initiation signals of MBP to express large amounts of fusion protein. Purification of the recombinant protein was performed in an amylose resin column (New England BioLabs) following the manufacturer's instructions. Purified protein was visualized after SDS-PAGE by Coomassie staining (see sections 2.6.2 and 2.12.1). Quantification of the purified fractions was achieved with the Protein 200 Assay in an Agilent 2100 Bioanalyser (Agilent Technologies) (see section 2.11.1). Fusion protein was cleaved with Factor Xa following the recommendations of the manufacturer. Results were visualized after SDS-PAGE by Coomassie staining and after western blot (see section 2.6.3) by using anti-MBP monoclonal antibody (New England BioLabs) and antiFGF23₂₀₇₋₂₂₂ polyclonal antibody (see table 8).

2.8.2 Expression in an eukaryotic system

The transfer of DNA into eukaryotic cells was accomplished with a stable transfection approach to establish clonal cell lines in which the transfected target gene is integrated into chromosomal DNA, from where it directs the synthesis of the target protein.

Human embryonic kidney cells (HEK293) were maintained on cell culture medium. Cells were stable transfected with empty pcDNA3.1 vector or vector expressing native FGF23, tagged FGF23 (FLAG/FGF23 and FGF23/His), mutant FGF23 (FGF23-R176Q, FGF23-R179Q and FGF23-S71G), as well as native PHEX, His-tagged PHEX and secPHEX recombinant proteins using EffecteneTM transfection reagent (QIAGEN, GmbH). This is a lipid-mediated transfection method (Felgner *et al.* 1994), based on the formation of artificial membrane vesicles (liposomes) that bind DNA molecules. The resulting liposomes adhere to and fuse with the negatively charged cell membrane. Following selection with 1000 µg/ml G418 (Calbiochem, GmbH) during four weeks, single colonies were plated in 24-well plates. When colonies had grown, they were transferred to culture flasks and the G418 concentration was reduced to 100 µg/ml. Integration and expression of the plasmid was examined by multiplex RT-PCR as described in section 2.3.3.

Cell culture medium: RPMI 1640 (1x) with HEPES medium, 10% FCS, 50 IU/ml penicillin and 50 µg/ml streptomycin. Add 100 µg/ml G418.

2.9 Cell culture

2.9.1 Preparation of conditioned medium

Confluent cells growing into a 75 mm² culture flask were washed once with PBS (PAA Laboratories, GmbH) and cultured overnight with 20 ml serum-free medium at 37°C in a humidified atmosphere of 5% CO₂/95% air. Conditioned medium was collected and concentrated 1:20 with Macrosep-omega 10K concentrators (PALL Life Sciences) (4500 x g, 120 min, 4°C). Protein content from the conditioned medium was examined after SDS-PAGE (12% gels for FGF23 and 7.5% gels for PHEX) by western blot analysis (see sections 2.6 and 2.13.1). Protein concentrations were determined using the Bradford protein assay (see section 2.11.2).

Serum-free medium: RPMI 1640 (1x) with HEPES medium, 50 IU/ml penicillin and 50 µg/ml streptomycin. Add 100 µg/ml G418.

2.9.2 Preparation of cells

Cells growing in a culture flask were collected and washed once with PBS. After recovering the cells by centrifugation at 500 x g for 2 min, pellets were lysed in 300 µl to 1000 µl of lysis buffer. A fraction of the cell lysate (100 µl) were mixed with 100 µl 5x Laemmli sample buffer and boiled for 5 min at 95°C. The protein content of the cells was examined after SDS-PAGE (12% gels for FGF23 and 7.5% gels for PHEX) by western blot analysis (see section 2.6).

Lysis buffer: 100 mM Tris, 1% SDS

Laemmli sample buffer: 4% SDS, 50 mM Tris/HCl pH 6.8, 10% β-mercaptoethanol, 20% glycerol, 0.2% bromophenol blue

2.9.3 Treatment with inhibitors

2.9.3.1 Inhibition of SPCs activity

HEK293 cells expressing native FGF23 were transferred into a 6-well culture plate (10⁴ cells/well) and cultured in cell culture medium (see section 2.8.2). Cells were washed once with PBS and cultured overnight with 1.5 ml serum-free medium (see section 2.9.1) in the presence of 0 µM, 0.13 µM, 1.3 µM, 13 µM, 26 µM and 39/52 µM concentrations of decanoyl-Arg-Val-Lys-Arg-chloromethyl ketone (Dec-RVKR-CMK) (BIOMOL Research

Laboratories), a specific inhibitor of SPC proteases. Conditioned medium was collected and concentrated to 100 μ l using a Microsep-omega 10K concentrator (PALL Life Sciences) by centrifugation at 4500 x g for 30 min at 4°C. Samples were analysed by SDS-PAGE and western blot (see section 2.6).

2.9.3.2 Inhibition of secPHEX activity

Different inhibitors, 1 mM EDTA, complete EDTA-plus protease inhibitor cocktail (Roche Diagnostics), complete EDTA-free protease inhibitor cocktail (Roche Diagnostics) or 1 mM Dec-RVKR-CMK (BIOMOL Research Laboratories) were handled following the manufacturer's instructions. Reaction samples were incubated with the inhibitors 15 min at RT before the addition of substrates. Following substrate addition, samples were then incubated at 37°C for 30 min. After incubation, 3 μ g of protein reaction sample were separated through SDS-PAGE and analysed by Silver staining (see section 2.12.2).

2.9.4 Treatment with glycosidases

2.9.4.1 N-glycosylation assay

Protein-containing conditioned medium (3 μ g) from HEK293 cells expressing native FGF23 and 1 μ g RNase B (Sigma) as assay control were mixed with glycosidases, PNGase F or Endo H, according to the manufacturer's protocol (New England BioLabs). Reaction mixtures were incubated for 1 h at 37°C.

2.9.4.2 O-glycosylation assay

Protein-containing conditioned medium (3 μ g) from HEK293 cells expressing native FGF23 and 1 μ g bovine fetuin (Sigma) as control were mixed with 4 mU neuraminidase type X (Sigma) in the presence of 20 mM phosphate buffer pH 6.5 and 0.2% BSA for 3 h at 37°C in a total volume of 25 μ l. After incubation, 2 mU O-glycosidase (Roche) were added to the reaction mixture and further incubated for 16 h at 37°C.

Reactions were stopped after incubation with 5x Laemmli sample buffer. Reaction products were analysed after SDS-PAGE by Coomassie staining or western blot analysis (see sections 2.6 and 2.12.1).

2.10 Protein purification

2.10.1 FGF23/His purification

Polyhistidine tracts bind tightly to a number of transition metals and transition metal chelate complexes. A protein carrying an exposed His-6 region will bind to a resin charged with divalent nickel ions. Contaminating proteins can be removed with appropriate washing, and a soluble competing chelator can then elute the protein of interest. To purify His-tagged FGF23, conditioned medium of HEK293 cells expressing FGF23/His protein was collected and concentrated 1:20 with Macrosep-omega 10K concentrators at 4°C. Concentrated conditioned medium was loaded onto a Ni-NTA spin column (QIAGEN) and FGF23/His protein was purified in a one-step procedure under native conditions by increasing the concentration of imidazole (20 mM – 250 mM) in the wash and elution buffers, following the manufacturer's instructions (QIAGEN). Fractions were analysed after SDS-PAGE by Silver staining (see section 2.12.2). The fraction containing pure FGF23/His was dialysed against PBS. Protein concentrations were determined by the Bradford method (see section 2.11.2).

2.11 Protein quantification

2.11.1 Agilent protein assay

Absolute quantification of protein from collected sample fractions after purification (see section 2.8.1) was performed with the help of an Agilent 2100 Bio analyser using the Protein 200 LabChip Kit (Agilent Technologies). The kit allows sizing and quantification of proteins ranging in size from 14 to 200 kDa. The Agilent 2100 Bio analyser detection is based on laser-induced fluorescence of an intercalating dye, which interacts with the protein/SDS complexes. Absolute quantification is enabled in combination with protein standards of known concentrations. Samples were mixed with the corresponding reagents following the manufacturer's instructions and colorimetric change was read in the analyser.

2.11.2 Bradford method

The Bradford method (Bradford 1976) was used to quantify the concentration of proteins in solution. The method consists of a dye-binding assay based on the differential color change of the dye Coomassie Brilliant Blue G-250 in response to various concentrations of protein. When binding to protein occurs, the dye stabilizes from a doubly-protonated red

form to a unprotonated blue form so the maximum absorbance of the acidic solution of Coomassie Brilliant Blue G-250 shifts from 465 nm to 595 nm. The Bradford assay has a high sensitivity (0.05 µg protein/ml). The Bio-Rad Protein Assay Kit I (Bio-Rad) was used for the Bradford assay following the manufacturer's instructions. 1 volume of Dye Reagent Concentrate was diluted with 4 volumes of ultra pure dH₂O. 990 µl of the diluted reagent were mixed with 10 µl of the protein sample and incubated for at least 5 min at RT. Sample buffer (10 µl) was used as blank value. Absorption was measured at 595 nm. A regression curve with a protein standard (BSA, 0.1-10 mg/ml) was set up to help the quantification of the results.

2.12 Protein staining

2.12.1 Colloidal Coomassie staining

The Colloidal Blue staining method described by Neuhoff (Neuhoff *et al.* 1988) is based on the colloidal properties of Coomassie Blue dyes. The free dye in solution is greatly reduced due to the hydrophobic effect, resulting in low background staining and high affinity binding of the dye to the proteins fixed in the gel, so proteins can be viewed as discrete blue bands. Colloidal Coomassie provides nanogram-level detection of proteins. The absorption of dye is approximately proportional to the amount of protein. After separation of the proteins by SDS-PAGE as described in section 2.6.2, gels were fixed on a rotating platform at low speed with 100 ml of solution A for 3 x 10 min. Following a rinse in solution B for 2 x 10 min, gels were incubated in solution C. After 10 min of shaking, 2% staining solution was added and incubated overnight. To remove some possible background after incubation, gels were immersed in dH₂O for 10 min. To make a permanent record, stained gels were scanned and dried as described in section 2.6.2.

Solution A: 30% ethanol, 2% orthophosphoric acid in dH₂O
Solution B: 2% orthophosphoric acid in dH₂O
Solution C: 2% phosphoric acid, 18% ethanol and 15% (NH₄)₂SO₄ in dH₂O
Staining solution: 2 g Coomassie G-250 in 100 ml hot dH₂O

2.12.2 Silver staining

Proteins were stained with silver nitrate following a modified procedure from the originally devised by Sammons *et al.* (Sammons *et al.* 1981). Silver staining allows detection

between 0.1-1.0 ng of polypeptide in a single band. The identification of proteins by silver staining is based on the differential reduction of silver ions that are bound to the side chains of amino acids. After separation of the proteins by SDS-PAGE (see section 2.6.2), the gel was immersed in fixing solution for 2 x 15 min on a rotating shaker at low speed. Following washing with 50% ethanol for 3 x 10 min and rinsing with sensitizer for 20 sec, gels were incubated in the silver nitrate solution for 15 min with gentle shaking. Silver nitrate solution was discarded and the gel was washed with ultra pure H₂O for 20 sec each. The gel was placed in developing solution until the stained bands of protein appeared. The reaction was stopped by washing the gel for 10 min in stopping solution. Stained gels were scanned and dried (see section 2.6.2).

Fixing solution:	50% methanol, 12% acetic acid and 500 µl/l formaldehyde 37% ultra pure H ₂ O
Washing solution:	50% ethanol in ultra pure H ₂ O
Sensitizer:	200 mg/l Na ₂ S ₂ O ₃ in ultra pure H ₂ O
Silver nitrate solution:	2 g/l AgNO ₃ , 750 µl/l formaldehyde 37% in ultra pure H ₂ O
Developing solution:	60 g/l Na ₂ CO ₃ , 5 mg/l Na ₂ S ₂ O ₃ and 500µl/l formaldehyde 37% in ultra pure H ₂ O
Stopping solution:	50% methanol, 12% acetic acid in ultra pure H ₂ O

2.12.3 Ponceau S

To confirm the transfer of proteins after western blotting, the entire area of the PVDF membranes were stained with the removable and insensitive stain Ponceau S (Muilerman *et al.* 1982, Salinovich and Montelaro 1986). Membranes were incubated for 3 min in a Ponceau S (Merck) staining solution followed by 3 min fading in 50 ml fading solution.

Ponceau S staining solution:	0.5 g Ponceau S, 1% acetic acid in dH ₂ O
Fading solution:	10% acetic acid, 50% methanol in dH ₂ O

2.13 Protein detection

2.13.1 Immunoblot

Proteins covalently bonded to a PVDF membrane can be detected with the help of antibodies. Membranes were pre-wetted in methanol and equilibrated for 5 min with 1x

PBS. Unreacted binding sites of the membrane were blocked in blocking solution for 1 h, to suppress non-specific adsorption of antibodies. After washing with 1x PBS/0.1% Tween 20 (1 x 15 min and 2 x 5 min), immobilized proteins were incubated for 2 h with a specific polyclonal antibody diluted in blocking solution. Antibodies are detailed in section 1.2.4. Membranes were again washed and incubated with a secondary Goat Anti-rabbit IgG (H+L) –HRP antibody (Bio-Rad) diluted 1:5000 in blocking solution, followed by washing (1 x 15 min and 2 x 5 min). Incubations were performed at RT on a rotator shaker. Antigen-antibody complexes were viewed by chemiluminescent reactions with ECL plus reagent (Amersham Biosciences) following the manufacturer's instructions and signals were developed with a WicoRex X-Ray film (Typon Medical Systems).

10x PBS: 80 g NaCl, 2 g KCl, 14.4 g Na₂HPO₄, 2.4 g KH₂PO₄ add dH₂O to 1 l. Adjust pH to 7.4 with HCl and autoclave

Blocking solution: 0.5% low-fat dry milk in 1 x PBS, 0.1% Tween 20

Washing solution: 1 x PBS, 0.1% Tween 20

2.13.2 Immunocytochemistry

HEK293 cells stable expressing mutant FGF23-S71G protein, native FGF23, and control HEK293 cells were cultured in culture medium (see section 2.8.2) on coated 8 chamber slides (Nunc) for 48 h. Cells were fixed in 4% paraformaldehyd for 15 min at room temperature, washed with PBS and permeabilized for 30 min followed by blocking for 30 min at 37°C. The primary antibody antiFGF23₁₄₈₋₁₆₃ against an N-terminal peptide was diluted to a concentration of 2.5 µg/ml, anti-calnexin [AF18] (Abcam), anti-Lamp1 [LY1C6] (Abcam) antibodies, monoclonal antibody against human mitochondria (Chemicon), and wheat germ agglutinin (WGA) Alexa Fluor 594 conjugate (Molecular Probes) were diluted in the blocking solution as recommended by the manufacturer and incubated for 1 h at 37°C. Slides were washed in PBS, 0.1% Igepal 3 times for 10 min. The same incubation and washing procedures were used for the secondary antibodies anti-rabbit Alexa fluor 350 nm and anti-mouse Alexa fluor 568 nm (Invitrogen) diluted 1:1000 in the blocking solution. Preparations were viewed using an ApoTome Microscope (Zeiss) and images were processed by using the AxioVision LE software (see section 3.2).

2.13.3 Enzyme-Linked Immunosorbent Assay (ELISA)

Determination of human FGF23 levels in plasma were measured by using a 2-site enzyme-

linked immunosorbent assay (Immutopics). The assay is based on the detection of FGF23 by binding to two antibodies directed against epitopes within the carboxyl terminal portion of FGF23. One antibody is immobilized onto a microtiter plate well to capture FGF23, and the second antibody conjugated to biotin is used to generate a signal with avidin-horseradish peroxidase. The enzymatic activity of the antibody bound to the protein is directly proportional to the amount of intact FGF23 in the sample.

Plasma was obtained after centrifugation (2500 x g for 10 min at RT) and separation of 10 ml EDTA-blood. Assay procedure was performed following the manufacturer's instructions. Absorbance was measured in a Synergy HT Multi Detection Microplate Reader (Synergy).

3. DATABASES AND COMPUTER PROGRAMMS

3.1 Databases

GenBank	http://www.ncbi.nlm.nih.gov/Genbank/index.html
NCBI	http://www.ncbi.nlm.nih.gov/
OMIM	http://www.ncbi.nlm.nih.gov/entrez/query.fcgi?db=OMIM&cmd=Limits
PubMed	http://www.ncbi.nlm.nih.gov/entrez/query.fcgi
Swiss-Prot	http://us.expasy.org/sprot/

3.2 Analysis tools and software packages

ExPASy	http://www.expasy.org/
Genome Browser	http://genome.ucsc.edu/
ImageJ Quantification	http://rsb.info.nih.gov/ij
AxioVision LE	http://www.zeiss.de/
Exon Primer	at the Genome Browser web page
PeptideMass	at the ExPASy web page
Tblastn	at the NCBI web page
Genewise	at the NCBI web page
Staden	MCR Laboratory of Molecular Biology, Cambridge, UK
ClustalWHUSAR	Heidelberg Unix Sequence Analysis Resources
PrettyboxHUSAR	Heidelberg Unix Sequence Analysis Resources, DKFZ, Heidelberg, Germany

C. RESULTS

1. CHARACTERIZATION OF THE FGF23 PROTEIN

1.1 Description of the FGF23 amino acid sequence

The complete human *FGF23* cDNA consists of 756 nucleotides that encode an unprocessed precursor protein of 251 amino acids (Fig. 7). Residues 1 through 24 serve as signal peptide that allows efficient secretion of the mature protein. The unprocessed precursor protein is predicted to have a molecular weight of 27.9 kDa (Swiss-Prot accession number Q9GZV9).

1	ATG TTG GGG GCC CGC CTC AGG CTC TGG GTC TGT GCC TTG TGC AGC GTC TGC AGC ATG AGC GTC CTC AGA	
	M L G A R L R L W V C A L C S V C S M S V L R	23
70	GCC TAT CCC AAT GCC TCC CCA CTG CTC GGC TCC AGC TGG GGT GGC CTG ATC CAC CTG TAC ACA GCC ACA	
	A Y P N A S P L L G S S W G G L I H L Y T A T	46
139	GCC AGG AAC AGC TAC CAC CTG CAG ATC CAC AAG AAT GGC CAT GTG GAT GGC GCA CCC CAT CAG ACC ATC	
	A R N S Y H L Q I H K N G H V D G A P H Q T I	69
	antiFGF23 ₄₈₋₆₇ antibody	
208	TAC AGT GCC CTG ATG ATC AGA TCA GAG GAT GCT GGC TTT GTG GTG ATT ACA GGT GTG ATG AGC AGA AGA	
	Y S A L M I R S E D A G F V V I T G V M S R R	92
	*	
277	TAC CTC TGC ATG GAT TTC AGA GGC AAC ATT TTT GGA TCA AAC TAT TTC GAC CCG GAG AAC TGC AGG TTC	
	Y L C M D F R G N I F G S H Y F D P E N C R F	115
346	CAA CAC CAG ACG CTG GAA AAC GGG TAC GAC GTC TAC CAC TCT CCT CAG TAT CAC TTC CTG GTC AGT CTG	
	Q H Q T L E N G Y D V Y H S P Q Y H F L V S L	138
415	GGC CGG GCG AAG AGA GCC TTC CTG CCA GGC ATG AAC CCA CCC CCG TAC TCC CAG TTC CTG TCC CGG AGG	
	G R A K R A F L P G M N P P P Y S Q F L S R R	161
	antiFGF23 ₁₄₈₋₁₆₃ antibody	
484	AAC GAG ATC CCC CTA ATT CAC TTC AAC ACC CCC ATA CCA CGG CGG CAC ACC CGG AGC GCC GAG GAC GAC	
	N E I P L I H F N T P I P R R H T R S A E D D	184
	* * antiFGF23 ₁₇₃₋₁₈₇ antibody	
553	TCG GAG CGG GAC CCC CTG AAC GTG CTG AAG CCC CGG GCC CGG ATG ACC CCG GCC CCG GCC TCC TGT TCA	
	S E R D P L N V L K P R A R M T P A P A S C S	207
622	CAG GAG CTC CCG AGC GCC GAG GAC AAC AGC CCG ATG GGC AGT GAC CCA TTA GGG GTG GTC AGG GGC GGT	
	Q E L P S A E D N S P M A S D P L G V V R G G	230
	antiFGF23 ₂₀₇₋₂₂₂ antibody	
691	CGA GTG AAC ACG CAC GCT GGG GGA ACG GGC CCG GAA GGC TGC CGC CCC TTC GCC AAG TTC ATC TAG	
	R V N T H A G G T G P E G C R P F A K F I *	251

Fig. 7. Nucleotide and amino acid sequence of the *FGF23* gene. Numbers on the left side indicate the nucleotide position and on the right side the amino acid position. Amino acids coding for the signal peptide are shown in bold. Mutated FGF23 amino acids causing ADHR and FTC are indicated with an asterisk (*). Polyclonal antibodies (antiFGF23₄₈₋₆₇, antiFGF23₁₄₈₋₁₆₃, antiFGF23₁₇₃₋₁₈₇ and antiFGF23₂₀₇₋₂₂₂) directed against underlined peptides were designed and generated in rabbits.

All human FGF paralogs share a 12-stranded β -sheet structure. The β -sheets are arranged in 3 similar lobes around a central axis forming an anti-parallel β -barrel (Harmer et al. 2004). The β -sheets are generally well preserved and the crystal structures superimpose in these areas. The intervening loops are less well conserved. An overview of the FGF2 structure is shown in the introduction (Fig. 4). FGF23 shares 25-36% amino acid identity with the other members of the FGF family in the common core sequence and is most closely related to FGF15, FGF19 and FGF21. With 251 amino acids, FGF23 is, as yet, the largest FGF, characterized by a large carboxy-terminal part of the protein.

In order to show the FGF23 evolutionary conservation, alignment of FGF23 from several vertebrate species was generated using ClustalW and Prettybox. The *FGF23* sequence was determined in *Tetraodon nigroviridis*, and *Danio rerio* by nested RT-PCR or in *Gallus gallus*, *Xenopus tropicalis*, and *Fugu rubripes* by prediction from the corresponding draft genome assemblies using tblastn and Genewise. *Homo sapiens* (AAG09917), *Mus musculus* (AAG09916), and *Rattus norvegicus* (BAB84108) FGF23 sequences were obtained from GenBank.

Alignment of the sequences showed high conservation within the N-terminal β -barrel structure and considerably lower homology within the C-terminal part (Fig. 8). Mutations at two arginine residues (p.R176 and p.R179) cause ADHR and at a serine (p.S71) cause FTC. These residues are conserved in all species investigated except for p.R179 which is not conserved in *Fugu rubripes* (Fig. 8). The two arginines, separated by only two amino acids (176RHTR179), define a potential subtilisin-like proprotein convertase (SPC) consensus cleavage site (RXXR motif). Interestingly, within the peptide fragment C-terminal of the proprotein convertase cleavage site, the homology is divergent among classes and only highly conserved within mammals and fish. Of note, the *Xenopus tropicalis* genome assembly (version 2) contained a second FGF23 homologous sequence (56% identity, 70% similarity) missing the proprotein convertase cleavage site (RXXR). According to a three-dimensional protein structure of FGF23 generated by modeling the protein sequence onto the superimposed crystal structure of FGFs (Harmer et al. 2004), serine 71 (p.S71) is situated at the end of the loop between strand 3 and 4 of the β -barrel structure. Arginine 176 and 179 (p.R176, p.R179) are located outside of the conserved β -barrel structure and could not be modeled.

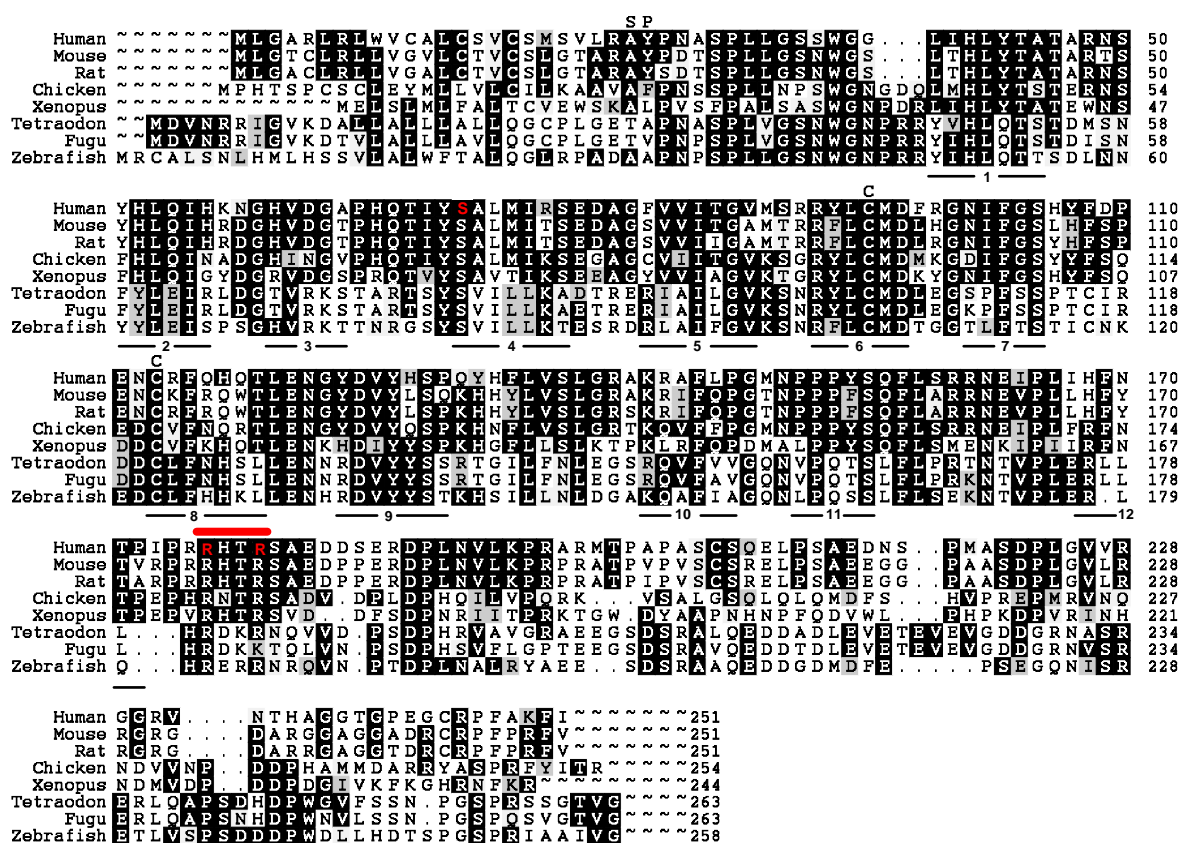


Fig. 8. Amino acid sequence alignment of FGF23. Human (AAG09917), mouse (AAG09916), rat (BAB84108), chicken, *Xenopus tropicalis*, *Fugu rubripes*, *Tetraodon nigroviridis*, and *Danio rerio* Fgf23 alignment was generated with ClustalW and Prettybox. Black and grey shadings represent identical and similar residues, respectively. The 12 β -strands that determine the core sequence are underlined. Within the N-terminal β -barrel structure the conservation is high between all species. Within the peptide fragment C-terminal of the proprotein convertase cleavage site, the homology is divergent among classes and only highly conserved among mammals and fishes. The p.S71 and the p.R176 sites (red) at which the p.S71G and p.R176Q mutations occurred are conserved in all species investigated. The p.R179 site (red) at which the p.R179Q or p.R179W mutations occurred is not conserved in *Fugu rubripes*. The signal peptide cleavage site is indicated by 'SP', the cysteines building a disulfide bond by 'C', and the proprotein convertase cleavage motif by a red bold line.

1.1.1 Expression analysis of FGF23 in human and mouse tissues

Total RNA was extracted from several human and mouse tissues or cell lines followed by reverse transcription to cDNA. All cDNA samples were checked by amplification with primers for the housekeeping gene *GAPDH* in order to confirm successful reverse transcription.

Nested RT-PCR analysis of RNA from human tissues with intron-spanning primers revealed an amplified FGF23 product in human whole fetus, heart, liver, thyroid/parathyroid, small intestine, testis, skeletal muscle, differentiated chondrocytes and

TIO tumor tissue. Fetal brain, fetal kidney, lung, brain, kidney, human osteosarcoma cells (SaOS), human embryonic 293 kidney cells (HEK293), prostate cancer cells (PC3), and human microvascular endothelial cells (HMEC-1) were negative. In mice, nested RT-PCR was positive in day 17 mouse embryo and spleen, but not in 12.5 mouse embryo, primary bone cell cultures from calvaria, limb bud cells, mouse osteoblastic cell line (MC3T3) and stimulated adult chondrocytes. Results are summarized in table 10.

Tab. 10. *FGF23* nested RT-PCR in human and mouse tissues and cell lines.

RT-PCR human	FGF23	RT-PCR mouse	Fgf 23
Whole fetus	yes	Embryo 12.5 days	no
Fetal brain	no	Embryo 17 days	yes
Fetal Kidney	no	Limb bud cells	no
Brain	no	Chondrocytes adult	no
Heart	yes	Bone calvaria	no
Small intestine	yes	MC3T3 osteoblasts	no
Kidney	no	Spleen	yes
Liver	yes		
Testis	yes		
Lung	no		
Skeletal muscle	yes		
Thyroid/parathyroid	yes		
TIO tumor tissue	yes		
Chondrocytes differentiated	yes		
Chondrocytes not differentiated	no		
PC3 prostate cancer cells	no		
HEK293 embryonic kidney cells	no		
HMEC-1 endothelial cells	no		
SaOS osteosarcoma cells	no		

1.2 FGF23 expression in *E.coli*

1.2.1 Generation of a prokaryotic FGF23 expression construct

A bacterial expression system was used to produce large amounts of FGF23 protein. The amplified *FGF23*-cDNA insert corresponding to amino acids 25-251 (*EcoRI/BamHI*) was directionally cloned into the pMAL-c2 expression vector. The pMAL-c2 vector encodes maltose-binding protein (MBP) followed by a polylinker sequence, serving as consensus cleavage site (IEGR) for a specific protease (Factor Xa) (Fig. 9). This construct results in the expression of a soluble N-terminal MBP-fusion protein with the possibility to release

the target protein from MBP by proteolytic cleavage after specific affinity chromatography purification.

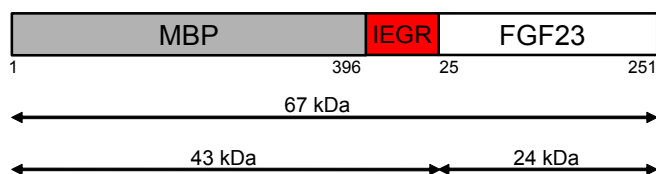


Fig. 9. MBP/FGF23 construct. Schematic representation of recombinant MBP/FGF23 fusion protein. Boxes represent recombinant MBP and FGF23 proteins linked by the consensus cleavage IEGR sequence (red). Numbers under the boxes indicate the amino acids constituting each protein. Numbers on the horizontal arrows indicate the molecular weight of MBP, FGF23 and MBP/FGF23 fusion protein calculated using the PeptideMass tool from the ExPASy proteomics server.

1.2.2 FGF23 expression and purification

E.coli XL-1 blue cells transformed with the *FGF23*pMAL construct were cultured and induced with IPTG to produce high amounts of MPB/FGF23 fusion protein. An aliquot of cells was collected before and after induction. Cells were lysed and 5 μ l of protein-containing cells were run through SDS-PAGE and stained with Coomassie. Results indicate that induced bacterial cells produced more fusion protein when compared with uninduced cells (Fig. 10 A).

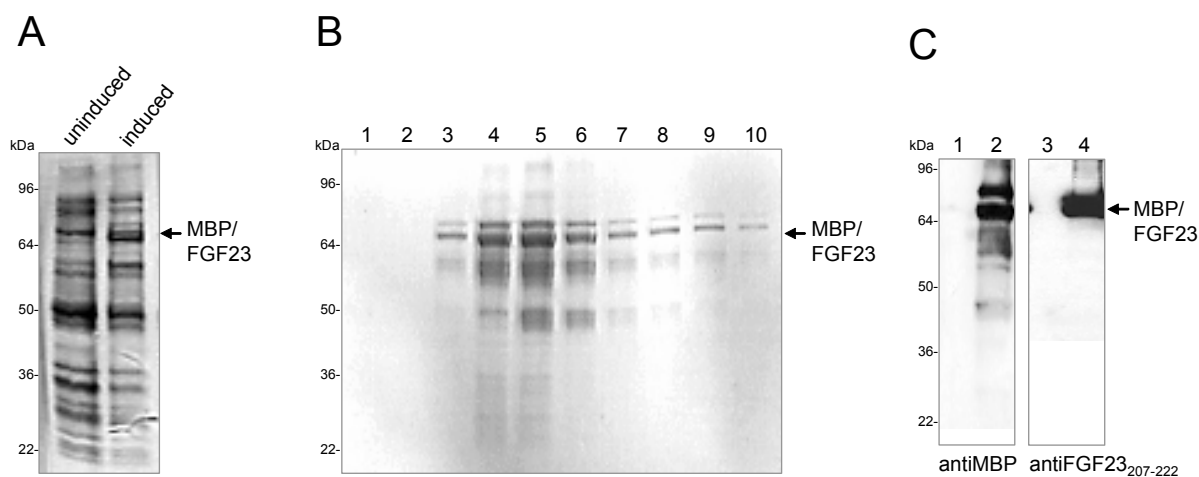


Fig. 10. MBP/FGF23 expression in *E.coli*. (A) Protein contained in bacterial cell lysate (5 μ l) from *FGF23*pMAL transformed *E.coli* cells before and after induction with IPTG and (B) elution fractions (5 μ l) from MBP/FGF23 affinity chromatography purification were analysed with Coomassie staining after 12% SDS-PAGE. A more intensive band around 67 kDa appeared after IPTG induction (induced). Purified protein mainly eluted between fractions 3 to 7 (lanes 3-7). (C) Protein (5 μ l) from elution fraction 5 and control elution were separated through 12% SDS-PAGE and analysed by western blot using anti-MBP or antiFGF23₂₀₇₋₂₂₂ antibodies. An immunoreactive band around 67 kDa was observed in the elution fraction 5 (lanes 2 and 4) whereas the control elution was negative (lanes 1 and 3). Molecular mass markers are indicated to the left.

Purification of MBP/FGF23 was performed by affinity chromatography through an amylose resin column. Bound material was eluted with maltose buffer and collected in 10 separated fractions. A major band of approximately 67 kDa, which corresponded to the expected molecular size of MBP/FGF23, mainly eluted between fractions 3 to 7. A Coomassie stained SDS-PAGE monitoring the 10-elution fractions is given in figure 10 B.

Protein-containing fraction 5 was analysed by western blot using specific anti-MBP and antiFGF23₂₀₇₋₂₂₂ antibodies and compared to control eluate. A prominent band was detected with both antibodies only in the eluate from *E.coli* cells transformed with MBP/FGF23. These results confirmed that the 67 kDa band observed with Coomassie staining was in fact MBP/FGF23 fusion protein (Fig. 10 C).

To quantify the amount of MBP/FGF23 present in the 10-elution fractions, protein samples were analysed with the help of an Agilent bioanalyser (Fig. 11). Absolute quantification yielded a MBP/FGF23 concentration of 29.4 $\mu\text{g/ml}$ in fraction 3, 64 $\mu\text{g/ml}$ in fraction 4, 94.4 $\mu\text{g/ml}$ in fraction 5, 72.9 $\mu\text{g/ml}$ in fraction 6, and 23.1 $\mu\text{g/ml}$ in fraction 7.

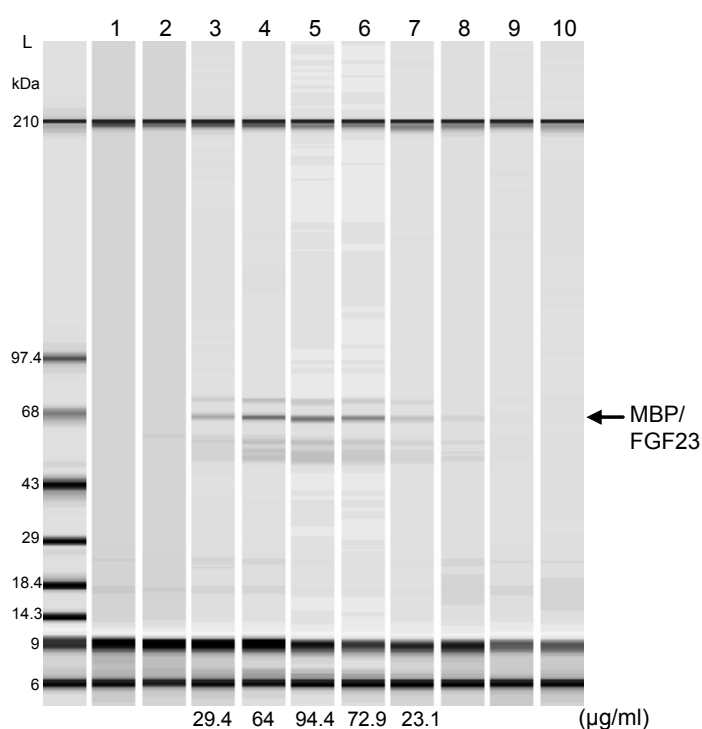


Fig. 11. MBP/FGF23 quantification. Absolute quantification of the 10-elution fractions (lanes 1 – 10) from MBP/FGF23 purification performed in an Agilent bioanalyser using a Protein 200 kit. Concentrations ($\mu\text{g/ml}$) are indicated at the bottom of the figure. Molecular masses of the ladder (L) are indicated to the left.

To separate MBP from FGF23, 1 μ g of pure MBP/FGF23 fusion protein was incubated with 10 ng Factor Xa for 8 and 24 hours at RT. After incubation, proteins were separated through 12% SDS-PAGE and visualized with Coomassie staining. Western blot analysis was also performed using antiFGF23₂₀₇₋₂₂₂ antibody. Peptides of molecular weights around 24 kDa for FGF23 and 43 kDa for MBP were expected after complete separation of MBP/FGF23 (see Fig. 9). However, a major 67 kDa band in addition to several minor bands around 30, 40, 49 and 62 kDa were detected after incubation with Factor Xa. The prominent MBP/FGF23 band (67 kDa) corresponded in size with the band of the fusion protein before incubation (Fig. 12). The same results were obtained when the incubation was conducted at 4°C. These results indicate incomplete and unspecific MBP/FGF23 proteolytic cleavage by Factor Xa. Presumably, inadequate three-dimensional conformation of the fusion protein prevented efficient cleavage by Factor Xa.

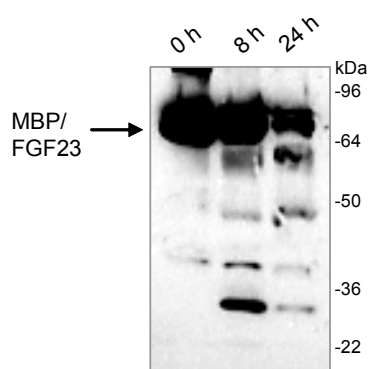


Fig. 12. MBP/FGF23 cleavage by Factor Xa. Western blot analysis with antiFGF23₂₀₇₋₂₂₂ antibody was performed after 12% SDS-PAGE loaded with 1 μ g pure MBP/FGF23 protein before incubation (0 h) and after 8 hours (8 h) or 24 hours (24 h) incubation with 10 ng Factor Xa. Appearance of several bands in addition to incomplete cleavage of MBP/FGF23 occurred after 8 hours and 24 hours incubation. The MBP/FGF23 band (67 kDa) remained intact in the control lane (0 h). Molecular mass markers are indicated to the left.

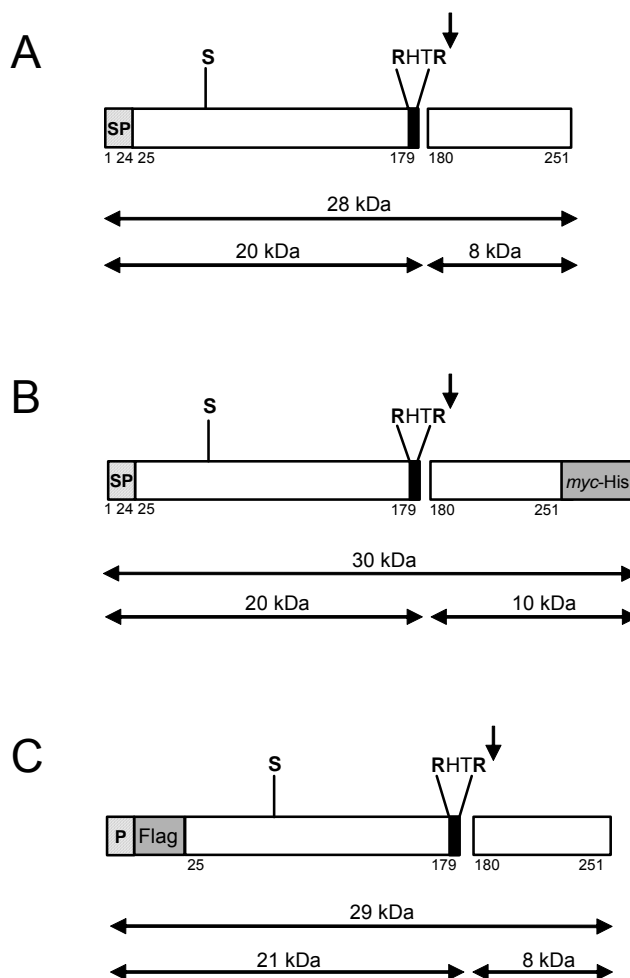
1.3 FGF23 expression in mammalian cells

1.3.1 Generation of recombinant tagged and untagged FGF23 constructs

To study the expression of the FGF23 protein in mammalian HEK293 cells, recombinant tagged and untagged FGF23 fusion constructs were created. The untagged *FGF23* plasmid was constructed by cloning the full-length *FGF23* cDNA (*HindIII/EcoRI*) into the pcDNA3.1 expression vector (Fig. 13). To construct the C-terminal *myc*-His-tagged *FGF23* plasmid stop codon at position c.754 was removed and the modified insert (*EcoRI/XbaI*) was cloned after PCR amplification into the pcDNA3.1/*myc*-His expression vector. The construct pcDNA/*FGF23*/His contained an in frame *myc* epitope (residues EQKLISEEDL) and a polyhistidine tag (residues HHHHHH) followed by an artificial stop codon, at the C-terminus of the FGF23 coding sequence (Fig. 13). Finally, a FLAG-tagged

FGF23 construct (pFLAG/CMV/*FGF23*) was provided by Michael J. Econs (Indiana University School of Medicine, Indianapolis). *FGF23* insert (*EcoRI/BamHI*) was directionally ligated into the pFLAG-CMV-3 expression vector (Sigma-Aldrich), which uses the preprotrypsin leader sequence to allow secretion of N-terminal FLAG tagged (residues DYKDDDDK) fusion proteins (Fig. 13). Molecular masses were predicted using the PeptideMass tool (ExpASy proteomics server).

Fig. 13. FGF23 recombinant proteins. Schematic representation of native FGF23 (A), *myc*-His-tagged FGF23 (FGF23/His) (B) and FLAG-tagged FGF23 (FLAG/FGF23) (C) recombinant proteins. Hatched boxes represent the signal peptide (SP) and the preprotrypsin leader sequence (P). Relative tag position (*myc*-His or FLAG) is indicated into the gray boxes. Amino acids mutated in ADHR or FTC are in bold. Vertical arrows represent SPC cleavage at the RHTR motif site (black box). Numbers on the horizontal arrows indicate the predicted molecular mass (kDa) of intact FGF23, as well as N- and C-terminal fragments.



1.3.2 Expression of tagged and untagged FGF23 in HEK293 cells and polyclonal antibody assessment

To determine whether the signal peptide encoded in the first 24 FGF23 residues is functional and FGF23 is indeed a secreted protein, FGF23 was expressed in HEK293 cells and its presence was determined both in cell lysate and in conditioned medium. Mammalian HEK293 cells were stable transfected with native FGF23 (pcDNA/*FGF23*), FLAG-tagged FGF23 (pFLAG/CMV/*FGF23*) and His-tagged FGF23

(pcDNA/*FGF23*/His) plasmids. Conditioned medium was collected and concentrated 1:20 and cell pellets were suspended in lysis buffer. *FGF23*/His from conditioned medium was further purified via a NiNTA-agarose column. Protein elution was performed under native conditions with an imidazol gradient buffer to avoid denaturation of the protein structure.

Affinity purified polyclonal antibodies to *FGF23* were generated in rabbits (Eurogentec). The antibodies were directed against peptides within the N-terminal (anti*FGF23*₄₈₋₆₇ and anti*FGF23*₁₄₈₋₁₆₃) and the C-terminal parts (anti*FGF23*₁₇₃₋₁₈₇ and anti*FGF23*₂₀₇₋₂₂₂) which are indicated in figure 7. To assess the specificity of the anti-*FGF23* polyclonal antibodies, western blot analysis was performed in conditioned medium and total cellular lysate using anti*FGF23*₄₈₋₆₇ (Fig. 14 A) and anti*FGF23*₁₇₃₋₁₈₇ (Fig. 14 B). Untransfected HEK293 cells were used as controls.

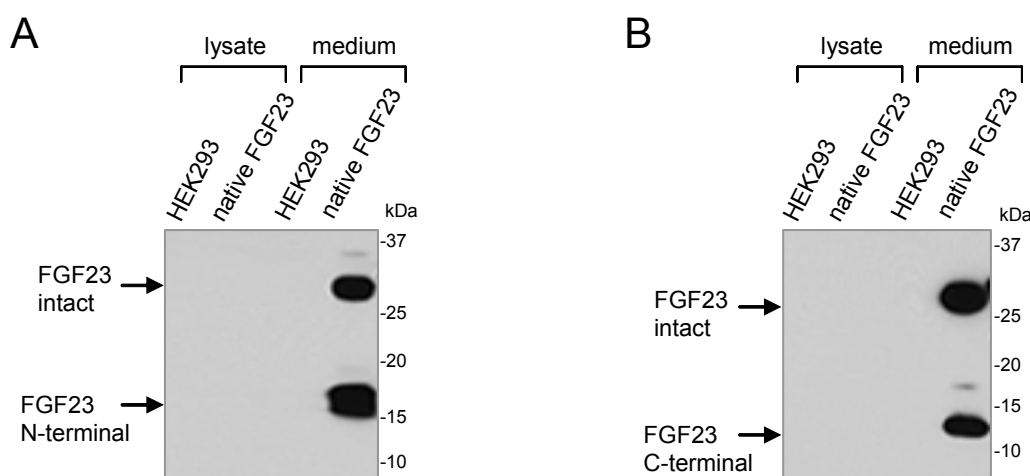


Fig. 14. Expression of *FGF23* in HEK293 cells. Protein (10 μ g of cell lysate and 3 μ g of concentrated conditioned medium) from native *FGF23*-expressing HEK293 cells as well as HEK293 control cells were previously separated on 12% SDS-PAGE and western blot analysis was performed with anti*FGF23*₄₈₋₆₇ (A) and anti*FGF23*₁₇₃₋₁₈₇ (B) antibodies. A band of 30 kDa was detected with both antibodies and two additional bands of 18 and 12 kDa were detected with anti*FGF23*₄₈₋₆₇ or anti*FGF23*₁₇₃₋₁₈₇ respectively in the conditioned medium. Control cells and cell lysates were negative. Molecular mass markers are indicated to the right.

In the conditioned medium of cells expressing native *FGF23*, a 30 kDa band corresponding to intact *FGF23*₂₅₋₂₅₁ protein was detected with both antibodies. In addition, two smaller bands around 18 and 12 kDa were detected with anti*FGF23*₄₈₋₆₇ or anti*FGF23*₁₇₃₋₁₈₇ antibodies respectively, which were supposed to be N- and C-terminal *FGF23* breakdown products. No immunoreactive bands were detected in the cell lysate.

The same bands were detected in the conditioned medium from HEK293 cells expressing FLAG/FGF23 and FGF23/His when analysed with anti-His (C-term)-HRP or anti-FLAG M2-HRP antibodies (Fig. 15). The FGF23/His and FLAG/FGF23 species migrate at a different rate because of the additional residues from the tags. These results confirm that FGF23 is a secreted peptide and that the smaller bands detected in the conditioned medium indeed correspond to N- and C-terminal FGF23 fragments, probably due to a partial processing of intact FGF23 during its biosynthesis in HEK293 cells. Pre-immune serum failed to detect a protein in all experiments. These results also provide evidence that the polyclonal affinity-purified anti-FGF23 antibodies specifically recognize the human FGF23 protein.

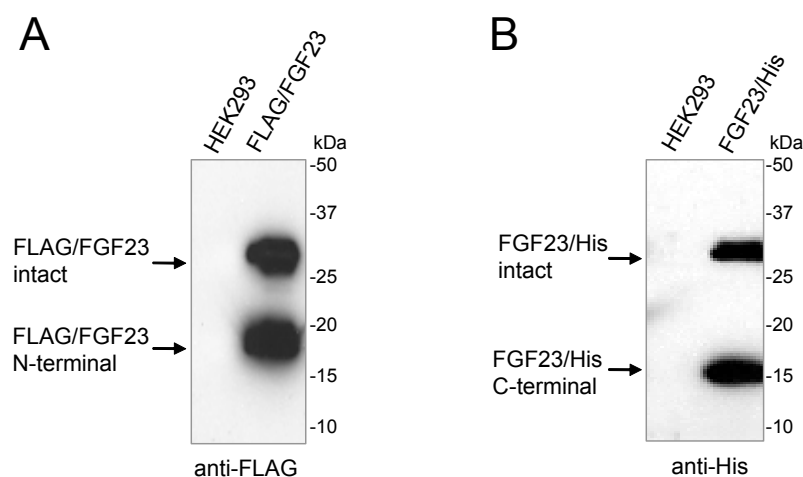


Fig. 15. Analysis of tagged FGF23 in HEK293 cells. Western blot analysis with anti-His (C-term)-HRP (A) and anti-FLAG M2-HRP (B) antibodies performed after separation on 12% SDS-PAGE of 3 μ g protein of concentrated conditioned medium from HEK293 cells expressing FLAG/FGF23 (A), FGF23/His (B) and control cells. A band around 32 kDa was recognized with both antibodies. Two additional bands around 20 and 15 kDa were recognized with anti-FLAG M2-HRP or anti-His (C-term)-HRP antibodies respectively. Molecular mass markers are indicated to the right.

1.3.3 Quantification of the FGF23 fraction in the conditioned medium

Total protein concentration in the conditioned medium after concentration was between 0.5 and 0.9 μ g/ μ l. To analyse how much of the protein fraction was constituted from FGF23, conditioned medium and purified FGF23/His were quantified by image analysis of Coomassie stained SDS-PAGE with the help of the ImageJ Quantification software. Results yielded an FGF23/total protein ratio of 4% (Fig. 16).

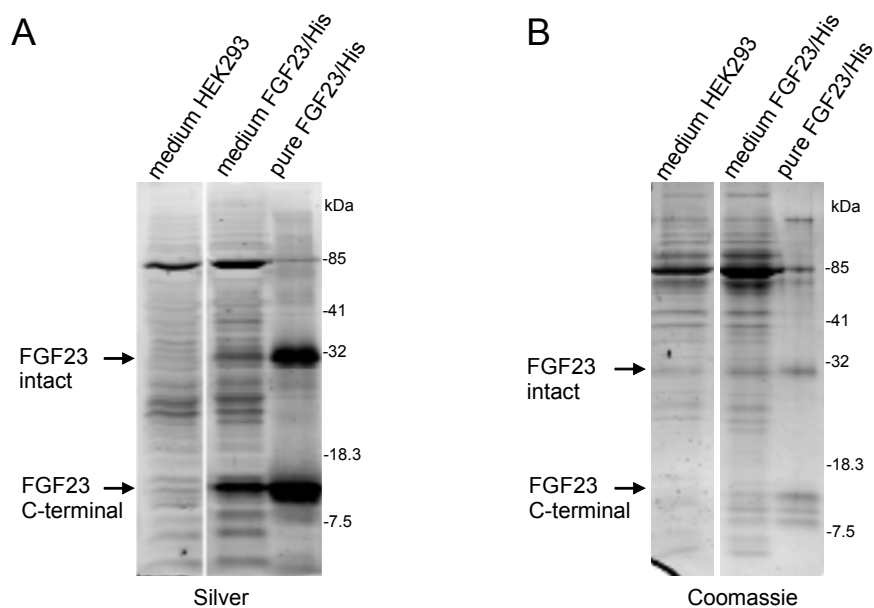


Fig. 16. FGF23 quantification in the conditioned medium. (A) Silver and (B) Coomassie-stained 12% SDS-PAGE of protein (3 μ g) of conditioned medium from FGF23/His-expressing HEK293 cells and control cells. Affinity purified FGF23/His protein (300 ng) was analysed with mass spectrometry. Quantification by image analysis of the Coomassie-stained SDS-PAGE yielded an FGF23/total protein ratio of 4%. Molecular mass markers are indicated to the right.

1.4 Protein characterization

1.4.1 Stability of native FGF23

The stability of FGF23 in the conditioned medium from FGF23 expressing-HEK293 cells was analysed in order to prove that the smaller FGF23 fragments are indeed products from a specific cleavage and not from unspecific degradation due to the presence of proteases in the conditioned medium.

Protein-containing conditioned medium of HEK293 cells expressing FGF23/His was collected and incubated without protease inhibitors at 37°C for 2 h or at RT for 2, 8 and 24 hours. Conditioned medium was then concentrated and 3 μ g protein was separated by SDS-PAGE. Western blot analysis using antiFGF23₁₇₃₋₁₈₇ revealed two immunoreactive bands of 32 and 14 kDa corresponding to intact FGF23₂₅₋₂₅₁ and the C-terminal FGF23₁₈₀₋₂₅₁ fragment, which did not present any signs of degradation after incubation (Fig. 17).

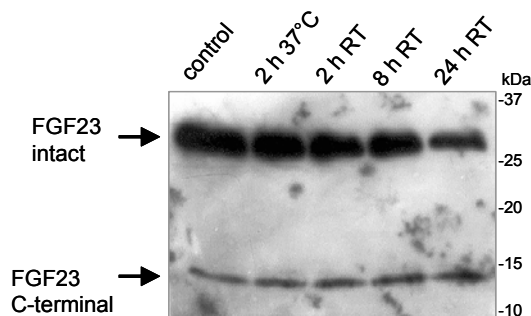


Fig. 17. FGF23 stability. Protein-containing conditioned medium from HEK293 cells expressing FGF23/His were incubated at 37 °C for 2 h or at RT for 2, 8, and 24 h. Following concentration, 3 µg proteins was separated through 12% SDS-PAGE and western blot analysis was performed using antiFGF23₁₇₃₋₁₈₇. The two bands around 32 and 14 kDa corresponding to intact FGF23₂₅₋₂₅₁/His and the C-terminal FGF23/His fragment remained stable during the whole incubation. Molecular mass markers are indicated to the right.

1.4.2 Intracellular versus extracellular cleavage of native FGF23

To determine whether the cleavage of FGF23 in HEK293 cells observed in vitro was an intra- or extracellular process, conditioned medium from HEK293 cells stable transfected with FGF23 was incubated with control HEK293 cells not expressing FGF23 for 24 h at 37°C and 5% CO₂. After incubation, the medium was collected, concentrated and subjected to western blot analysis using antiFGF23₁₇₃₋₁₈₇. There was no change in the ratio of the 30 kDa band to the 12 kDa band regardless of the treatment of the conditioned medium (Fig. 18), indicating that FGF23 cleavage occurred intracellularly, either before or during cellular secretion, and not by extracellular proteases expressed by HEK293 cells.

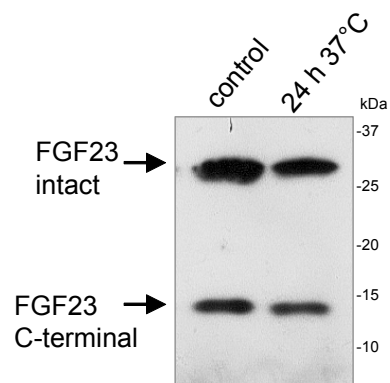


Fig. 18. Analysis of extracellular exposure of FGF23 to HEK293 cells. Conditioned medium from FGF23 expressing-HEK293 cells was incubated for 24 h with HEK293 control cells in a confluent 25 cm² culture flask at 37°C and 5% CO₂. After concentration, 3 µg protein-containing conditioned medium was separated through 12% SDS-PAGE and western blot analysis was performed using antiFGF23₁₇₃₋₁₈₇. There was no difference in the intensity of the 30 kDa and 12 kDa bands after the treatment. Molecular mass markers are indicated to the right.

1.4.3 Glycosylation of native FGF23

Carbohydrates in the form of asparagines-linked (N-linked) or serine/threonine-linked (O-linked) oligosaccharides are major structural components of many eukaryotic proteins. N-linked oligosaccharides may contribute 3.5 kDa or more per structure to the mass of a glycoprotein. O-linked sugars, although usually less massive than N-linked structures, may

be more numerous. The diversity of oligosaccharide structures often results in heterogeneity in the mass and charge of glycoproteins.

To characterize the glycosylation state of FGF23, conditioned medium of HEK293 cells expressing native FGF23 was submitted to deglycosylation by PNGase F or endo H to remove N-linked carbohydrates and neuraminidase type X followed by O-glycosidase treatment to remove O-linked carbohydrates. RNase B and bovine fetuin were used as positive controls in the N-deglycosylation and O-deglycosylation assays respectively.

Western blot analysis with antiFGF23₄₈₋₆₇ or antiFGF23₁₇₃₋₁₈₇ antibodies revealed that FGF23 was not sensitive to PNGase F or Endo H digestion (Fig. 19).

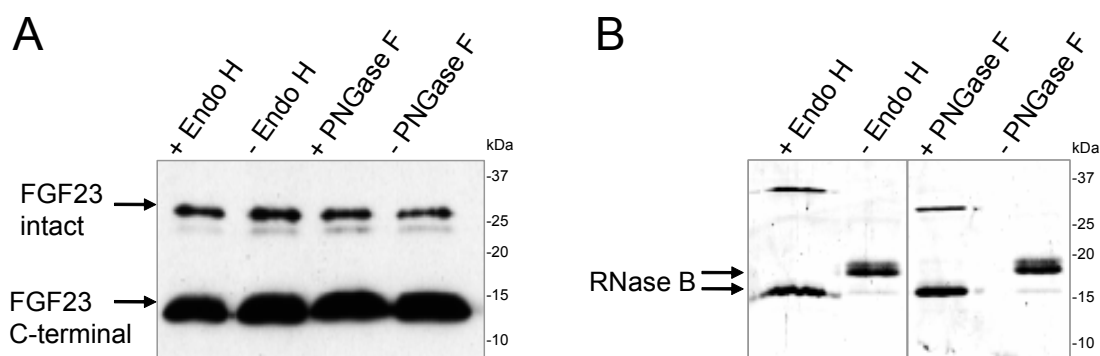


Fig. 19. Treatment of native FGF23 with N-deglycosidases. (A) Protein-containing conditioned medium (2 μ g) of FGF23 expressing-HEK293 cells was treated with 1 U PNGase F or Endo H for 1 h at 37°C to remove N-linked oligosaccharides. Samples were visualized after separation through 12% SDS-PAGE by western blot analysis using antiFGF23₁₇₃₋₁₈₇ antibody. (B) 1 μ g RNase B was used as internal control and visualized by Coomassie staining of 12% SDS-PAGE. No difference in the mobility of native FGF23 was observed before and after treatment. Molecular mass markers are indicated to the right.

In contrast, neuraminidase and O-glycosidase treatment revealed that intact FGF23₂₅₋₂₅₁ (30 kDa) and both N-terminal (18 kDa) and C-terminal (12 kDa) fragments were O-glycosylated, since their electrophoretic mobility increased after digestion (Fig. 20). The double band of 18 kDa corresponding to the N-terminal FGF23 fragment turned into a single band after treatment with glycosidases which indicates heterogeneity in the glycosylation state of this fragment (Fig. 20 A). Monitoring of RNase B and bovine fetuin with Coomassie stain after SDS-PAGE showed a noticeable increase in mobility of both enzymes after deglycosylation (Fig. 19 B and 20 B).

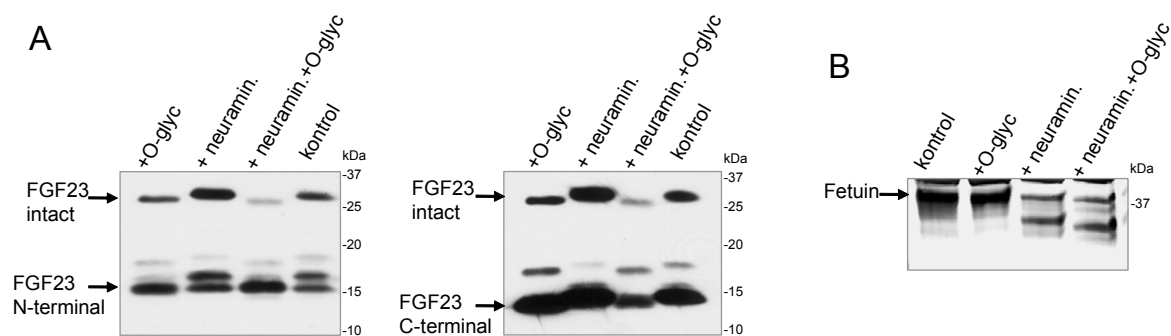


Fig. 20. Treatment of native FGF23 with O-glycosidases. (A) Protein-containing conditioned medium (2 μ g) of FGF23 expressing-HEK293 cells was treated with 4 mU neuraminidase type X for 3 h at 37°C followed by 2 mU O-glycosidase for 16 h at 37°C. Samples were separated by 12% SDS-PAGE and visualized by western blot analysis using anti-FGF23₄₈₋₆₇ or anti-FGF23₁₇₃₋₁₈₇ antibodies. (B) 1 μ g bovine fetuin as internal control was treated under the same conditions and viewed by Coomassie staining of 12% SDS-PAGE. Native FGF23 mobility increased after neuraminidase followed by O-glycosidase treatment. Molecular mass markers are indicated to the right.

1.4.4 Purification of FGF23/His and mass spectrometry analysis

His-tagged FGF23 present in the conditioned medium of HEK293 cells was purified after concentration by a Ni-NTA agarose spin column under native conditions. The fraction containing pure FGF23/His was dialyzed against PBS and proteins were separated through 12% SDS-PAGE and silver stained (Fig. 16). The 32 kDa and 14 kDa fragments were excised from the gel and digested with trypsin *in situ*. The tryptic peptides were extracted from the gel slices and analysed by mass spectrometry. The mass spectrometry analysis was performed by Hans Zischka (Institute of Human Genetics, GSF Neuherberg).

Figure 21 shows the MALDI-TOF spectrum of the 14 kDa protein fragment. Four tryptic peptides with masses of 918.51, 1450.75, 1855.82, and 1941.91 Da matched to the human C-terminal FGF23 sequence with 48% coverage. Insufficient data were obtained to identify the 32 kDa protein by MALDI-TOF.

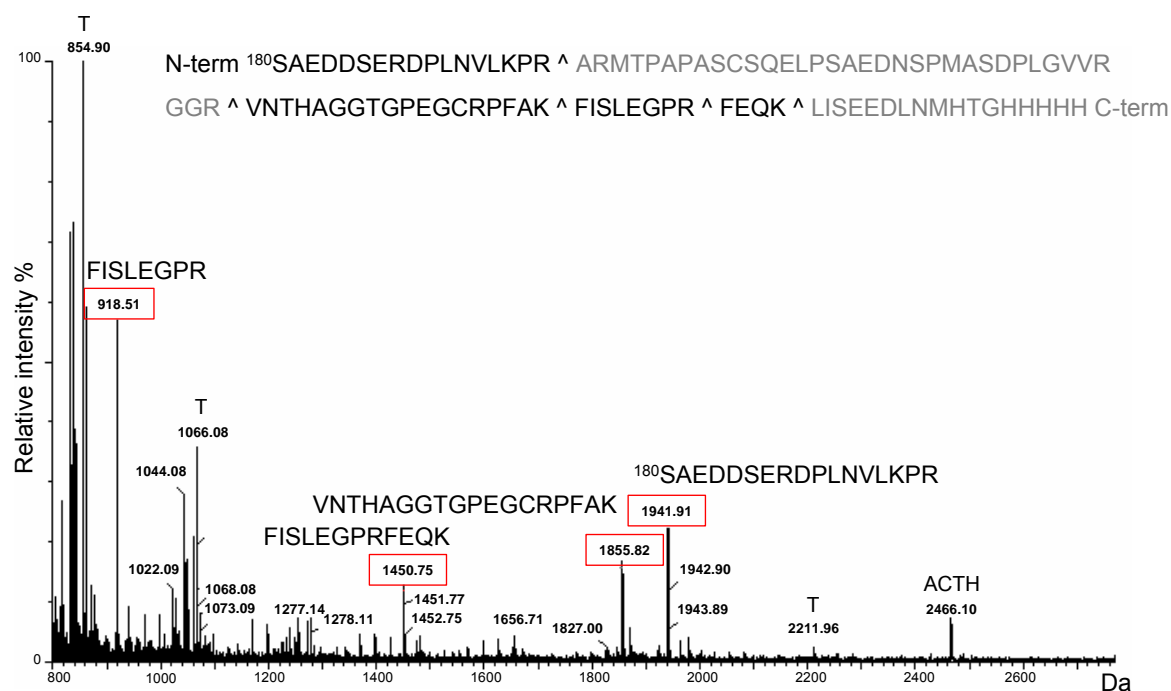


Fig. 21 Mass spectrometric analysis of the FGF23/His C-terminal fragment. FGF23/His was affinity purified and separated by SDS-PAGE. The 14 kDa band was subjected to gel digestion with trypsin, and the extracted peptides were analysed by MALDI-TOF. Four peptide masses (918.51, 1450.75, 1855.82, and 1941.91) matched the human FGF23 C-terminal fragment with 48% sequence coverage. T indicates tryptic peptides derived from trypsin and ACTH was used as internal control. Molecular masses are given in Daltons (Da). The C-terminal FGF23 sequence starting at amino acid position 180 is shown in the upper part of the figure. Tryptic peptides obtained from the mass spectrometric analysis are indicated in black, (^) indicates trypsin cleavage sites.

2. CHARACTERIZATION OF FGF23 MUTANT PROTEINS

2.1 Mutation analysis in FTC

In previous studies, the ADHR Consortium (The ADHR Consortium, 2000) identified the FGF23 gene as causative factor for autosomal dominant hypophosphatemic rickets (ADHR) by a positional cloning approach (see introduction 2.2.1). Mutations affecting two argenines, p.R176Q (c.527G>A), p.R179W (c.535C>T) and p.R179Q (c.536G>A), were found in four families that showed a male-to-male transmission of the trait and clinical features compatible with ADHR (Tab. 11).

In the present study, a mutation analysis was performed in two families with Austrian (family 1) and Spanish (family 2) origin that presented the clinical features of familial

tumoral calcinosis (FTC) with hyperphosphatemia (see introduction 3.1). FTC is inherited in an autosomal recessive mode. Biallelic mutations in the *GALNT3* gene have been described in two large families as the cause of FTC (Topaz *et al.* 2004). Therefore, *GALNT3* was considered as the first candidate gene for mutation screening.

Tab. 11. Mutations found in *FGF23* and *GALNT3* genes as causative factors for ADHR and FTC.

Disease	Gene	Mutation	Amino acid
ADHR	<i>FGF23</i>	c.527G>A	p.R176Q
ADHR	<i>FGF23</i>	c.535C>T	p.R179W
ADHR	<i>FGF23</i>	c.536G>A	p.R179Q
FTC	<i>FGF23</i>	c.211A>G	p.S71G
FTC	<i>GALNT3</i>	c.985G>A	p.G329R

ADHR: autosomal dominant hypophosphatemic rickets, FTC: familial tumoral calcinosis, *FGF23*: fibroblast growth factor 23, *GALNT3*: N-acetylgalactosaminyltransferase 3.

Using genomic DNA and balanced primer pairs, the ten *GALNT3* coding exons were screened for pathogenic mutations in all members of the Austrian (family 1) and Spanish (family 2) families. A homozygous missense mutation (c.985G>A) in exon 4 resulting in the amino acid substitution glycine to arginine (p.G329R) was found in the two affected individuals (mother and son) from family 2. The same homozygous mutation was found in the healthy daughter. The father was heterozygous and the mutation was not found in 1250 sequenced control alleles (Fig. 22 B). In contrast, no mutation was found in the patient from family 1.

After exclusion of *GALNT3* mutations in the affected individual from family 1, direct sequencing of the three *FGF23* exons identified a homozygous missense mutation (c.211A>G) at the last nucleotide of the first exon. This finding constitutes the first description of a *FGF23* mutation in this condition and demonstrates allelic heterogeneity of the disease. The mutation c.211A>G leads to a missense mutation replacing a serine by a glycine (p.S71G). The parents and one sister were heterozygous for the mutation (Fig. 22 A), which was not found in 256 control alleles sequenced previously by the ADHR Consortium in the year 2000. I concluded that the novel *FGF23* mutation c.211A>G and *GALNT3* mutation c.985G>A were causative for the autosomal recessive transmission of FTC in these families.

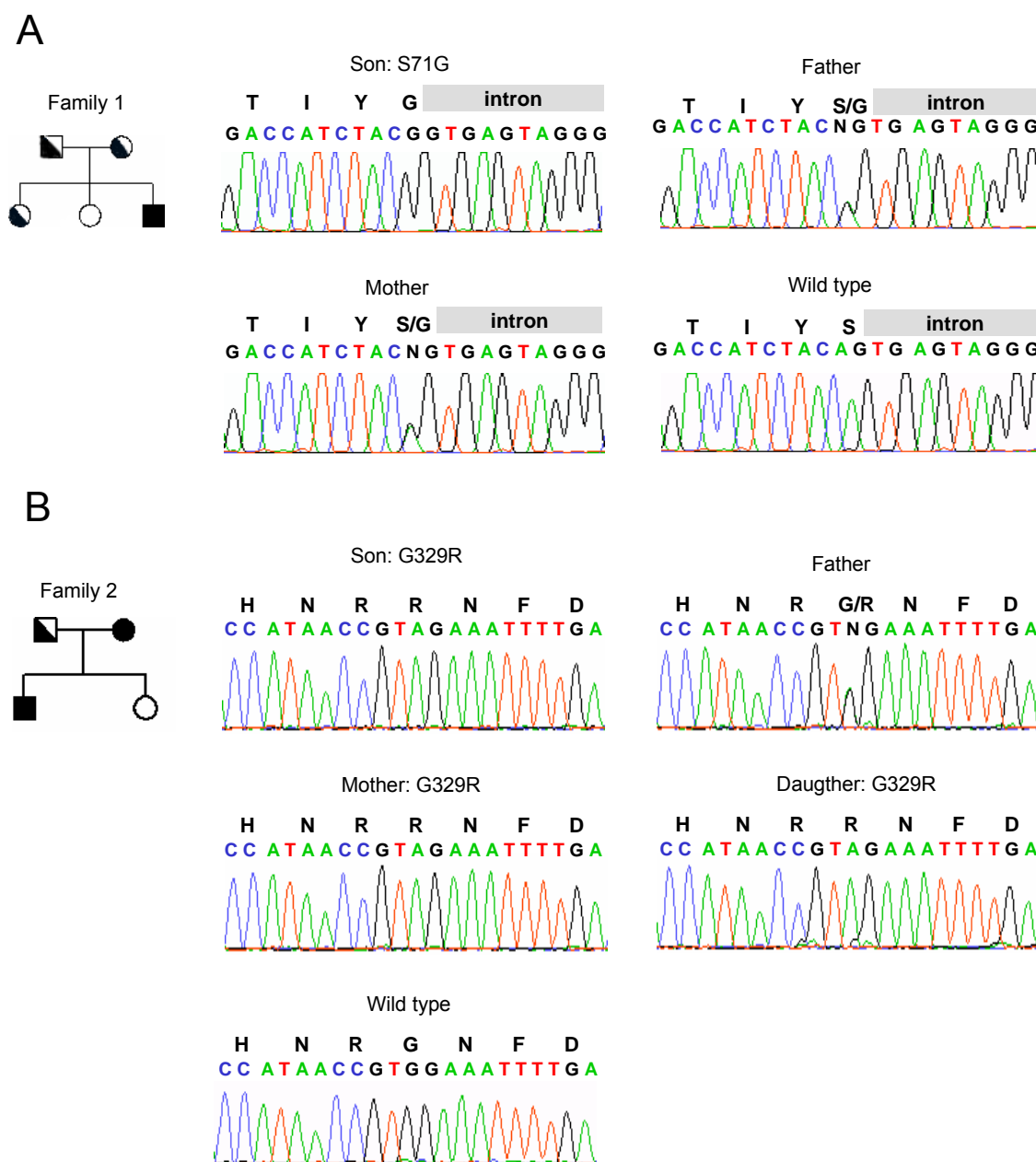


Fig. 22. Mutation analysis. Pedigrees from the Austrian (family 1) and Spanish (family 2) families affected with FTC and electropherograms of the family members. (A) Segregation of the *FGF23* c.211A>G transition (p.S71G) within family 1. The affected individual is homozygous for the mutation, the parents and one sister heterozygous. (B) Segregation of the *GALNT3* c.985G>A transition (p.G329R) within family 2. Three individuals are homozygous for the mutation although one of them (daughter) is not affected. The father is heterozygous.

2.2 FGF23 mutant proteins and expression in mammalian cells

ADHR mutations p.R176Q, p.R179W, and p.R179Q lead to replacement of either of two critical arginine residues within a potential subtilisin-like proprotein convertase (SPC) minimum consensus cleavage site: 176RHTR179 (RXXR motif). SPCs are the major

endoproteolytic processing enzymes of the secretory pathway for a wide variety of hormone and neuropeptide precursors. If native FGF23 cleavage occurs at this site, it can be hypothesized that ADHR mutations interfere with the hydrolysis by SPCs.

The FTC mutation in FGF23 leads to substitution of a serine by a glycine (p.S71G). Although the mutation is localized at the last nucleotide of exon 1 (c.211A) it is unlikely to cause aberrant splicing because it introduces a G which is most frequently used at this position and therefore increases the splice site consensus value as defined by Shapiro and Senapathy (Shapiro and Senapathy 1987). This serine (p. 71S) is situated at the end of the loop between strand 3 and 4 of the FGF β -barrel according to structure modeling (Harmer *et al.* 2004) and it could be involved in post-translational modifications such as glycosylation or in the correct folding of the mature protein.

In order to investigate whether FGF23 mutant proteins were expressed and secreted in mammalian cells in a similar manner as the native protein, *FGF23* expression plasmids carrying p.R176Q (pcDNA/*FGF23*R176Q/His), p.R179Q (pcDNA/*FGF23*R179Q/His) and p.S71G (pcDNA/*FGF23*S71G) mutations were created by site directed mutagenesis and stable transfected in HEK293 cells.

2.2.1 Analysis of the ADHR FGF23-R176Q and –R179Q mutant proteins

Western blot analysis of conditioned medium and total cellular lysate from HEK293 cells transfected with His-tagged FGF23-R176Q and FGF23-R179Q was performed using antiFGF23₁₇₃₋₁₈₇ antibody. Untransfected HEK293 cells and cells transfected with native FGF23/His were used as internal controls. Results revealed a 32 kDa band corresponding to intact FGF23-R176Q/His and FGF23-R179Q/His proteins (Fig. 23). No additional bands corresponding to processed products were detected in the conditioned medium from mutant FGF23/His-expressing HEK293 cells. In contrast, wild type FGF23/His resolves in two immunoreactive bands intact FGF23 (FGF23₂₅₋₂₅₁/His) and C-terminal fragment (FGF23₁₈₀₋₂₅₁/His). Total cellular lysates and control cells were negative (Fig. 23).

These results indicate that FGF23-R176Q and FGF23-R179Q mutant proteins are secreted primarily as the intact protein species. Most likely, mutant proteins escape from proteolytic cleavage because the ADHR mutations may disrupt the cleavage motif 176RXXR179 recognized by SPCs.

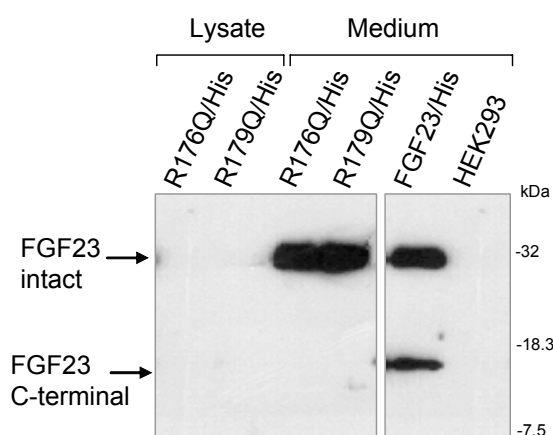


Fig. 23. Expression of mutant FGF23-R176Q/His and FGF23-R179Q/His in HEK293 cells. Western blot analysis with antiFGF23₁₇₃₋₁₈₇ antibody against C-terminal FGF23 peptide was performed after 12% SDS-PAGE of 5 µg protein-containing concentrated conditioned medium and cell lysate from FGF23/His-, FGF23-R176Q/His- and FGF23-R179Q/His-expressing HEK293 cells and control cells. Bands of 32 and 12 kDa were detected in the conditioned medium from cells expressing FGF23/His whereas only a 32 kDa band was detected in the conditioned medium from cells expressing mutant FGF23-R176Q and FGF23-R179Q. Cell lysates were negative. Molecular mass markers are indicated to the right.

2.2.1.1 Inhibition of FGF23 processing at the RHTR site

To determine whether FGF23 is processed at the 176RHTR179 site during its biosynthesis by SPC proteases, we used Decanoyl-Arg-Val-Lys-Arg-chloromethyl ketone (Dec-RVKR-CMK). This is a highly specific, irreversible and cell permeable competitive inhibitor of proprotein convertases: furin/SPC1 (Ki= 1.0 nM), SPC2/PC2 (Ki= 0.36 nM), SPC3/PC1/PC3 (Ki= 2.0 nM), SPC4/PACE4 (Ki= 3.6 nM), SPC6/PC5/PC6 and SPC7/PC7/PC8 (Ki= 0.12 nM) (Denault *et al.* 1995, Bowler *et al.* 2002). The typical concentration range used in tissue culture is 25-100 µM. Increasing concentrations of Dec-RVKR-CMK to 52 µM were added to the culture medium of HEK293 cells expressing native FGF23. Western blot analysis of the conditioned medium with antiFGF23₁₇₃₋₁₈₇ showed dosage-dependent inhibition of FGF23 cleavage. Complete inhibition of cleavage was achieved with 39 µM Dec-RVKR-CMK (Fig. 24).

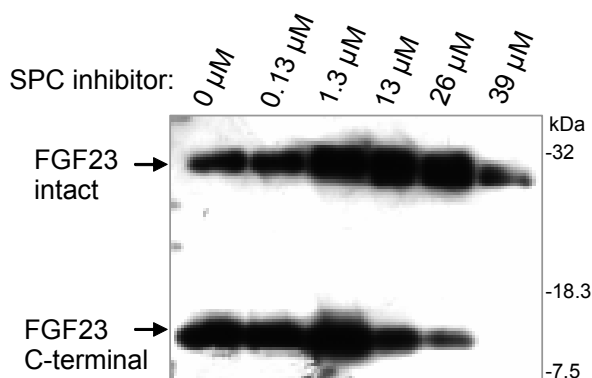


Fig. 24. Inhibition of proteolytic cleavage of FGF23 by a SPC inhibitor. HEK293 cells expressing native FGF23 were cultured overnight in 6-well culture plates with 1.5 ml serum-free medium in the presence of different concentrations of Dec-RVKR-CMK. Samples were concentrated to 100 µl using a Microsep-omega 10K concentrator. Proteins (3 µg) were separated through 12% SDS/PAGE and incubated with anti-FGF23 polyclonal antibody (antiFGF23₁₇₃₋₁₈₇). FGF23 cleavage was completely prevented at a concentration of 39 µM Dec-RVKR-CMK. Molecular mass markers are indicated to the right.

Quantification was performed by using the ImageJ Quantification software. Two replicates at an inhibitor concentration of 26 μM and four replicates at all other inhibitor concentrations resulted in the following mean values for the ratio of C-terminal to intact plus C-terminal protein: 59% at 0 μM inhibitor, 52% at 0.13 μM , 44% at 1.3 μM , 29% at 13 μM , 18% at 26 μM , 4% at 39/52 μM indicating a marked reduction of the amount of C-terminal fragment at higher inhibitor concentrations. These results show that members of the SPC family of proteases are required for FGF23 processing.

2.2.1.2 Expression of SPCs in HEK293 cells and in mice osteoblasts

To test whether FGF23 cleavage by proprotein convertases in cultured cells could be of physiological significance, the expression of this family of proteases was analysed in HEK293 cells and in mice osteoblasts where Fgf23 expression has been documented by real-time quantitative RT-PCR (Liu *et al.* 2003).

A semi-quantitative multiplex PCR was performed in cDNAs from HEK293 cells and from mice osteoblasts to determine the expression of the different SPCs. SPC2, SPC4, SPC6 and SPC7 could be amplified from HEK293 cells at the same expression level as GAPDH (Fig. 25 A). Spc1, Spc2, Spc3, Spc4 and Spc7 expression was detected in mice osteoblasts (Fig. 25 B). These results suggested that FGF23 cleavage could be of biological significance because of the parallel expression of SPC2, SPC4 and SPC7 in HEK293 cells as well as in mice osteoblasts. Thus, SPCs are likely to be responsible for the processing of FGF23 also *in vivo*.

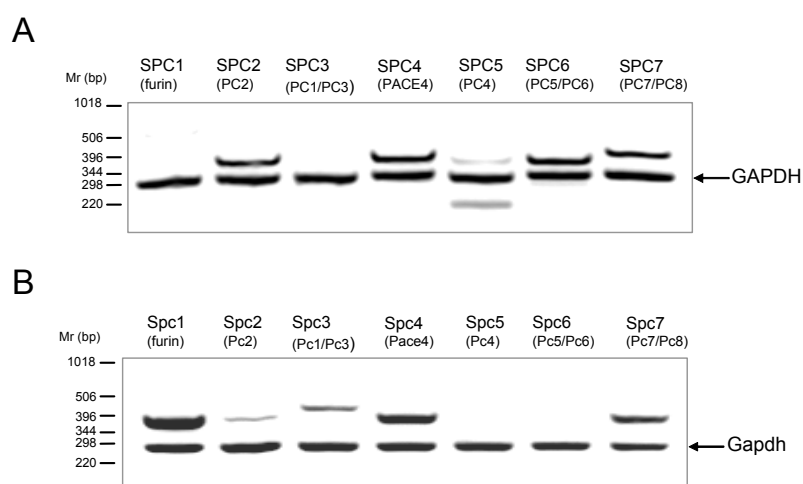


Fig. 25. Expression of subtilisin-like proprotein convertases in HEK293 cells and mice osteoblasts. First-strand cDNA (10 ng) was used as template for a semi-quantitative multiplex PCR with the corresponding SPC/Spc and GAPDH/Gapdh primers. PCR amplification products were detected for SPC 2, 4, 6, and 7 in HEK293 cells (A) and Spc 1, 2, 3, 4, and 7 in mice osteoblasts (B).

2.2.2 Analysis of the FTC FGF23-S71G mutant protein

Expression and processing of mutant FGF23-S71G in HEK293 cells was analysed in the conditioned medium and in cell lysate by western blot analysis using antiFGF23₄₈₋₆₇ and antiFGF23₁₇₃₋₁₈₇ polyclonal antibodies (Fig. 26). Untransfected HEK293 cells and cells transfected with native FGF23 or empty pcDNA3.1 vector were used as internal controls.

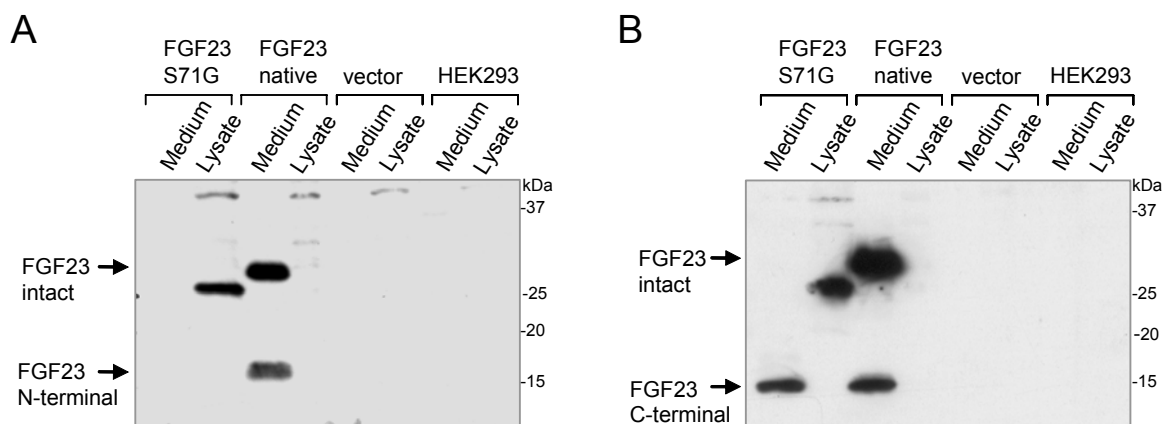


Fig. 26. Expression of mutant FGF23-S71G in HEK293 cells. Western blot analysis using anti-FGF23 polyclonal antibodies against the N-terminal (antiFGF23₄₈₋₆₇) (A) and the C-terminal (antiFGF23₁₇₃₋₁₈₇) peptides (B) were performed in the conditioned medium and the cell lysate of HEK293 cells expressing mutant FGF23-S71G, native FGF23, HEK293 cells stable transfected with empty pcDNA3.1 vector as well as untransfected HEK293 cells. Bands of 30, 18 and 12 kDa were detected in the conditioned medium of cells expressing native FGF23 whereas only a 12 kDa band was detected in the conditioned medium from cells expressing mutant FGF23-S71G. In addition, a 25 kDa band was detected in the cell lysate from cells expressing mutant FGF23-S71G. Controls were negative. Molecular mass markers are indicated to the right.

In the conditioned medium of cells expressing native FGF23 immunoreactive bands of approximately 30, 18 and 12 kDa were detected, corresponding to secrete intact FGF23₂₅₋₂₅₁ (30 kDa), N-terminal FGF23₂₅₋₁₇₉ (18 kDa) and C-terminal FGF23₁₈₀₋₂₅₁ (12 kDa) respectively. Sometimes after 1 day of exposure, a slight band corresponding to intact FGF23₂₅₋₂₅₁ was detected in the cell lysate. In contrast, conditioned medium of cells expressing mutant FGF23-S71G contained almost exclusively C-terminal FGF23₁₈₀₋₂₅₁ (12 kDa). Only very slight bands of intact FGF23₂₅₋₂₅₁ and N-terminal FGF23₂₅₋₁₇₉ were detected in 7 of 10 and 4 of 5 experiments, respectively. Surprisingly, we detected a prominent band of approximately 25 kDa with both antibodies within the cell lysates. Other bands were not detected. Although this band migrated faster than the FGF23₂₅₋₂₅₁ detected in the conditioned media, it most probably represents intact FGF23₂₅₋₂₅₁ in another folding state. Alternatively, the difference in the apparent molecular weight may be caused

by post-translational modifications or digestions at the N- or C-terminal ends. Taken together, these results demonstrate that most of the mutant intact FGF23-S71G protein remains trapped within the cells whereas only the C-terminal fragment is secreted.

2.2.2.1 Subcellular localization of the FGF23-S71G mutant protein

As a consequence of a mutation, proteins may be misfolded and degraded by the ubiquitin-proteasome system, may be transported to lysosomes or may be retained within the endoplasmic reticulum or Golgi apparatus (Tsai *et al.* 2002).

In order to study the subcellular localization of the mutant protein, immunocytochemistry experiments were performed in stable transfected HEK293 cells expressing mutant and wild-type protein. Untransfected HEK293 cells were used as controls. Primary antibodies against FGF23 (antiFGF23₁₄₈₋₁₆₃) and fluorochrome-labelled secondary antibodies were used to detect the proteins. FGF23-S71G, but not native protein, was detected within the cells (Fig. 27).

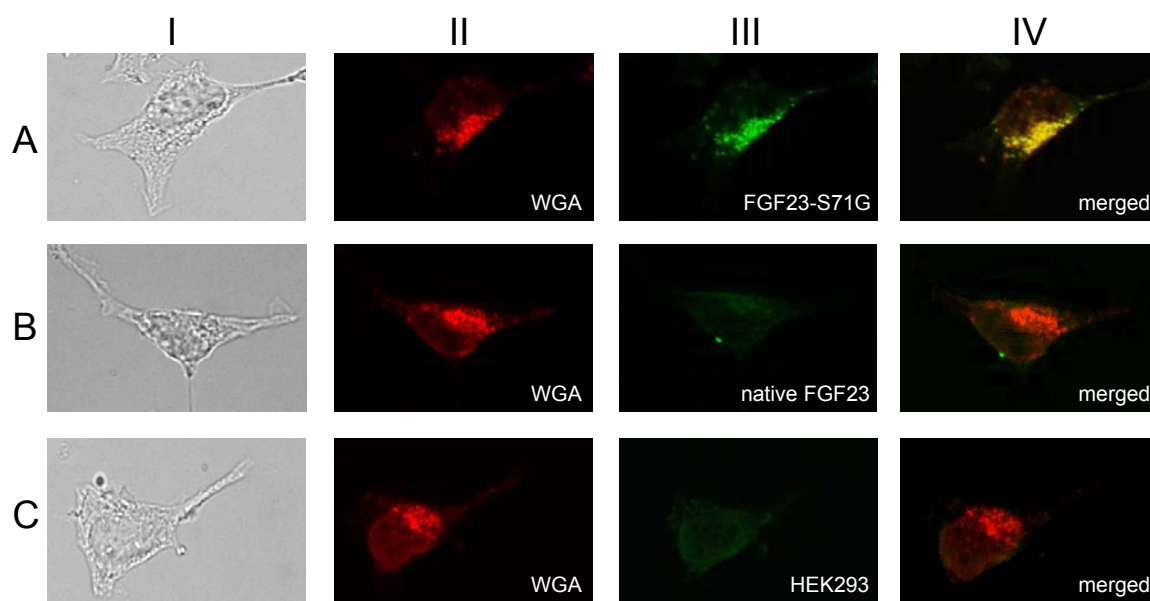


Fig. 27. Subcellular localization of FGF23-S71G. Light microscopy images of HEK293 cells (column I) stable transfected with FGF23-S71G (A), native FGF23 (B) and untransfected HEK293 cells (C). Cells were stained with WGA Alexa Fluor 594 conjugate (red; column II) and antiFGF23₁₄₈₋₁₆₃ antibody (green; column III). Merged images of the double-stained cells are shown in column IV. FGF23-S71G protein co-localized with the Golgi compartment specific WGA staining, whereas native FGF23 was not detected within the cells. HEK293 control cells showed no cross-reaction.

Antibodies and markers against different cellular organelles were used for co-localization studies. Localization in endoplasmic reticulum, lysosomes and mitochondria was excluded

by using antibodies against calnexin, lysosome-associated membrane protein 1 and a 60 kDa nonglycosylated protein component of mitochondria respectively. The green fluorescence of antiFGF23₁₄₈₋₁₆₃ was localized to the polar perinuclear structure of the Golgi apparatus and perfectly co-localized with the red label of the Golgi marker WGA Alexa Fluor 594 conjugate (Fig. 27 A). Thus, FGF23-S71G is retained within the Golgi complex.

2.2.2.2 Quantification of plasma FGF23 levels

To investigate the effect of mutant FGF23-S71G *in vivo*, circulating FGF23 plasma levels were measured in the FTC patient, his parents, 2 sisters and 5 controls with a commercially available ELISA sandwich that uses antibodies against the C-terminal FGF23 fragment (Tab. 12). This assay detects intact FGF23 and C-terminal fragment. The FGF23 levels of normal controls ranged from 25 to 78 RU/ml (median 42 RU/ml), thus being within the normal range, which is below 150 RU/ml described for this assay (Jonsson *et al.* 2003). Also, the parents and sisters of the patient showed plasma levels within the normal range (45, 112, 92 and 39 RU/ml). In contrast, the affected individual had a markedly elevated FGF23 level of 1077 RU/ml. Most probably, these elevated levels are the result of increased production and secretion of the C-terminal FGF23 fragment.

Tab. 12. FGF23 detection in plasma of normal controls and family members with FTC.

Group	Sex	Mutation S71G	FGF23 RU/ml
Control I	F	no	40
Control II	F	no	51
Control III	M	no	25
Control IV	F	no	78
Control V	M	no	42
Father	M	heterozygous	45
Mother	F	heterozygous	112
Unaffected child	F	heterozygous	59
Unaffected child	F	no	92
Affected child	M	homozygous	1077

3. FGF23 A SUBSTRATE OF THE PHEX ENDOPEPTIDASE

The vast majority of active peptides are generated by selective cleavage of precursors at sites that contain one or more basic amino acids. First, one or more endopeptidases cleave the precursor to generate intermediates containing C-terminal basic residues. The major peptide-processing endopeptidases are SPCs (Zhou *et al.* 1998, Seidah and Chretien 1997). Subsequently, a carboxypeptidase was shown to be necessary for removal of the carboxy-terminal basic residues (arginine or lysine) exposed by the endopeptidases (Fricker 1988, Wei 2003).

It has long been discussed whether FGF23 is a substrate of the PHEX endopeptidase which is mutated in X-linked hypophosphatemic rickets (XLH) (see introduction 2.1). To study the ability of PHEX to degrade FGF23, co-culture experiments with HEK293 cells expressing native FGF23 or PHEX proteins as well as FGF23 incubation with membrane fractions containing PHEX were performed. FGF23 cleavage was not observed in co-incubation experiments. By the use of membrane fractions, partial FGF23 cleavage with PHEX-containing membranes as well as with control membranes that did not contain PHEX was observed in some experiments. Most likely, this unspecific cleavage was caused by other proteases within the membrane fraction. To reduce this contaminating effect I decided to follow the strategy described by Boileau *et al.* (2001) to create a secreted and soluble form of the PHEX protein (secPHEX) that allowed incubation experiments without the use of membrane fractions.

3.1 Expression of secPHEX in HEK293 cells

3.1.1 Generation of recombinant PHEX constructs

A C-terminal His-tagged *PHEX* plasmid was constructed by cloning the full-length *PHEX* cDNA (*NotI/XbaI*) into the pcDNA3.1/myc-His expression vector after removal of the stop codon at position 2863 (pcDNA/*PHEX*/His) (Fig. 28 A).

To create a secreted and soluble PHEX, the signal peptide/membrane anchor domain (SA domain) of the protein was transformed into a cleavage-competent signal sequence. Site-directed mutations in eight codons and deletion of four codons by PCR mutagenesis were introduced into the *PHEX* coding sequence previously cloned into the pBS vector (pBS/*PHEX*). The restriction fragment (*NotI/XbaI*) containing the sec*PHEX* sequence was

digested and subcloned into the pcDNA3.1 expression vector (pcDNA/secPHEX) (Fig. 28 B).

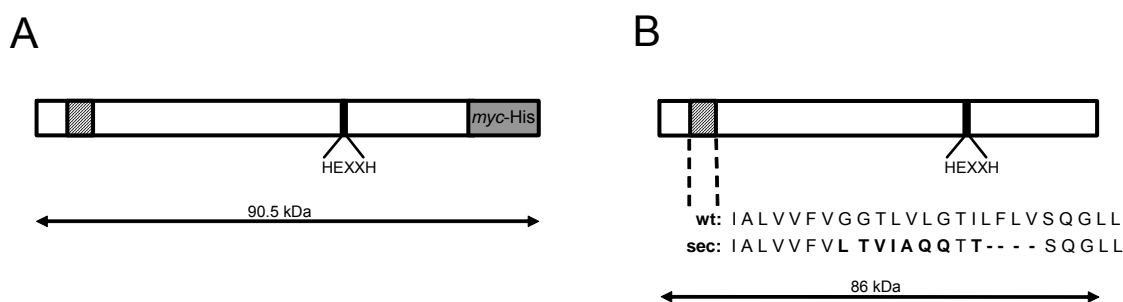


Fig. 28. secPHEX recombinant protein. Schematic representation of His tagged PHEX (PHEX/His) (A) and secreted PHEX (secPHEX) (B) recombinant proteins. The hatched box represents the transmembrane domain and the black box the zinc-binding domain (HEXXH). *Myc*-His tag is shown at the C-terminal end of the box. Amino acid sequences of the wild-type (**wt**) and the mutated (**sec**) transmembrane domains are presented in the one-letter code. In the **sec** sequence, bold letters indicate the amino acids mutated by site-directed mutagenesis PCR, whereas hyphens (-) depict deleted residues (adapted from Boileau *et al.* 2001). Numbers on the horizontal arrows indicate the predicted molecular mass (kDa) of the PHEX recombinant proteins. Molecular masses were predicted using the PeptideMass tool from the ExpASY proteomics server.

3.1.2 Expression of PHEX and secPHEX in HEK293 cells

To determine whether secPHEX was properly secreted, mammalian HEK293 cells were stable transfected with His-tagged PHEX (pcDNA/PHEX/His) and secPHEX (pcDNA/secPHEX). HEK293 cells stable transfected with pcDNA3.1 vector were used as controls. A polyclonal antibody against human PHEX was generated in rabbits and affinity purified (Eurogentec). In order to assess the specificity of the antiPHEX₁₇₁₋₁₈₅ antibody, western blot analysis was performed in the conditioned medium and total cellular lysate.

In the cell lysate of cells expressing PHEX/His, a resolving band of approximately 100 kDa corresponding to intact PHEX/His was detected with antiPHEX₁₇₁₋₁₈₅ whereas the conditioned medium was negative. The same band was detected with anti-His (C-term)-HRP antibody in the cell lysate of PHEX/His-expressing HEK293 cells. Control cells were negative. This data confirmed the specificity of antiPHEX₁₇₁₋₁₈₅ antibody (Fig. 29 A). Also, secPHEX was only detected in the conditioned medium whereas cell lysates were negative (Fig. 29 B).

These results show that secPHEX was correctly secreted and that the polyclonal affinity-purified anti-PHEX antibody recognizes specifically the human PHEX protein. Pre-immune serum failed to detect a protein in all experiments.

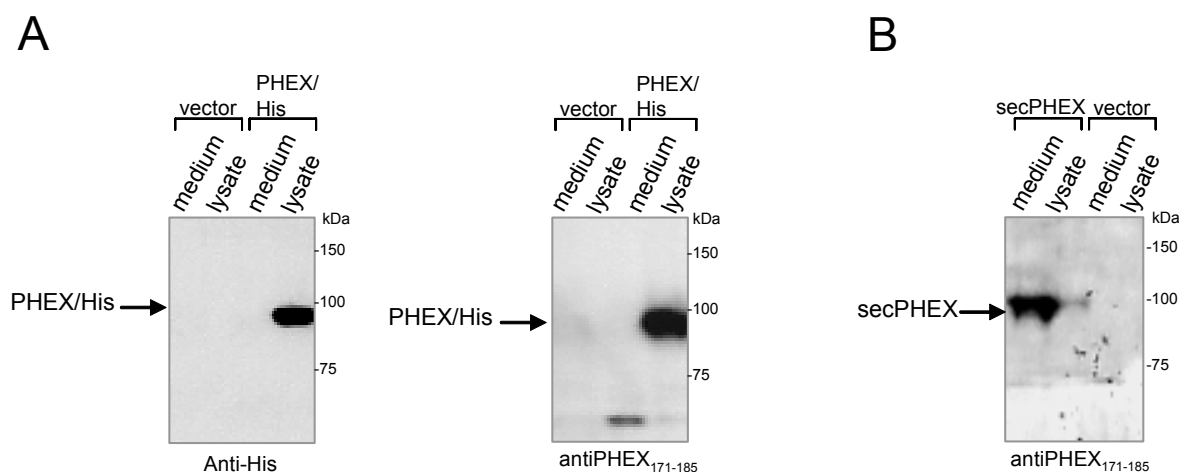


Fig. 29. Detection of secPHEX in the conditioned medium Protein (10 μ g of cell lysate and 3 μ g of concentrated conditioned medium) from PHEX/His and secPHEX-expressing HEK293 cells as well as HEK293 control cells were separated on 12% SDS-PAGE and western blot analysis was performed with antiPHEX₁₇₁₋₁₈₅ and anti-His (C-term)-HRP antibodies. A band around 100 kDa was detected with antiPHEX₁₇₁₋₁₈₅ and with anti-His (C-term)-HRP in the cell lysate and not in the conditioned medium from PHEX/His-expressing cells. In the conditioned medium from cells expressing secreted PHEX (secPHEX) a resolving band around 100 kDa was detected with antiPHEX₁₇₁₋₁₈₅. Cell lysate of secPHEX-expressing HEK293 cells and control cells were negative. Molecular mass markers are indicated to the right.

3.1.3 Quantification of the secPHEX fraction in the conditioned medium

Total protein concentration in the conditioned medium after concentration was 0.9 μ g/ μ l. To analyse how much of the protein fraction was constituted of secPHEX; conditioned medium was quantified by image analysis of Coomassie stained SDS-PAGE. The quantification yielded a secPHEX/total protein ratio of 8% (Fig. 30).

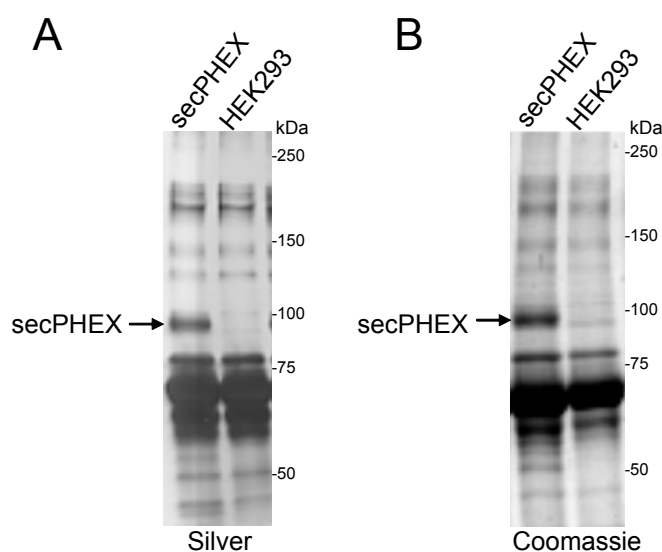


Fig. 30. secPHEX quantification in the conditioned medium. (A) Silver- and (B) Coomassie-stained 7.5% SDS-PAGE loaded with 3 μ g protein of conditioned medium from secPHEX-expressing HEK293 cells and control cells. Quantification of the Coomassie-stained SDS-PAGE yielded a secPHEX/total protein ratio of 8%. Molecular mass markers are indicated to the right.

3.2 Endopeptidase activity of secPHEX

3.2.1 Analysis of the secPHEX activity

In order to determine whether secPHEX had endopeptidase activity, PTHrP₁₀₇₋₁₃₉ was used as control substrate. Digestion of PTHrP₁₀₇₋₁₃₉ by secPHEX has been demonstrated and results in the production of four degradation products by cleavage N-terminal of three aspartate residues (Boileau *et al.* 2001). pH was optimized in order to ensure maximal secPHEX activity by determining activity at pH between 7.2 and 5.2. PTHrP₁₀₇₋₁₃₉ cleavage was tested in the conditioned medium from secPHEX-expressing HEK293 cells and in the conditioned medium from HEK293 control cells. Degradation was observed after 30 min incubation in the presence of secPHEX, but not in the control samples. Activity was only observed at pH 7.2 (Fig. 31).

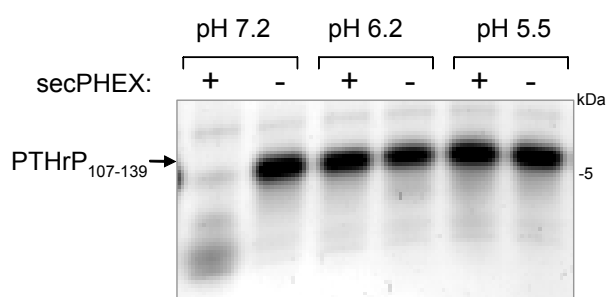


Fig. 31. Analysis of secPHEX activity. Silver-stained 16.5% Tris-tricine gels showing the degradation of PTHrP₁₀₇₋₁₃₉ by secPHEX protein. PTHrP₁₀₇₋₁₃₉ (1 µg) was incubated for 30 min at 37°C with 5 µg of protein from concentrated conditioned medium from secPHEX-expressing HEK293 cells and control cells under decreasing pH conditions. Specific degradation of PTHrP₁₀₇₋₁₃₉ was only observed at pH 7.2.

3.2.2 Inhibition of secPHEX activity

The effect of different inhibitors interfering with secPHEX activity was next examined. Complete mini EDTA-free tablets that efficiently inhibit serine and cysteine proteases but not metalloproteases, complete mini EDTA-plus tablets to inhibit maximal protease activity, and 1 mM EDTA that inhibits specific metalloproteases were mixed with conditioned medium for 15 min before addition of the substrate. Results indicate that 100% inhibition of secPHEX activity was only achieved in the presence of EDTA (Fig. 32).

These results provided evidence that PTHrP₁₀₇₋₁₃₉ was specifically degraded due to the secPHEX activity and not by other extracellular proteases present in the conditioned medium. To rule out the possibility that Dec-RVKR-CMK interferes with the activity of secPHEX, we also examined the effect of this inhibitor. Cleavage of PTHrP₁₀₇₋₁₃₉ by secPHEX was not inhibited in the presence of Dec-RVKR-CMK (Fig. 32).

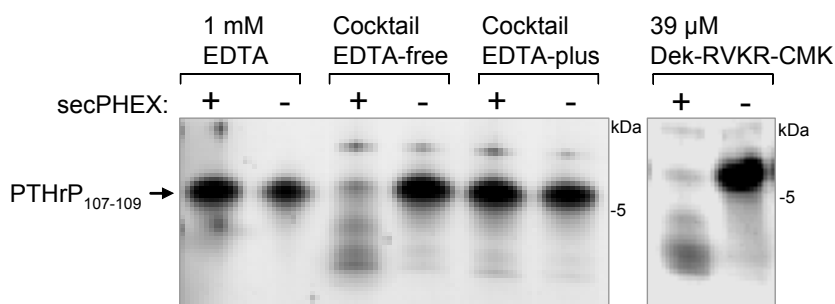


Fig. 32. Inhibition of secPHEX. secPHEX activity was studied in the presence of different inhibitors. Reaction mixtures, 5 μg of protein-containing conditioned medium premixed with inhibitor and then incubated with 1 μg PTHrP₁₀₇₋₁₃₉, were subjected to a 16.5% Tris-tricine gel and silver stained. Inhibition was achieved with 1 mM EDTA or complete EDTA-plus protease inhibitor cocktail, but not with complete EDTA-free protease inhibitor cocktail or 39 μM Dec-RVKR-CMK. Molecular mass markers are indicated to the right.

3.3 secPHEX co-incubation with FGF23

To investigate whether FGF23 is a PHEX substrate, different FGF23 protein constructs were co-incubated with secPHEX. Concentrated conditioned medium from HEK293 cells expressing N-terminal FLAG-tagged FGF23 (FLAG/FGF23) and affinity purified C-terminal His-tagged FGF23 (FGF23/His) were mixed with concentrated conditioned medium from secPHEX-expressing HEK293 cells or untransfected HEK293 control cells. Samples were incubated at pH 7.2 and 37°C for up to 3 h. Western blot analysis using anti-FLAG M2-HRP and anti-His (C-term)-HRP antibodies revealed three bands corresponding to intact (FGF23₂₅₋₂₅₁) (30 kDa) and N-terminal (FGF23₂₅₋₁₇₉) (18 kDa) or C-terminal (FGF23₁₈₀₋₂₅₁) (12 kDa) fragments (Fig. 33). None of the tagged proteins showed specific cleavage or significant degradation.

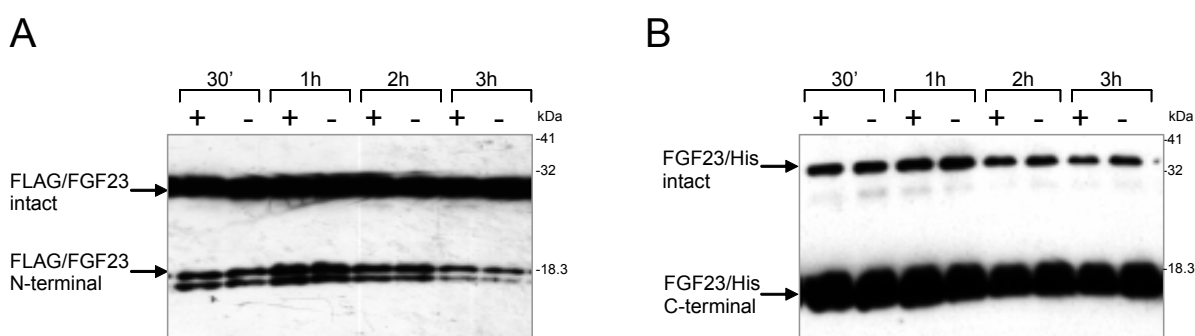


Fig. 33. Assessment of tagged FGF23 hydrolysis by western blot analysis. Protein-containing conditioned medium (3 μg) from HEK293 cells expressing or not expressing secPHEX were mixed with 3 μg of FLAG/FGF23 protein from concentrated conditioned medium (A) or 300 ng of FGF23/His purified protein (B). Samples were incubated at pH 7.2 and 37°C for 30 min up to 3 h. Proteins were separated through 12%

SDS-PAGE and analysed by western blot using anti-FLAG M2-HRP or anti-His (C-term)-HRP antibodies. Bands around 32 and 18 kDa or 14 kDa showed no signs of degradation. (+) refers to conditioned medium samples from secPHEX expressing-HEK293 cells and (-) refers to conditioned medium from untransfected HEK293 of control cells. Molecular mass markers are indicated to the right.

secPHEX stability during the experiment was proven by performing a western blot with antiPHEX₁₇₁₋₁₈₅ polyclonal antibody (Fig. 34). SecPHEX was unaltered after 3 h at 37 °C.

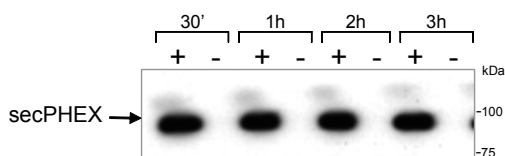


Fig. 34. Analysis of the secPHEX stability. Western blot using anti-PHEX₁₇₁₋₁₈₅ antibody was performed to verify the stability of secPHEX after the assay. (+) refers to conditioned medium samples from secPHEX expressing-HEK293 cells and (-) refers to conditioned medium from untransfected HEK293 of control cells. A stable band around 100 kDa appeared only in the conditioned medium from secPHEX-expressing HEK293 cells. Molecular mass markers are indicated to the right.

To prove that the tags within the fusion proteins did not interfere with the cleavage process, the same experiment was performed with native FGF23. Western blot analysis using antiFGF23₁₇₃₋₁₈₇ antibody revealed no specific cleavage or significant degradation of intact (FGF23₂₅₋₂₅₁) and N-terminal (FGF23₂₅₋₁₇₉) or C-terminal (FGF23₁₈₀₋₂₅₁) fragments (Fig. 35 A).

To rule out the possibility that the lack of carboxypeptidase activity in this assay disrupts degradation of FGF23 by secPHEX, the C-terminal arginine residue (p.R179) in the FGF23₂₅₋₁₇₉ intermediate after SPC cleavage was removed. Native FGF23₂₅₋₁₇₈ expression plasmid (pcDNA/FGF23₂₅₋₁₇₈) was stable transfected in HEK293 cells and conditioned medium was prepared. A co-incubation assay was conducted under the same conditions (Fig. 35 B). Degradation or cleavage could not be shown.

The assay was finally performed with only intact FGF23. Conditioned medium was harvested after inhibition of FGF23 cleavage by SPCs with Dec-RVKR-CMK and again samples were incubated in the presence and absence of secPHEX (Fig. 35 C). In these experiments, neither intact FGF23 nor FGF23₂₅₋₁₇₈ fragment showed specific cleavage or signs of degradation.

SecPHEX was also able to degrade PTHrP₁₀₇₋₁₃₉ after the addition of conditioned medium from FGF23₁₋₂₅₁-expressing cells indicating that FGF23 does not interfere with secPHEX endopeptidase activity.

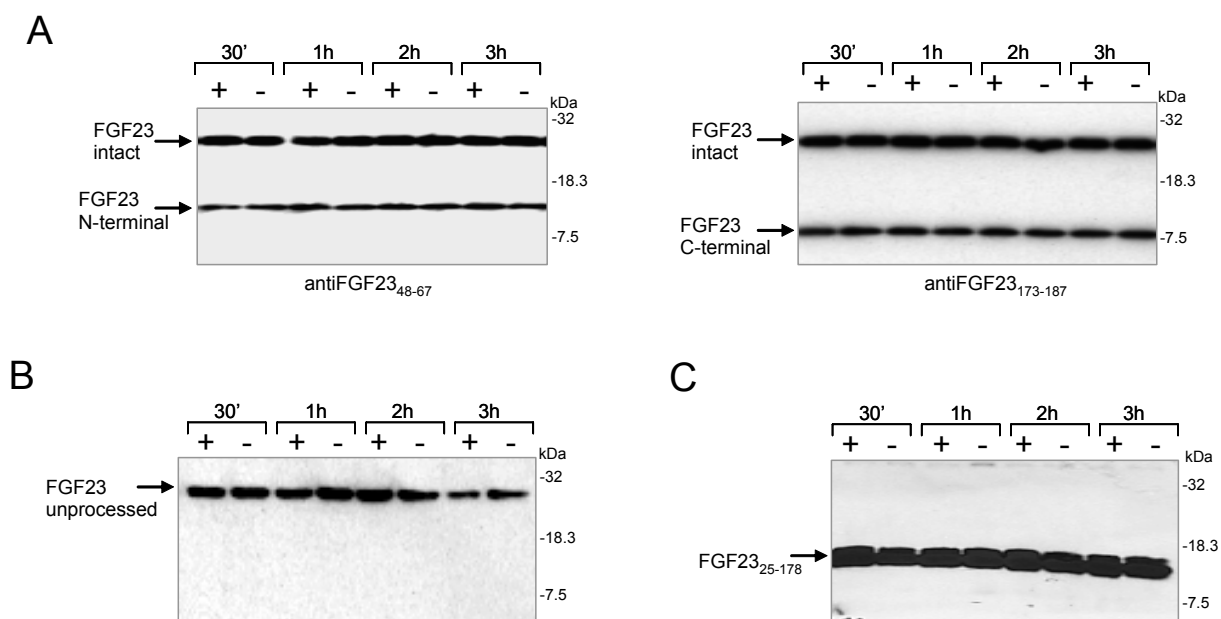


Fig. 35. Assessment of native FGF23 hydrolysis by western blot analysis. Proteins (3 μ g) of conditioned medium from HEK293 cells expressing (+) or not expressing (-) secPHEX were mixed with 3 μ g protein of conditioned medium from HEK293 cells expressing native FGF23 (A), unprocessed native FGF23 (B) or FGF23₂₅₋₁₇₈ fragment (C). Bands of 30, 18 and 12 kDa appeared and presented no signs of degradation or specific cleavage. Samples were incubated at pH 7.2 and 37°C for 30 min up to 3 h. Proteins were separated on 12% SDS-PAGE and immunoblotted using antiFGF23₄₈₋₆₇ or antiFGF23₁₇₃₋₁₈₇ antibodies.

D. DISCUSSION

1. NATIVE FGF23

This project is based on the study of a novel hormone, FGF23, which is mutated in patients with the renal phosphate wasting disorder ADHR (The ADHR Consortium 2000). FGF23 is located on the chromosome 12p13 only 55 kb separated from FGF6 (The ADHR Consortium 2000). Clustering of FGF genes have been reported and supports a model of local gene duplications and chromosomal translocations during evolution (Itoh and Ornitz 2004). Since the increase in the number of FGF genes is associated with the period of main evolutionary change that coincided with the origin of vertebrates, an important function of FGF/FGFR interactions has been proposed in the development of the skeletal system (Coulter *et al.* 1997).

1.1 Overview of the FGF23 sequence

FGF23 contains a predicted ORF of 251 amino acids and is the longest FGF member described up to now. Together with FGF21 and FGF19, FGF23 belongs to the FGF19 subfamily (Fig. 36). Members of the same subfamily show increased sequence similarity, structure and biochemical properties (Ornitz and Itoh 2001). All FGFs share a common core sequence with 12 β -strands that determines the characteristic three-dimensional β -barrel structure of this protein family (see introduction Fig. 4). Alignment of the core sequence between FGF23 and the other family members showed a 25-36% amino acid identity (The ADHR Consortium 2000). The last four residues in the core sequence of FGF23 define a subtilisin-like proprotein convertase (SPC) motif conserved in all species except in *Fugu rubripes*. FGF23 alignment among species shows a high homology at the N-terminal part but not at the part C-terminal from the SPC cleavage site (see results Fig. 7). FGF23 has the longest C-terminal fragment among the members of the FGF family.

Interestingly, all *FGF23* mutations reported so far in ADHR (p.R176Q, p.R179Q, p.R179W) are located at the SPC cleavage motif (RXXR) and are conserved among species from fish to mammals (see results Fig. 8); these mutations make the protein resistant to cleavage by SPCs. The novel *FGF23* mutation (p.S71G) found in patients with autosomal recessive FTC (see results Tab. 11) is located in the conserved N-terminal β -

barrel structure. The serine residue at position p.S71 is also conserved among species, from fish to mammals (see results Fig. 8). According to structure modeling, it is situated at the end of the loop between strand 3 and 4 of the FGF β -barrel structure (Harmer *et al.* 2004). This serine probably has an important function since mutant FGF23-S71G remains stacked inside the cells interrupting its maturation process.

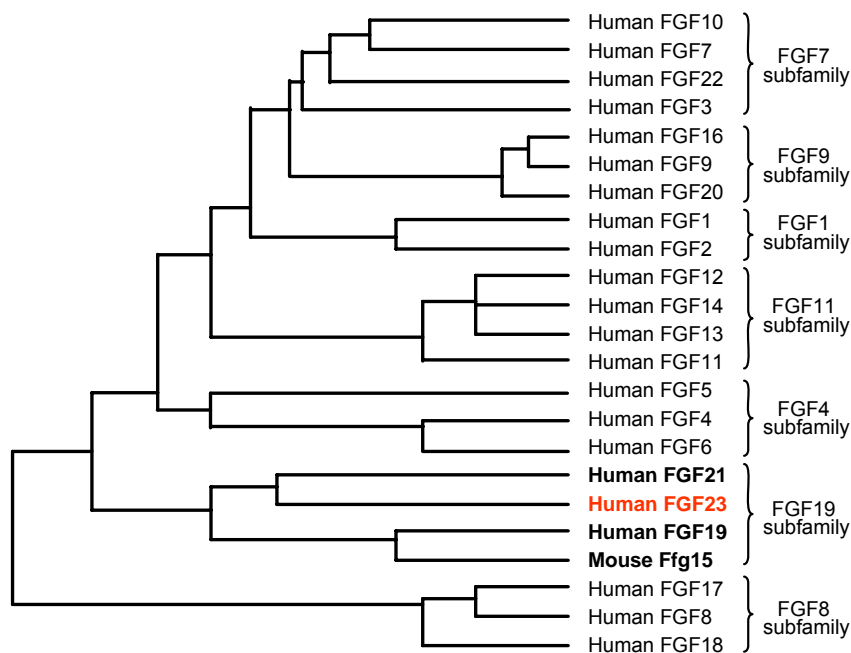


Fig. 36. The evolutionary relationships within the human fibroblast growth factor (FGF) gene family. Twenty-two FGF encoding genes have been identified in the human genome. Phylogenetic analysis suggests that these genes can be arranged into seven subfamilies, each containing two to four members. Branch lengths are proportional to the evolutionary distance between each gene. Human FGF15 and mouse Fgf19 have not been identified. Since human FGF19 is most closely related to mouse Fgf15 (51% amino acid identity), Fgf15 is thought to be the ortholog of human FGF19 (Adapted from Itoh and Ornitz 2004).

The first 24 residues from the predicted FGF23 protein sequence determine a putative signal peptide. Members of the FGF family are often paracrine factors, but it is possible to identify some FGFs to be present in serum (Ikemoto *et al.* 1999, Larsson *et al.* 2002). Most FGFs have N-terminal signal peptides and are readily secreted from cells. FGFs 1, 2, 9, 16 and 20 lack obvious, cleavable N-terminal signal peptides but can be nevertheless secreted. FGF22 remains attached to the cell surface rather than being secreted. FGFs 11-14 lack also signal peptides, remain intracellular and function within cells in a receptor-independent manner (for review see Itoh and Ornitz 2004). Thus, a question that arose in the present study was whether FGF23 is a secreted factor as well.

1.2 FGF23 is a secreted protein

The analysis performed in this study demonstrates that FGF23 is in fact a secreted protein with a molecular mass of around 30 kDa. When plasmids containing the native FGF23 protein were stable transfected into HEK293 cells, FGF23 was detected in the supernatant but not in the cell lysate using specific antiFGF23 antibodies, antiFGF23₄₈₋₆₇ and antiFGF23₁₇₃₋₁₈₇ (see results Fig. 14). Two additional N- and C-terminal fragments around 18 and 12 kDa respectively were also detected with the corresponding antibodies indicating cleavage of FGF23 during or after biosynthesis. The same cleavage products were observed when N- and C-terminal tagged FGF23 protein constructs were transfected into HEK293 cells and detected with antibodies directed against the tags (see results Fig. 15). Expression of FGF23 in cells from other species including opossum kidney (OK/E), African green monkey kidney (COS-7), and Chinese hamster ovary (CHO) demonstrated the same processing (White *et al.* 2001, Shimada *et al.* 2001).

Mass spectrometry analysis confirmed that the smaller 12 kDa fragment belongs to the C-terminal part of the FGF23 protein (see results Fig. 21). Unfortunately, determination of the first residue from the C-terminal FGF23 fragment was not possible by peptide mass fingerprinting. Shimada *et al.* showed by amino acid sequencing that the smaller product had p.S180 at its N-terminus. The preceding amino acid sequence of p.S180, 176RHTR179 agrees with the SPC consensus proteolytic cleavage sequence RXXR (Shimada *et al.* 2001).

Specificity of the cleavage was analysed by adding conditioned medium containing native FGF23 to untransfected HEK293 cells, indicating that no further cleavage occurs after secretion (see results Fig. 18). In addition, intact FGF23 as well as N- and C-terminal fragments are stable peptides, since incubation of FGF23 at room temperature up to 24 hours and at 37°C did not alter the stability of the protein (see results Fig. 17).

Taken together, these results provided evidence that FGF23 is a secreted protein that undergoes partial cleavage into two fragments, FGF23₂₅₋₁₇₉ and FGF23₁₈₀₋₂₅₁, during biosynthesis in HEK293 cells and ruled out the possibility that the smaller FGF23 fragments were products of unspecific degradation. The observation that the SPC cleavage site (RXXR) is highly conserved among species and that FGF23 proteolysis was confirmed in other cell systems suggest a physiological relevance of the FGF23 cleavage.

1.3 Analysis of the FGF23 cleavage

The processing of prepro- and pro-polypeptides to a mature form is critical for proper secretion. Many of the secreted factors that influence renal and bone mineral homeostasis, such as the bone morphogenic proteins (BMPs) (Constam and Robertson 1999), parathyroid hormone (PTH) (Hendy *et al.* 1995), and PTH-related peptide (PTHrP) (Liu *et al.* 1995) undergo cleavage by the subtilisin-like proprotein convertase family. Complete inhibition of FGF23 cleavage using the SPC inhibitor Dek-RVKR-CMK indicates that native FGF23 is specifically cleaved by enzymes of this family in HEK293 cells (see results Fig. 24).

Evidence supporting the cleavage and activation by SPCs include FGF related growth factors that play important roles in bone growth and development such as platelet-derived growth factor (PDGF)-A and -B (Ostman *et al.* 1992), pro-transformant growth factor β (pro-TGF β) (Dubois *et al.* 2001), and insulin-like growth factor (IGF)-I and -II (Duguay *et al.* 1997 and 1998). Furthermore, some secreted factors are processed by more than one SPC family member, such as bone morphogenic protein-4 (BMP4), which shows enhanced cleavage in the presence of SPC1 or SPC6 (Cui *et al.* 1998). Most tissues and cell lines express more than one SPC (Bergeron *et al.* 2000). It can not be excluded that the cells that secrete FGF23 *in vivo* express other SPCs than the model HEK293 system used for the present studies implying other modifications to FGF23 in its natural tissue.

Recent reports show that bone is the predominant site of Fgf23 expression in mice (Liu *et al.* 2003). To provide evidence whether FGF23 cleavage by proprotein convertases is of physiological significance, expression of SPCs in mouse osteoblasts as well as in HEK293 cells was examined (see results Fig. 25). The finding that SPC2, SPC4, and SPC7 are expressed in osteoblasts as well as in HEK293 cells raised the possibility that FGF23 is also cleaved by SPCs *in vivo*. Furthermore, we demonstrated that cleavage of FGF23 occurs intracellularly, before or during secretion, where localization of SPC2, SPC4, and SPC7 has been reported (Thomas 2002).

1.4 FGF23 glycosylation

Intact FGF23 is predicted to have a molecular mass of 27.9 kDa (Swiss-Prot accession number Q9GZV9). Provided that a molecular mass of 30 kDa was estimated by SDS-

PAGE, our findings could imply that FGF23 undergoes post-translational modifications. More than half of all proteins and many lipids in biological systems are glycosylated (Van de Steen *et al.* 1998). While N-linked oligosaccharides are characterized by big structures producing large changes in the molecular mass of the protein (more than 3.5 kDa), O-linked sugars are usually less massive although they can be more numerous. As the difference between predicted (27.9 kDa) and SDS-PAGE observed (30 kDa) molecular mass of FGF23 is not any greater than 2-3 kDa, FGF23 may undergo O-glycosylation. The use of N-glycosidases failed to deglycosylate FGF23 whereas O-glycosidase and neuraminidase treatment resulted in a decrease of the molecular mass of intact FGF23 as well as both N- and C-terminal FGF23 fragments (see results Figs. 19 and 20). Thus, we conclude that FGF23 is O-glycosylated at the N- and C-terminal fragment.

O-linked sugars can be very heterogeneous and eight core structures have been identified so far. The most common modification of the core is mono-, di- or tri-sialylation (Hounsell *et al.* 1996). The oligosaccharides linked to FGF23 must be composed by a sialylated N-acetyl galactosamine (GalNAc) residue (Fig. 37) since O-glycosidase could only remove the sugar chain after incubation with neuraminidase. Thus, elimination of external sialic acid (NeuAc) with neuraminidase, followed by the elimination of the GalNAc core with O-glycosidase, resulted in a slight advance of the FGF23 migration (see results Fig. 20).

A consensus primary amino acid sequence for O-glycosylation has not been clearly defined. However, there is substantial evidence that serine and threonine residues, often in combination with proline, alanine, glycine, or valine, are potential sites of O-glycosylation (Kirnarsky *et al.* 1998). O-glycosylation is a post-translational and postfolding event. Therefore, only exposed serines and threonines will be glycosylated. In accordance with this, mucin-type O-glycosylation occurs mostly on β -turns of the secondary structure or other regions with an extended conformation, and in regions with low hydrophobicity (Van de Steen *et al.* 1998).

O-linked glycosylation plays a major role in determining the structure of the fully folded protein; it is essential in the recognition process for protein-protein interactions and contributes to the activity of signalling molecules (Van de Steen *et al.* 1998). Our results show that native FGF23 is O-glycosylated at the N- and C-terminal fragments. Also, Shimada *et al.* reported variations of the number of O-linked sugar chains in the FGF23-R176Q and -R179Q mutant proteins (Shimada *et al.* 2002). More experiments will be

necessary to confirm these data because O-linked glycosylation could play an important role in modulating the physiological function of FGF23.

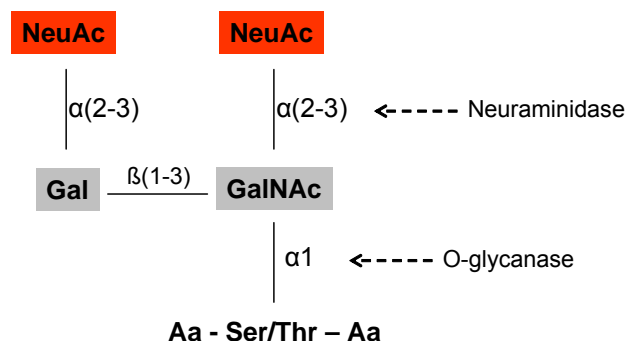


Fig. 37. O-linked glycosylation. The most common type in mammals is the mucin-type oligosaccharide. This structure includes an O-linked N-acetylgalactosamine (GalNAc) residue directly attached to a serine or threonine, followed by β 1-3 linked galactose (Gal) and α 2-3 linked N-acetylneuraminic acid (NeuAc).

1.5 FGF23 expression in human and mouse tissues

Multiple tissue Northern blots of human mRNAs failed to detect FGF23 transcripts and nested RT-PCR was required to detect FGF23 in RNA from human tissues such as whole fetus, heart, liver, thyroid/parathyroid, small intestine, testis, skeletal muscle, differentiated chondrocytes, and TIO tumor tissue (see results Tab. 10). FGF23 expression in heart, liver, and TIO was confirmed by another group (Shimada *et al.* 2001). In mice the Fgf23 transcript was detectable in 17 days embryo and spleen (see results Tab. 10). Fgf23 expression by RT-PCR was also demonstrated in brain, thymus, small intestine and heart of adult mice. Expression of Fgf23 in the ventrolateral thalamic nucleus of the brain was reported by *in situ* hybridization (Yamashita *et al.* 2000).

In accordance to our results, Mirams *et al.* confirmed the detection of FGF23 expression in liver and in the human hepatoma cell line (HUH-7) by real-time RT-PCR (Mirams *et al.* 2004). This finding could indicate a physiological role of FGF23 in the liver.

The same group found FGF23 expression in kidney tissue, in human embryonic kidney (HEK293) and opossum kidney (OK/E) cell lines. Liu *et al.* also detected low levels of Fgf23 mRNA expression in mouse kidney (Liu *et al.* 2003). In contrast, our results were negative for FGF23 expression in kidney and in HEK293 cells.

TIO tumors express abundant amounts of FGF23 mRNA, and FGF23 protein could be visualized by western blot analysis of tumor extracts (White *et al.* 2001). In addition, FGF23 was detected at high levels in serum from TIO patients but not from healthy controls (Yamazaki *et al.* 2002) suggesting that FGF23 is expressed and secreted into the circulation at low levels under normal circumstances.

1.5.1 FGF23 expression in bone

Although it has been supposed that bone is the source of FGF23, the principal site of secretion of circulating FGF23 is unknown. The investigations performed could neither show FGF23 transcripts in mice calvaria nor in human osteosarcoma cells (SaOS) and mouse osteoblastic cell line (MC3T3). Also other groups found no evidence for expression of FGF23 in bone (Yamashita *et al.* 2000, Guo *et al.* 2001 and 2002, Liu *et al.* 2002, White *et al.* 2001, Bai *et al.* 2003). However, recent studies could detect FGF23 expression in human bone by real-time quantitative RT-PCR (Mirams *et al.* 2004), and in osteogenic cells of trabecular bone by *in situ* hybridization (Riminucci *et al.* 2003). The expression of FGF23 in human bone is consistent with expression analyses in mice and rats where expression has been reported to be highest in bone (Liu *et al.* 2003, Ijuin *et al.* 2004). Ijuin *et al.* also showed a positive correlation of the amount of Fgf23 protein with osteoblast differentiation and bone nodule formation. These findings strongly suggest that FGF23 may be directly involved in bone formation independently of its systemic actions.

2. AUTOSOMAL DOMINANT HYPOPHOSPHATEMIC RICKETS

2.1 FGF23-R176Q and -R179Q mutant proteins are resistant to cleavage

In contrast to native FGF23 protein that is sensitive to protease cleavage during its biosynthesis, FGF23-R176Q, -R179W and -R179Q mutant proteins are resistant to cleavage after stable transfection into HEK293 cells (see results Fig. 23). Most probably, the mutations disrupt the 176RXXR179 motif of a SPC cleavage site. Secretion of the intact FGF23 may stabilize the protein and lead to renal phosphate wasting in ADHR patients.

If FGF23 is normally co-expressed with the SPC enzymes then the majority of native FGF23 will probably be cleaved into fragments during secretion. In the case of TIO,

increased FGF23 expression may overwhelm SPCs activity, and the major portion of FGF23 would be secreted in its intact form. In support of this idea, only the 30 kDa FGF23 protein species was detected in a tumor causing TIO. Both p.R176 and p.R179 FGF23 mutations were not detected in DNA from this tumor (White *et al.* 2001).

2.2 ADHR mutations cause gain of protein function

ADHR does not arise from FGF23 haploinsufficiency because the experiments performed in this study demonstrated that the mutants are efficiently translated and secreted by mammalian cells (see results Fig. 23). Furthermore, FGF23 protein has been detected in TIO tumors (White *et al.* 2001) and circulates at high levels in serum from patients with TIO (Yamazaki *et al.* 2002, Jonsson *et al.* 2003). As serum phosphate levels become normal after resection of the tumors, it is likely that intact FGF23 functions as the phosphaturic factor in these conditions.

Studies in mice showed that administration of intact FGF23₂₅₋₂₅₁ (Shimada *et al.* 2001) or through subcutaneous implantation of cells expressing FGF23 into nude mice (Shimada *et al.* 2002, Bai *et al.* 2003) caused renal phosphate wasting. Others demonstrated that administration of FGF23-R179Q (Segawa *et al.* 2003) or FGF23-R176Q (Bai *et al.* 2003) significantly decreased renal Na/Pi cotransport activity in kidneys from normal rats. Taken together, these data provide evidence that FGF23 is a phosphaturic substance and that ADHR does not arise from inactivating mutations in a phosphate conserving factor. Rather, ADHR mutations enhance the phosphaturic activity of FGF23.

Because the SPC family is often associated with activation of their substrates, we cannot rule out a possible biological role for the FGF23 cleavage products under normal physiological conditions, perhaps as autocrine or paracrine agents, as in the case of other members of the FGF family (Hannon *et al.* 1996, Hurley *et al.* 1994). Interestingly, the C-terminal fragment of neuronal growth factor β (NGF β) produced by partial SPC cleavage binds to tyrosine kinase receptors (Trk) promoting neuronal innervations and survival whereas intact pro-NGF β binds to the neurotrophin receptor (p75NTR) thereby activating apoptosis (Bono *et al.* 1999).

2.3 Searching for the FGF23 receptor

Four functional FGF receptors have been identified in humans (Itoh and Ornitz 2004). However, it remains to be solved which receptor(s) is involved in FGF23 signalling. Preliminary reports demonstrate that FGF23 binds to the FGFR2 and FGFR4 receptors, both of which are expressed in the kidney and FGF23-R179Q showed preferentially binding to FGFR4 (Jonsson *et al.* 2001). Yamashita *et al.* showed FGF23 binding to FGFR3c and FGFR2c but not to FGFR1c by the Biacore system. FGF23 binding to FGFR3c inhibited renal phosphate reabsorption *in vitro* through a MAPK-dependent mechanism (Yamashita *et al.* 2002). A mutation in the FGFR1 was recently found to be the cause of the novel syndrome osteoglophonic dysplasia (White *et al.* 2005). The renal phosphate wasting and the elevated FGF23 levels in some of these patients raised the question whether FGF23 binds the FGFR1 receptor.

3. FAMILIAL TUMORAL CALCINOSIS WITH HYPERPHOSPHATEMIA

3.1 FGF23 in familial tumoral calcinosis

3.1.1 FGF23-S71G mutant protein is not secreted

Autosomal recessive familial tumoral calcinosis (FTC) with hyperphosphatemia is characterized as being the metabolic mirror image of the hypophosphatemic conditions (see introduction Tab. 1). Sequence analysis of the *FGF23* gene in an affected individual revealed a homozygous missense mutation, encoding a p.S71G substitution, whereas non-affected family members were either heterozygous or homozygous for the wild-type allele (see results Fig. 22). The heterozygous parents and one heterozygous sister showed no abnormalities in clinical and biochemical parameters, including serum FGF23 levels (see results Tab. 12), indicating that the expression of one *FGF23* allele can compensate the manifestation of FTC. This is consistent with recent reports that showed viability of Fgf23 heterozygous mice (Shimada *et al.* 2004, Sitara *et al.* 2004).

In contrast to native FGF23 that is secreted into the medium, cell culture experiments demonstrated that the intact FGF23-S71G isoform is retained within the Golgi complex whereas only the C-terminal fragment is secreted (see results Figs. 26 and 27). Retention in the Golgi complex has also been reported in other mutant proteins (Mulders *et al.* 1998,

Sabbagh *et al.* 2001 and 2003). The N-terminal fragment was not detectable, neither within the cell nor in the conditioned medium, suggesting that this fragment is degraded.

3.1.2 FTC mutation causes “loss” of function

In order to show whether the *in vitro* experiments I performed reflect the *in vivo* situation, FGF23 in serum was measured with a commercially available FGF23 sandwich ELISA that uses polyclonal antibodies against peptides within the C-terminal part of FGF23 thereby measuring intact FGF23 as well as the C-terminal fragment. Markedly elevated FGF23 levels were found in the affected individual. Most probably, these levels represent elevated concentrations of the C-terminal fragment as demonstrated by the cell culture experiments. In contrast to hypophosphatemia in ADHR which is caused by gain of function mutations of FGF23, and in TIO which is caused by over expression of FGF23, these results indicate that hyperphosphatemia in FTC is caused by a loss or reduction of FGF23 function due to loss or at least decrease of intact FGF23 in the circulation.

It has been shown that over expression of both intact FGF23 (Shimada *et al.* 2002) or FGF23-R176Q, -R179Q (Segawa *et al.* 2003, Bai *et al.* 2003) in mice is associated with hypophosphatemia reflecting the TIO and ADHR situations in human disease. It is less well established whether N-terminal FGF23₂₅₋₁₇₉ or C-terminal FGF23₁₈₀₋₂₅₁ alone causes renal phosphate wasting. There is only a single report demonstrating that the administration of intact FGF23 to rodents caused renal phosphate wasting whereas the administration of N-terminal FGF23₂₅₋₁₇₉ and C-terminal FGF23₁₈₀₋₂₅₁ did not (Shimada *et al.* 2002). The results of this study exclude the possibility that the C-terminal fragment alone can cause phosphate wasting.

Hyperphosphatemia due to increased renal phosphate reabsorption and increased 1,25-dihydroxyvitamin D serum levels have also been found in Fgf23 null-mice (Shimada *et al.* 2004, Sitara *et al.* 2004). However this mouse model showed in addition severe bone tissue abnormalities, severe growth retardation and reduced life span possibly because of marked vascular calcification in the kidneys, impaired renal function and hypoglycemia. These differences between the mouse model and human FTC, either due to *FGF23* or *GALNT3* mutations, can either be explained by residual function of FGF23 in humans or by inadequacy of the mouse model. A residual function may be explained by low levels of

mutated intact FGF23, but a physiological function of the abundant C-terminal fragment cannot be excluded.

3.2 GALNT3 in familial tumoral calcinosis

In a second family presenting the characteristic features of FTC with hyperphosphatemia mutations in the *GALNT3* gene were found. Sequence analysis of the *GALNT3* gene in the affected individuals (mother and son) revealed a homozygous missense mutation, encoding a p.G329R substitution (see results Fig. 22). These findings are consistent with autosomal recessive inheritance. The same homozygous mutation was found in the healthy daughter. Since the clinical manifestations of FTC may be variable (see introduction 3.1) and her mother was first diagnosed at the age of 44 years (Blay *et al.* 2001), underdiagnosis of the disease due to low penetrance or late onset could have occurred in this family member.

GALNT3 is an N-acetylgalactosaminyltransferase responsible for the initiation of O-linked glycosylation. A nonsense mutation causing premature termination of protein translation and an aberrant splice site mutation in the *GALNT3* gene have already been described in individuals with FTC (Topaz *et al.* 2004). The missense mutation p.G329R is situated between the catalytic domain and the ricin-like domain, in a linker region that contains several residues important for the maintenance of the three-dimensional enzyme structure (Fritz *et al.* 2004). This glycine (p.G329) is highly conserved among species (Schwientek *et al.* 2002) and within members of the same family (Bennett *et al.* 1999) suggesting an important role of this residue in the linker region.

The fact that FTC can be caused by mutations in a glycosyltransferase, GALNT3, or in a glycosylated factor, FGF23, suggests that FGF23 could be a substrate of GALNT3. Elevated FGF23 levels have recently been reported in two families with FTC due to mutations in the *GALNT3* gene (Topaz *et al.* 2004). Although we demonstrated that mature FGF23 contains O-linked sugars, it is unlikely that the serine substituted in FGF23-S71G is O-glycosylated. According to structure modeling, this serine is solvent inaccessible (Harmer *et al.* 2004) and would sterically not allow O-glycosylation. Nevertheless, our results do not exclude that FGF23 is O-glycosylated by GALNT3 in other candidate sites and further experiments are necessary to prove whether there is a physiological interaction between FGF23 and GALNT3.

4. FGF23 IN X-LINKED HYPOPHOSPHATEMIC RICKETS

4.1. Does PHEX function as an endopeptidase?

Studies with *Hyp* and *Gy* mouse models together with the phenotypic similarities between ADHR, XLH and TIO, suggested that PHEX, a type II membrane protein with endopeptidase activity, and FGF23, a circulating phosphaturic hormone, are involved in the same pathway of the phosphate homeostasis. Loss of function mutations of PHEX and gain of function mutations of FGF23 formed the basis for a hypothesis to explain the common pathogenesis of these hypophosphatemic disorders (see introduction 2). According to this hypothesis FGF23 might be a substrate of PHEX, but this has not been proven yet (Strewler 2001, Jan de Beur *et al.* 2002).

PHEX contains key residues required for catalytic activity of small peptides (Campos *et al.* 2003), but a defined physiological substrate remains to be identified. PHEX does cleave at the N-terminus of acidic amino acid residues (Asp or Glu) and has a strong preference for Asp (Boileau *et al.* 2001, Campos *et al.* 2003). This was shown by PHEX cleavage analysis of small internally quenched synthetic fluorogenic peptides (IQFP) (Campos *et al.* 2003).

Degradation of FGF23 by PHEX in an *in vitro* translation system has initially been reported (Bowe *et al.* 2001), but has not been confirmed by others. More likely, degradation in the *in vitro* translation system is caused by the presence of contaminating enzymes in the reticulolysate (Liu *et al.* 2003). FGF23 processing by PHEX was also excluded using co-expression of tagged FGF23 and tagged PHEX (Liu *et al.* 2003). Further, membranes from cells expressing recombinant PHEX have been used to assess endopeptidase activity on potential substrates. Reports concerning PHEX degradation of PTH are also inconsistent (Jean *et al.* 1995, Lipman *et al.* 1998). Guo *et al.* excluded PHEX cleavage of stanniocalcin 1, casein and a FGF23 peptide (amino acid 172-186) but reported specific cleavage of [Leu]enkaphalin (Guo *et al.* 2001). Boileau *et al.*, using a secreted form of PHEX, showed that it cleaves PTHrP₁₀₇₋₁₃₉ (Boileau *et al.* 2001).

On the other hand, members of the FGF family, such as FGF3, are processed by SPC protease cleavage before further hydrolysis can occur. Antoine *et al.* showed that *Xenopus* and mouse *Fgf3* homologs are proteolytically processed at RQRR or RLRR motifs,

respectively, from a 31 kDa form to a 27 kDa species with increased biological activity and alternatively extracellular cleavage by exogenous plasminogen was determined *in vitro* (Antoine *et al.* 2000).

4.2 Co-incubation of FGF23 and PHEX in an optimized assay

The purpose of this experiment was to minimize possible contaminating proteases. Therefore, I followed the strategy proposed by Boileau *et al.* (Boileau *et al.* 2001) to create a recombinant secreted form of the PHEX protein (see results Fig. 28) that allowed to work with conditioned medium from transfected cells (see results Figs. 29 and 30). Further, by using untagged PHEX and FGF23 was excluded possible interfering of tags with the cleavage process. Recombinant secPHEX catalytic activity was demonstrated by the degradation of PHTrP₁₀₇₋₁₃₉ (see results Figs. 31 and 32).

In this assay, secPHEX failed to hydrolyze intact FGF23₂₅₋₂₅₁ (see results Figs. 33 and 35) thereby excluding the possibility that PHEX in addition to SPCs cleaves FGF23 at the RHTR site. Also, the N-terminal (FGF23₂₅₋₁₇₉ and FGF23₂₅₋₁₇₈) and C-terminal (FGF23₁₈₀₋₂₅₁) fragments were not processed (see results Figs. 33 and 35) providing evidence against the possibility that FGF23 is cleaved at the sites detected within peptides derived from PHTrP₁₀₇₋₁₃₉, FGF23 and MEPE (Campos *et al.* 2003, Boileau *et al.* 2001). These results do not exclude the possibility that co-factors are required for the processing of the FGF23 protein by PHEX (Benet-Pagès *et al.* 2004).

On the other hand, it is unlikely that PHEX substrate specificity observed within small synthetic peptides can be extended to larger proteins due to incompatible three-dimensional structures that limit enzyme substrate interactions. The PHEX protein is similar to the NEP family of zinc metallopeptidases in several functional aspects such as conservation of the residues important for sequestering the zinc ion, stabilization of the transition state, and catalysis (Turner *et al.* 2001). The natural substrates for NEP are small (< 3 kDa), and this is also likely for PHEX (Oefener *et al.* 2000, Campos *et al.* 2003). Therefore, intact FGF23 (30 kDa) as well as N- and C- terminal fragments (18 kDa and 12 kDa) would be excluded as substrates because of their size.

Finally, since phosphaturic activity *in vivo* has only been ascribed to intact FGF23 so far, SPCs are likely to regulate FGF23 activity by inactivation whereas further processing of FGF23 may not have biological relevance at least in phosphate regulation.

4.3 PHEX proteolytic function remains unclear

Although other potential PHEX substrates such as MEPE (Guo *et al.* 2002) and DMP1 (Lemire *et al.* 1997) have been proposed, cleavage by PHEX has not been proven yet. PTHrP₁₀₇₋₁₃₉ is the only naturally occurring, small-peptide substrate cleaved by PHEX (Boileau *et al.* 2001). Bony fish is the simplest organism containing a PHEX ortholog. However, PTHrP₁₀₇₋₁₃₉ is absent in bony fish (Bianchetti *et al.* 2002), suggesting that PTHrP₁₀₇₋₁₃₉ either is an unlikely PHEX substrate or has emerged as an alternative substrate in higher organisms.

Notably, it has been demonstrated *in vitro* that PHEX binds but does not cleave MEPE (Guo *et al.* 2002, Rowe *et al.* 2004) and osteocalcin (Boileau *et al.* 2001). Further experiments are needed to confirm the nature of PHEX and its cell-surface interactions with MEPE, osteocalcin, and perhaps other matrix proteins. Moreover, since KELL protein binding to the XK protein does not implicate proteolytic cleavage (Lee *et al.* 1999, 2000, 2003), it is reasonable to speculate that PHEX may well function as a matrix-protein ligand.

The fact that FGF23 cannot be cleaved by PHEX leaves the question open whether PHEX may regulate FGF23 action by another mechanism than enzyme/substrate interaction. Recent results obtained in the double compound *Hyp*/*Fgf23* null mice showed elevated serum phosphate levels that were indistinguishable from those of *Fgf23* *-/-* animals (Sitara *et al.* 2004). This data provides further evidence that *Phex* is either directly or indirectly involved in the regulation or degradation of FGF23. An alternative hypothesis is that inactivating PHEX mutations can somehow upregulate FGF23 expression (Liu *et al.* 2003). This would suggest that increased circulating FGF23 in *Hyp* mice and in patients with XLH might be due to increased synthesis rather than reduced clearance. Furthermore, other possible PHEX substrates remain to be determined in order to elucidate the function of PHEX within phosphate homeostasis.

5. A MORE COMPLEX MODEL TO EXPLAIN PHOSPHATE REGULATION

The data provided in this study unravelled novel protein interactions of FGF23 that play an important role in modulating FGF23 function and therefore have physiological relevance in the hypophosphatemic disorders (Fig. 38). The experiments I performed demonstrated that FGF23 is cleaved by SPCs and this cleavage must be physiologically relevant since mutations disrupting the cleavage motif site are responsible for ADHR.

The demonstration that FGF23 can cause FTC, which is characterized by hyperphosphatemia, provided additional evidence about the importance of FGF23 in the regulation of phosphate homeostasis and suggests that FGF23 interacts with GALNT3, a glycosyltransferase that could be responsible for O-glycosylation of FGF23. It can be concluded that FGF23 mutations in hypophosphatemic rickets and FTC have opposite effects on phosphate homeostasis. Finally, the construction of an assay to test possible PHEX substrates demonstrated that PHEX does neither cleave FGF23 before nor directly after SPCs processing.

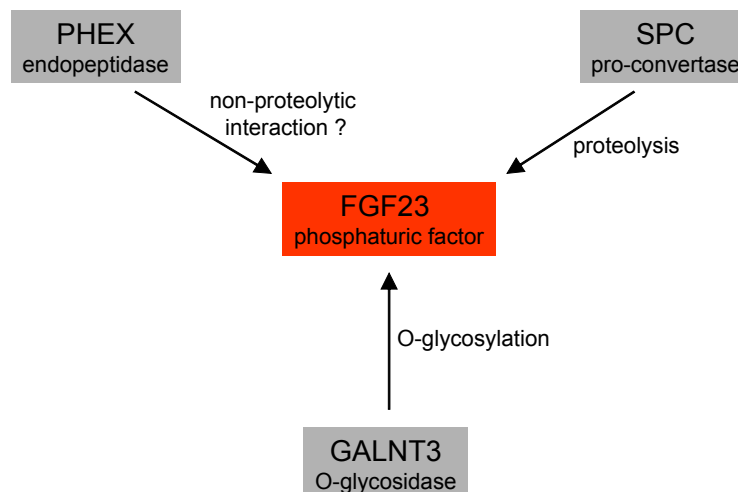


Fig. 38. Proteins involved in the modification of FGF23. FGF23 is cleaved by a subtilisin-like proprotein convertase (SPC) at the RXXR site whereas FGF23 proteolytic cleavage by PHEX could not be confirmed, leaving the question open whether FGF23 interacts with PHEX in a non-proteolytic way. In addition, FGF23 is O-glycosylated most likely by GALNT3.

Although our results showed that the model proposed has support for ADHR and TIO, there are a number of inconsistencies with regard to XLH, that raise concerns about whether a simple enzyme/substrate hypothesis is correct (see introduction 4). The

demonstration that other hormones such as FRP4 and MEPE are also overexpressed in TIO tumors and that MEPE causes inhibition of mineralization *in vivo* (Gowen *et al.* 2003), indicates that the pathophysiological mechanisms in these disorders are more complex. Since the bone phenotype in ADHR patients as well as in *Hyp* mice is not completely rescued by dietary phosphorus and vitamin D supplementation, a primary osteoblast defect has been suggested to cause these disorders in addition to renal phosphate wasting. Whether FGF23 has direct effects on bone mineralization has not been described yet.

Although the physiological function of FGF23 is not completely understood, there is strong evidence that indicates a very specific and independent effect of FGF23 in the regulation of phosphate homeostasis. Further studies will be important to understand the significance of the FGF23 cleavage as well as the possible function of FGF23 cleavage fragments. Identifying specific receptors for FGF23 will also generate valuable information about extra-renal or extra-skeletal actions as well as potential autocrine or paracrine actions of FGF23.

REFERENCES

- Adelman, R. D. & Solhaug, M. J. (2000) Phosphorus, 16th edn. W.B. Saunders Company, Philadelphia
- Antoine, M., Daum, M., Kohl, R., Blecken, V., Close, M. J., Peters, G. & Kiefer, P. (2000) NH₂-terminal cleavage of xenopus fibroblast growth factor 3 is necessary for optimal biological activity and receptor binding. *Cell Growth Differ* 11, 593-605
- Aono, Y., Shimada, T., Yamazaki, Y., Hasegawa, H., Hino, R., Takeuchi, Y., Fujita, T., Fukumoto, S., Nagano, N., Wada, M., Yamashita, T. (2003) The neutralization of FGF23 ameliorates hypophosphatemia and rickets in *Hyp* mice. *J Bone Miner Res* 18:S16
- Avioli, L. V., Birge, S., Lee, S. W. & Slatopolsky, E. (1968) The metabolic fate of vitamin D₃-3H in chronic renal failure. *J Clin Invest* 47, 2239-2252
- Bai, X., Miao, D., Panda, D., Grady, S., McKee, M. D., Goltzman, D. & Karaplis, A. C. (2002) Partial rescue of the *Hyp* phenotype by osteoblast-targeted PHEX (phosphate-regulating gene with homologies to endopeptidases on the X chromosome) expression. *Mol Endocrinol* 16, 2913-2925
- Bai, X. Y., Miao, D., Goltzman, D. & Karaplis, A. C. (2003) The autosomal dominant hypophosphatemic rickets R176Q mutation in fibroblast growth factor 23 resists proteolytic cleavage and enhances in vivo biological potency. *J Biol Chem* 278, 9843-9849
- Benet-Pages, A., Lorenz-Depiereux, B., Zischka, H., White, K. E., Econs, M. J. & Strom, T. M. (2004) FGF23 is processed by proprotein convertases but not by PHEX. *Bone* 35, 455-462
- Benet-Pages, A., Orlik, P., Strom, T. M. & Lorenz-Depiereux, B. (2005) An FGF23 missense mutation causes familial tumoral calcinosis with hyperphosphatemia. *Hum Mol Genet* 14, 385-390
- Bennett, E. P., Hassan, H., Hollingsworth, M. A. & Clausen, H. (1999) A novel human UDP-N-acetyl-D-galactosamine:polypeptide N-acetylgalactosaminyltransferase, GalNAc-T7, with specificity for partial GalNAc-glycosylated acceptor substrates. *FEBS Lett* 460, 226-230
- Bennett, E. P., Hassan, H., Mandel, U., Hollingsworth, M. A., Akisawa, N., Ikematsu, Y., Merckx, G., van Kessel, A. G., Olofsson, S. & Clausen, H. (1999) Cloning and characterization of a close homologue of human UDP-N-acetyl-alpha-D-galactosamine:Polypeptide N-acetylgalactosaminyltransferase-T3, designated GalNAc-T6. Evidence for genetic but not functional redundancy. *J Biol Chem* 274, 25362-25370
- Bergeron, F., Leduc, R. & Day, R. (2000) Subtilase-like pro-protein convertases: from molecular specificity to therapeutic applications. *J Mol Endocrinol* 24, 1-22
- Berndt, T., Craig, T. A., Bowe, A. E., Vassiliadis, J., Reczek, D., Finnegan, R., Jan De Beur, S. M., Schiavi, S. C. & Kumar, R. (2003) Secreted frizzled-related protein 4 is a potent tumor-derived phosphaturic agent. *J Clin Invest* 112, 785-794
- Bianchetti, L., Oudet, C. & Poch, O. (2002) M13 endopeptidases: New conserved motifs correlated with structure, and simultaneous phylogenetic occurrence of PHEX and the bony fish. *Proteins* 47, 481-488
- Blay, P., Fernandez-Martinez, J. M. & Diaz-Lopez, B. (2001) Vertebral involvement in hyperphosphatemic tumoral calcinosis. *Bone* 28, 316-318
- Boileau, G., Tenenhouse, H. S., Desgroseillers, L. & Crine, P. (2001) Characterization of

- PHEX endopeptidase catalytic activity: identification of parathyroid-hormone-related peptide 107-139 as a substrate and osteocalcin, PPI and phosphate as inhibitors. *Biochem J* 355, 707-713
- Bonjour, J. P. & Caverzasio, J. (1984) Phosphate transport in the kidney. *Rev Physiol Biochem Pharmacol* 100, 161-214
- Bono, F., Lamarche, I., Bornia, J., Savi, P., Della Valle, G. & Herbert, J. M. (1999) Nerve growth factor (NGF) exerts its pro-apoptotic effect via the P75NTR receptor in a cell cycle-dependent manner. *FEBS Lett* 457, 93-97
- Bowe, A. E., Finnegan, R., Jan de Beur, S. M., Cho, J., Levine, M. A., Kumar, R. & Schiavi, S. C. (2001) FGF-23 inhibits renal tubular phosphate transport and is a PHEX substrate. *Biochem Biophys Res Commun* 284, 977-981
- Bowler, R. P., Nicks, M., Olsen, D. A., Thogersen, I. B., Valnickova, Z., Hojrup, P., Franzusoff, A., Enghild, J. J. & Crapo, J. D. (2002) Furin proteolytically processes the heparin-binding region of extracellular superoxide dismutase. *J Biol Chem* 277, 16505-16511
- Brame, L. A., White, K. E. & Econs, M. J. (2004) Renal phosphate wasting disorders: clinical features and pathogenesis. *Semin Nephrol* 24, 39-47
- Bringhurst, F. R., Demay, M. B. & Kronenberg, H. M. (1988) Hormones and disorders of mineral metabolism, 9th edn. W.B. Saunders Company, Philadelphia, Pennsylvania. pp 1155-1209
- Bushinsky, D. A., Riera, G. S., Favus, M. J. & Coe, F. L. (1985) Evidence that blood ionized calcium can regulate serum 1,25(OH)₂D₃ independently of parathyroid hormone and phosphorus in the rat. *J Clin Invest* 76, 1599-1604
- Cai, Q., Hodgson, S. F., Kao, P. C., Lennon, V. A., Klee, G. G., Zinsmeister, A. R. & Kumar, R. (1994) Brief report: inhibition of renal phosphate transport by a tumor product in a patient with oncogenic osteomalacia. *N Engl J Med* 330, 1645-1649
- Campos, M., Couture, C., Hirata, I. Y., Juliano, M. A., Loisel, T. P., Crine, P., Juliano, L., Boileau, G. & Carmona, A. K. (2003) Human recombinant endopeptidase PHEX has a strict S1' specificity for acidic residues and cleaves peptides derived from fibroblast growth factor-23 and matrix extracellular phosphoglycoprotein. *Biochem J* 373, 271-279
- Clarke, E., Swischuk, L. E. & Hayden, C. K., Jr. (1984) Tumoral calcinosis, diaphysitis, and hyperphosphatemia. *Radiology* 151, 643-646
- Constam, D. B. & Robertson, E. J. (1999) Regulation of bone morphogenetic protein activity by pro domains and proprotein convertases. *J Cell Biol* 144, 139-149
- Coulier, F., Pontarotti, P., Roubin, R., Hartung, H., Goldfarb, M. & Birnbaum, D. (1997) Of worms and men: an evolutionary perspective on the fibroblast growth factor (FGF) and FGF receptor families. *J Mol Evol* 44, 43-56
- Crine, P., Dion, N. & Boileau, G. (1997) Endopeptidase-24.11. BIOS Scientific Publisher Ltd., Oxford. pp 77-98
- Cui, Y., Jean, F., Thomas, G. & Christian, J. L. (1998) BMP-4 is proteolytically activated by furin and/or PC6 during vertebrate embryonic development. *Embo J* 17, 4735-4743
- DeLuca, H. F. (1982) Metabolism and molecular mechanism of action of vitamin D: 1981. *Biochem Soc Trans* 10, 147-158
- Denault, J. B., D'Orleans-Juste, P., Masaki, T. & Leduc, R. (1995) Inhibition of convertase-related processing of proendothelin-1. *J Cardiovasc Pharmacol* 26 Suppl 3, S47-50
- Drezner, M. K. (2000) PHEX gene and hypophosphatemia. *Kidney Int* 57, 9-18
- Drezner, M. K. (2003) Hypophosphatemic rickets. *Endocr Dev* 6, 126-155

- Dubois, C. M., Blanchette, F., Laprise, M. H., Leduc, R., Grondin, F. & Seidah, N. G. (2001) Evidence that furin is an authentic transforming growth factor-beta1-converting enzyme. *Am J Pathol* 158, 305-316
- Duguay, S. J., Jin, Y., Stein, J., Duguay, A. N., Gardner, P. & Steiner, D. F. (1998) Post-translational processing of the insulin-like growth factor-2 precursor. Analysis of O-glycosylation and endoproteolysis. *J Biol Chem* 273, 18443-18451
- Duguay, S. J., Milewski, W. M., Young, B. D., Nakayama, K. & Steiner, D. F. (1997) Processing of wild-type and mutant proinsulin-like growth factor-1A by subtilisin-related proprotein convertases. *J Biol Chem* 272, 6663-6670
- Duret, M. H. (1899) Tumeurs multiples et singulieres des bourses sereuses. *Bull.Mem.Soc.Ant. Paris*, 725-731
- Ecarot-Charrier, B., Glorieux, F. H., Travers, R., Desbarats, M., Bouchard, F. & Hinek, A. (1988) Defective bone formation by transplanted Hyp mouse bone cells into normal mice. *Endocrinology* 123, 768-773
- Econs, M. J., Feussner, J. R., Samsa, G. P., Effman, E. L., Vogler, J. B., Martinez, S., Friedman, N. E., Quarles, L. D. & Drezner, M. K. (1991) X-linked hypophosphatemic rickets without "rickets". *Skeletal Radiol* 20, 109-114
- Econs, M. J., McEnery, P. T., Lennon, F. & Speer, M. C. (1997) Autosomal dominant hypophosphatemic rickets is linked to chromosome 12p13. *J Clin Invest* 100, 2653-2657
- Econs, M. J. & Strom, T. M. (1999) The molecular basis of hypophosphatemic rickets. Humana Press, Totowa, New Jersey. pp 39-55
- Entesarian, M., Matsson, H., Klar, J., Bergendal, B., Olson, L., Arakaki, R., Hayashi, Y., Ohuchi, H., Falahat, B., Bolstad, A. I., Jonsson, R., Wahren-Herlenius, M. & Dahl, N. (2005) Mutations in the gene encoding fibroblast growth factor 10 are associated with aplasia of lacrimal and salivary glands. *Nat Genet* 37, 125-127
- Felgner, J. H., Kumar, R., Sridhar, C. N., Wheeler, C. J., Tsai, Y. J., Border, R., Ramsey, P., Martin, M. & Felgner, P. L. (1994) Enhanced gene delivery and mechanism studies with a novel series of cationic lipid formulations. *J Biol Chem* 269, 2550-2561
- Fricker, L. D. (1988) Carboxypeptidase E. *Annu Rev Physiol* 50, 309-321
- Fritz, T. A., Hurley, J. H., Trinh, L. B., Shiloach, J. & Tabak, L. A. (2004) The beginnings of mucin biosynthesis: the crystal structure of UDP-GalNAc:polypeptide alpha-N-acetylgalactosaminyltransferase-T1. *Proc Natl Acad Sci U S A* 101, 15307-15312
- Garabedian, M., Holick, M. F., Deluca, H. F. & Boyle, I. T. (1972) Control of 25-hydroxycholecalciferol metabolism by parathyroid glands. *Proc Natl Acad Sci U S A* 69, 1673-1676
- Ghaddar, G., Ruchon, A. F., Carpentier, M., Marcinkiewicz, M., Seidah, N. G., Crine, P., Desgroseillers, L. & Boileau, G. (2000) Molecular cloning and biochemical characterization of a new mouse testis soluble-zinc-metallopeptidase of the neprilysin family. *Biochem J* 347, 419-429
- Gowen, L. C., Petersen, D. N., Mansolf, A. L., Qi, H., Stock, J. L., Tkalcevic, G. T., Simmons, H. A., Crawford, D. T., Chidsey-Frink, K. L., Ke, H. Z., McNeish, J. D. & Brown, T. A. (2003) Targeted disruption of the osteoblast/osteocyte factor 45 gene (OF45) results in increased bone formation and bone mass. *J Biol Chem* 278, 1998-2007
- Greenberg, B. G., Winters, R. W. & Graham, J. B. (1960) The normal range of serum inorganic phosphorus and its utility as a discriminant in the diagnosis of congenital hypophosphatemia. *J Clin Endocrinol Metab* 20, 364-379
- Guo, R., Liu, S., Spurney, R. F. & Quarles, L. D. (2001) Analysis of recombinant Phex: an

- endopeptidase in search of a substrate. *Am J Physiol Endocrinol Metab* 281, E837-847
- Guo, R., Rowe, P. S., Liu, S., Simpson, L. G., Xiao, Z. S. & Darryl Quarles, L. D. (2002) Inhibition of MEPE cleavage by Phex. *Biochem Biophys Res Commun* 297, 38-45
- Hannon, K., Kudla, A. J., McAvoy, M. J., Clase, K. L. & Olwin, B. B. (1996) Differentially expressed fibroblast growth factors regulate skeletal muscle development through autocrine and paracrine mechanisms. *J Cell Biol* 132, 1151-1159
- Hardy, D. C., Murphy, W. A., Siegel, B. A., Reid, I. R. & Whyte, M. P. (1989) X-linked hypophosphatemia in adults: prevalence of skeletal radiographic and scintigraphic features. *Radiology* 171, 403-414
- Harmer, N. J., Pellegrini, L., Chirgadze, D., Fernandez-Recio, J. & Blundell, T. L. (2004) The crystal structure of fibroblast growth factor (FGF) 19 reveals novel features of the FGF family and offers a structural basis for its unusual receptor affinity. *Biochemistry* 43, 629-640
- Harris, C. A., Sutton, R. A. & Dirks, J. H. (1977) Effects of hypercalcemia on calcium and phosphate ultrafilterability and tubular reabsorption in the rat. *Am J Physiol* 233, F201-206
- Hendy, G. N., Bennett, H. P., Gibbs, B. F., Lazure, C., Day, R. & Seidah, N. G. (1995) Parathyroid hormone is preferentially cleaved to parathyroid hormone by the prohormone convertase furin. A mass spectrometric study. *J Biol Chem* 270, 9517-9525
- Holden, H. M., Tronrud, D. E., Monzingo, A. F., Weaver, L. H. & Matthews, B. W. (1987) Slow- and fast-binding inhibitors of thermolysin display different modes of binding: crystallographic analysis of extended phosphoramidate transition-state analogues. *Biochemistry* 26, 8542-8553
- Hopkins, T., Howard, J. E. & Eisenberg, H. (1952) Ultrafiltration studies on calcium and phosphorus in human serum. *Bull Johns Hopkins Hosp* 91, 1-21
- Hounsell, E. F., Davies, M. J. & Renouf, D. V. (1996) O-linked protein glycosylation structure and function. *Glycoconj J* 13, 19-26
- Hughes, M. R., Brumbaugh, P. F., Hussler, M. R., Wergedal, J. E. & Baylink, D. J. (1975) Regulation of serum 1 α ,25-dihydroxyvitamin D₃ by calcium and phosphate in the rat. *Science* 190, 578-580
- Hurley, M. M., Abreu, C., Gronowicz, G., Kawaguchi, H. & Lorenzo, J. (1994) Expression and regulation of basic fibroblast growth factor mRNA levels in mouse osteoblastic MC3T3-E1 cells. *J Biol Chem* 269, 9392-9396
- Ijuin, C., Wang, H., Tanne, K., Audin, J. E., Maeda, N. & Yoshiko, Y. (2004) FGF23 expression during osteoblast development and matrix mineralization in vitro and vivo suggest that FGF23 may be a local regulator of bone formation. *J.Bone.Minor.Res* SU195
- Ikemoto, M., Hasegawa, K., Kihara, Y., Iwakura, A., Komeda, M., Yamazato, A. & Fujita, M. (1999) Development of enzyme-linked immunosorbent assay for acidic fibroblast growth factor and its clinical application. *Clin Chim Acta* 283, 171-182
- Inclan, A., Leon, P. & Camejo, M. G. (1943) Tumoral calcinosis. *J.A.M.A*, 490-495
- Itoh, N. & Ornitz, D. M. (2004) Evolution of the Fgf and Fgfr gene families. *Trends Genet* 20, 563-569
- Jan de Beur, S. M. & Levine, M. A. (2002) Molecular pathogenesis of hypophosphatemic rickets. *J Clin Endocrinol Metab* 87, 2467-2473
- Jean, F., Boudreault, A., Basak, A., Seidah, N. G. & Lazure, C. (1995) Fluorescent peptidyl substrates as an aid in studying the substrate specificity of human

- prohormone convertase PC1 and human furin and designing a potent irreversible inhibitor. *J Biol Chem* 270, 19225-19231
- Johnson, G. D., Swenson, H. R., Ramage, R. & Ahn, K. (2002) Mapping the active site of endothelin-converting enzyme-1 through subsite specificity and mutagenesis studies: a comparison with neprilysin. *Arch Biochem Biophys* 398, 240-248
- Jonsson, K., Pragnell, M., Larsson, T., White, K. E., Econs, M. J. & Schiavi, S. C. (2001) Recombinant FGF23 interacts in vitro with FGF receptors 2 and 4. *J.Bone.Minor.Res* 16
- Jonsson, K. B., Zahradnik, R., Larsson, T., White, K. E., Sugimoto, T., Imanishi, Y., Yamamoto, T., Hampson, G., Koshiyama, H., Ljunggren, O., Oba, K., Yang, I. M., Miyauchi, A., Econs, M. J., Lavigne, J. & Juppner, H. (2003) Fibroblast growth factor 23 in oncogenic osteomalacia and X-linked hypophosphatemia. *N Engl J Med* 348, 1656-1663
- Kawashima, H. & Kurokawa, K. (1986) Metabolism and sites of action of vitamin D in the kidney. *Kidney Int* 29, 98-107
- Kirnarsky, L., Nomoto, M., Ikematsu, Y., Hassan, H., Bennett, E. P., Cerny, R. L., Clausen, H., Hollingsworth, M. A. & Sherman, S. (1998) Structural analysis of peptide substrates for mucin-type O-glycosylation. *Biochemistry* 37, 12811-1281
- Kumar, R. (2002) New insights into phosphate homeostasis: fibroblast growth factor 23 and frizzled-related protein-4 are phosphaturic factors derived from tumors associated with osteomalacia. *Curr Opin Nephrol Hypertens* 11, 577-553
- Lajeunesse, D., Meyer, R. A., Jr. & Hamel, L. (1996) Direct demonstration of a humorally-mediated inhibition of renal phosphate transport in the Hyp mouse. *Kidney Int* 50, 1531-1538
- Larsson, A., Skoldenberg, E. & Ericson, H. (2002) Serum and plasma levels of FGF-2 and VEGF in healthy blood donors. *Angiogenesis* 5, 107-110
- Lee, D. B., Walling, M. W. & Corry, D. B. (1986) Phosphate transport across rat jejunum: influence of sodium, pH, and 1,25-dihydroxyvitamin D₃. *Am J Physiol* 251, G90-95
- Lee, S., Debnath, A. K. & Redman, C. M. (2003) Active amino acids of the Kell blood group protein and model of the ectodomain based on the structure of neutral endopeptidase 24.11. *Blood* 102, 3028-3034
- Lee, S., Lin, M., Mele, A., Cao, Y., Farmar, J., Russo, D. & Redman, C. (1999) Proteolytic processing of big endothelin-3 by the kell blood group protein. *Blood* 94, 1440-1450
- Lee, S., Russo, D. & Redman, C. M. (2000) The Kell blood group system: Kell and XK membrane proteins. *Semin Hematol* 37, 113-121
- Lemire, I., Lazure, C., Crine, P. & Boileau, G. (1997) Secretion of a type II integral membrane protein induced by mutation of the transmembrane segment. *Biochem J* 322, 335-342
- Lipman, M. L., Panda, D., Bennett, H. P., Henderson, J. E., Shane, E., Shen, Y., Goltzman, D. & Karaplis, A. C. (1998) Cloning of human PEX cDNA. Expression, subcellular localization, and endopeptidase activity. *J Biol Chem* 273, 13729-13737
- Liu, B., Goltzman, D. & Rabbani, S. A. (1995) Processing of pro-PTHrP by the prohormone convertase, furin: effect on biological activity. *Am J Physiol* 268, E832-838
- Liu, S., Guo, R., Simpson, L. G., Xiao, Z. S., Burnham, C. E. & Quarles, L. D. (2003) Regulation of fibroblastic growth factor 23 expression but not degradation by PHEX. *J Biol Chem* 278, 37419-37426
- Liu, S., Guo, R., Tu, Q. & Quarles, L. D. (2002) Overexpression of Phex in osteoblasts

- fails to rescue the Hyp mouse phenotype. *J Biol Chem* 277, 3686-3697
- Lorenz, B., Francis, F., Gempel, K., Boddich, A., Josten, M., Schmahl, W., Schmidt, J., Lehrach, H., Meitinger, T. & Strom, T. M. (1998) Spermine deficiency in Gy mice caused by deletion of the spermine synthase gene. *Hum Mol Genet* 7, 541-547
- Lufkin, E. G., Kumar, R. & Heath, H., 3rd (1983) Hyperphosphatemic tumoral calcinosis: effects of phosphate depletion on vitamin D metabolism, and of acute hypocalcemia on parathyroid hormone secretion and action. *J Clin Endocrinol Metab* 56, 1319-1322
- Lyles, K. W. & Drezner, M. K. (1982) Parathyroid hormone effects on serum 1,25-dihydroxyvitamin D levels in patients with X-linked hypophosphatemic rickets: evidence for abnormal 25-hydroxyvitamin D-1-hydroxylase activity. *J Clin Endocrinol Metab* 54, 638-644
- Markowitz, M., Rotkin, L. & Rosen, J. F. (1981) Circadian rhythms of blood minerals in humans. *Science* 213, 672-674
- Martinez, S. (2002) Tumoral calcinosis: 12 years later. *Semin Musculoskelet Radiol* 6, 331-339
- Meyer, R. A., Jr., Henley, C. M., Meyer, M. H., Morgan, P. L., McDonald, A. G., Mills, C. & Price, D. K. (1998) Partial deletion of both the spermine synthase gene and the Pex gene in the X-linked hypophosphatemic, gyro (Gy) mouse. *Genomics* 48, 289-295
- Meyer, R. A., Jr., Meyer, M. H. & Gray, R. W. (1989) Parabiosis suggests a humoral factor is involved in X-linked hypophosphatemia in mice. *J Bone Miner Res* 4, 493-500
- Miller, S. A., Dykes, D. D. & Polesky, H. F. (1988) A simple salting out procedure for extracting DNA from human nucleated cells. *Nucleic Acids Res* 16, 1215
- Mirams, M., Robinson, B. G., Mason, R. S. & Nelson, A. E. (2004) Bone as a source of FGF23: regulation by phosphate? *Bone* 35, 1192-1199
- Mitnick, P. D., Goldfarb, S., Slatopolsky, E., Lemann, J., Jr., Gray, R. W. & Agus, Z. S. (1980) Calcium and phosphate metabolism in tumoral calcinosis. *Ann Intern Med* 92, 482-487
- Morgan, J. M., Hawley, W. L., Chenoweth, A. I., Retan, W. J. & Diethelm, A. G. (1974) Renal transplantation in hypophosphatemia with vitamin D-resistant rickets. *Arch Intern Med* 134, 549-552
- Muillerman, H. G., ter Hart, H. G. & Van Dijk, W. (1982) Specific detection of inactive enzyme protein after polyacrylamide gel electrophoresis by a new enzyme-immunoassay method using unspecific antiserum and partially purified active enzyme: application to rat liver phosphodiesterase I. *Anal Biochem* 120, 46-51
- Mulders, S. M., Bichet, D. G., Rijss, J. P., Kamsteeg, E. J., Arthus, M. F., Lonergan, M., Fujiwara, M., Morgan, K., Leijendekker, R., van der Sluijs, P., van Os, C. H. & Deen, P. M. (1998) An aquaporin-2 water channel mutant which causes autosomal dominant nephrogenic diabetes insipidus is retained in the Golgi complex. *J Clin Invest* 102, 57-66
- Murer, H. & Biber, J. (1996) Control of proximal tubular apical Na/Pi cotransport. *Exp Nephrol* 4, 201-204
- Murer, H., Hernando, N., Forster, I. & Biber, J. (2001) Molecular aspects in the regulation of renal inorganic phosphate reabsorption: the type IIa sodium/inorganic phosphate co-transporter as the key player. *Curr Opin Nephrol Hypertens* 10, 555-561
- Murer, H., Werner, A., Reshkin, S., Wuarin, F. & Biber, J. (1991) Cellular mechanisms in proximal tubular reabsorption of inorganic phosphate. *Am J Physiol* 260, C885-899
- Nesbitt, T., Coffman, T. M., Griffiths, R. & Drezner, M. K. (1992) Crosstransplantation of kidneys in normal and Hyp mice. Evidence that the Hyp mouse phenotype is

- unrelated to an intrinsic renal defect. *J Clin Invest* 89, 1453-1459
- Neuhoff, V., Arold, N., Taube, D. & Ehrhardt, W. (1988) Improved staining of proteins in polyacrylamide gels including isoelectric focusing gels with clear background at nanogram sensitivity using Coomassie Brilliant Blue G-250 and R-250. *Electrophoresis* 9, 255-262
- Oefner, C., D'Arcy, A., Hennig, M., Winkler, F. K. & Dale, G. E. (2000) Structure of human neutral endopeptidase (Neprilysin) complexed with phosphoramidon. *J Mol Biol* 296, 341-349
- Omdahl, J. L., Gray, R. W., Boyle, I. T., Knutson, J. & DeLuca, H. F. (1972) Regulation of metabolism of 25-hydroxycholecalciferol by kidney tissue in vitro by dietary calcium. *Nat New Biol* 237, 63-64
- Ornitz, D. M. & Itoh, N. (2001) Fibroblast growth factors. *Genome Biol* 2, REVIEWS3005
- Ostman, A., Thyberg, J., Westermark, B. & Heldin, C. H. (1992) PDGF-AA and PDGF-BB biosynthesis: proprotein processing in the Golgi complex and lysosomal degradation of PDGF-BB retained intracellularly. *J Cell Biol* 118, 509-519
- Palmer, P. E. (1966) Tumoural calcinosis. *Br J Radiol* 39, 518-525
- Pastoriza-Munoz, E., Colindres, R. E., Lassiter, W. E. & Lechene, C. (1978) Effect of parathyroid hormone on phosphate reabsorption in rat distal convolution. *Am J Physiol* 235, F321-330
- Pfister, M. F., Ruf, I., Stange, G., Ziegler, U., Lederer, E., Biber, J. & Murer, H. (1998) Parathyroid hormone leads to the lysosomal degradation of the renal type II Na/Pi cotransporter. *Proc Natl Acad Sci U S A* 95, 1909-1914
- Polisson, R. P., Martinez, S., Khoury, M., Harrell, R. M., Lyles, K. W., Friedman, N., Harrelson, J. M., Reisner, E. & Drezner, M. K. (1985) Calcification of entheses associated with X-linked hypophosphatemic osteomalacia. *N Engl J Med* 313, 1-6
- Popovtzer, M. M. & Wald, H. (1981) Evidence for interference of 25(OH)vitamin D3 with phosphaturic action of glucagon. *Am J Physiol* 240, F269-275
- Rajesh, V. T. (2000) Pathogenesis of Dent's disease and related syndromes of X-linked nephrolithiasis. *Kidney Int* 57, 787-793
- Reid, I. R., Hardy, D. C., Murphy, W. A., Teitelbaum, S. L., Bergfeld, M. A. & Whyte, M. P. (1989) X-linked hypophosphatemia: a clinical, biochemical, and histopathologic assessment of morbidity in adults. *Medicine (Baltimore)* 68, 336-352
- Riminucci, M., Collins, M. T., Fedarko, N. S., Cherman, N., Corsi, A., White, K. E., Waguespack, S., Gupta, A., Hannon, T., Econs, M. J., Bianco, P. & Gehron Robey, P. (2003) FGF-23 in fibrous dysplasia of bone and its relationship to renal phosphate wasting. *J Clin Invest* 112, 683-692
- Rizzoli, R., Fleisch, H. & Bonjour, J. P. (1977) Effect of thyroparathyroidectomy of calcium metabolism in rats: role of 1,25-dihydroxyvitamin D3. *Am J Physiol* 233, E160-164
- Roques, B. P., Noble, F., Dauge, V., Fournie-Zaluski, M. C. & Beaumont, A. (1993) Neutral endopeptidase 24.11: structure, inhibition, and experimental and clinical pharmacology. *Pharmacol Rev* 45, 87-146
- Rost, C. R., Bikle, D. D. & Kaplan, R. A. (1981) In vitro stimulation of 25-hydroxycholecalciferol 1 alpha-hydroxylation by parathyroid hormone in chick kidney slices: evidence for a role for adenosine 3',5'-monophosphate. *Endocrinology* 108, 1002-1006
- Rowe, P. S. (1997) The PEX gene: its role in X-linked rickets, osteomalacia, and bone mineral metabolism. *Exp Nephrol* 5, 355-363
- Rowe, P. S., de Zoysa, P. A., Dong, R., Wang, H. R., White, K. E., Econs, M. J. & Oudet, C. L. (2000) MEPE, a new gene expressed in bone marrow and tumors causing

- osteomalacia. *Genomics* 67, 54-68
- Rowe, P. S., Kumagai, Y., Gutierrez, G., Garrett, I. R., Blacher, R., Rosen, D., Cundy, J., Navvab, S., Chen, D., Drezner, M. K., Quarles, L. D. & Mundy, G. R. (2004) MEPE has the properties of an osteoblastic phosphatonin and minihabin. *Bone* 34, 303-319
- Ruchon, A. F., Marcinkiewicz, M., Siegfried, G., Tenenhouse, H. S., DesGroseillers, L., Crine, P. & Boileau, G. (1998) Pex mRNA is localized in developing mouse osteoblasts and odontoblasts. *J Histochem Cytochem* 46, 459-468
- Sabbagh, Y., Boileau, G., Campos, M., Carmona, A. K. & Tenenhouse, H. S. (2003) Structure and function of disease-causing missense mutations in the PHEX gene. *J Clin Endocrinol Metab* 88, 2213-2222
- Sabbagh, Y., Boileau, G., DesGroseillers, L. & Tenenhouse, H. S. (2001) Disease-causing missense mutations in the PHEX gene interfere with membrane targeting of the recombinant protein. *Hum Mol Genet* 10, 1539-1546
- Saiki, R. K., Gelfand, D. H., Stoffel, S., Scharf, S. J., Higuchi, R., Horn, G. T., Mullis, K. B. & Erlich, H. A. (1988) Primer-directed enzymatic amplification of DNA with a thermostable DNA polymerase. *Science* 239, 487-491
- Sambrook, J., Fritsch, E. F. & Maniatis, T. (1989) *Molecular Cloning: a laboratory manual*, 2nd edn. Cold Spring Harbor Laboratory Press, Cold Spring Harbor
- Sammons, D.W., Adams, L.D., and Nishizawa, E.E. (1981) Ultrasensitive silver-based color staining of polypeptides in polyacrilamide gels. *Electrophoresis* 2, 135-141
- Schwientek, T., Bennett, E. P., Flores, C., Thacker, J., Hollmann, M., Reis, C. A., Behrens, J., Mandel, U., Keck, B., Schafer, M. A., Haselmann, K., Zubarev, R., Roepstorff, P., Burchell, J. M., Taylor-Papadimitriou, J., Hollingsworth, M. A. & Clausen, H. (2002) Functional conservation of subfamilies of putative UDP-N-acetylgalactosamine:polypeptide N-acetylgalactosaminyltransferases in *Drosophila*, *Caenorhabditis elegans*, and mammals. One subfamily composed of I(2)35Aa is essential in *Drosophila*. *J Biol Chem* 277, 22623-22638
- Segawa, H., Kawakami, E., Kaneko, I., Kuwahata, M., Ito, M., Kusano, K., Saito, H., Fukushima, N. & Miyamoto, K. (2003) Effect of hydrolysis-resistant FGF23-R179Q on dietary phosphate regulation of the renal type-II Na/Pi transporter. *Pflugers Arch* 446, 585-592
- Seidah, N. G. & Chretien, M. (1997) Eukaryotic protein processing: endoproteolysis of precursor proteins. *Curr Opin Biotechnol* 8, 602-607
- Seidah, N. G. & Chretien, M. (1999) Proprotein and prohormone convertases: a family of subtilases generating diverse bioactive polypeptides. *Brain Res* 848, 45-62
- Shimada, T., Kakitani, M., Yamazaki, Y., Hasegawa, H., Takeuchi, Y., Fujita, T., Fukumoto, S., Tomizuka, K. & Yamashita, T. (2004) Targeted ablation of Fgf23 demonstrates an essential physiological role of FGF23 in phosphate and vitamin D metabolism. *J Clin Invest* 113, 561-568
- Shimada, T., Mizutani, S., Muto, T., Yoneya, T., Hino, R., Takeda, S., Takeuchi, Y., Fujita, T., Fukumoto, S. & Yamashita, T. (2001) Cloning and characterization of FGF23 as a causative factor of tumor-induced osteomalacia. *Proc Natl Acad Sci USA* 98, 6500-6505
- Shimada, T., Muto, T., Urakawa, I., Yoneya, T., Yamazaki, Y., Okawa, K., Takeuchi, Y., Fujita, T., Fukumoto, S. & Yamashita, T. (2002) Mutant FGF-23 responsible for autosomal dominant hypophosphatemic rickets is resistant to proteolytic cleavage and causes hypophosphatemia in vivo. *Endocrinology* 143, 3179-3182
- Shinki, T., Shimada, H., Wakino, S., Anazawa, H., Hayashi, M., Saruta, T., DeLuca, H. F. & Suda, T. (1997) Cloning and expression of rat 25-hydroxyvitamin D3-1alpha-

- hydroxylase cDNA. *Proc Natl Acad Sci U S A* 94, 12920-12925
- Sitara, D., Razzaque, M. S., Hesse, M., Yoganathan, S., Taguchi, T., Erben, R. G., H, J. A.-P. & Lanske, B. (2004) Homozygous ablation of fibroblast growth factor-23 results in hyperphosphatemia and impaired skeletogenesis, and reverses hypophosphatemia in PheX-deficient mice. *Matrix Biol* 23, 421-432
- Slavin, R. E., Wen, J., Kumar, D. & Evans, E. B. (1993) Familial tumoral calcinosis. A clinical, histopathologic, and ultrastructural study with an analysis of its calcifying process and pathogenesis. *Am J Surg Pathol* 17, 788-802
- Strewler, G. J. (2001) FGF23, hypophosphatemia, and rickets: has phosphatonin been found? *Proc Natl Acad Sci U S A* 98, 5945-5946
- Strom, T. M., Francis, F., Lorenz, B., Boddich, A., Econs, M. J., Lehrach, H. & Meitinger, T. (1997) Pex gene deletions in Gy and Hyp mice provide mouse models for X-linked hypophosphatemia. *Hum Mol Genet* 6, 165-171
- Strom, T. M. & Lorenz-Depiereux, B. (2001) Monogen vererbte Hypophosphatämien, 1st edn. Springer-Verlag Berlin, Heidelberg. pp 365-381
- Tanaka, Y. & Deluca, H. F. (1973) The control of 25-hydroxyvitamin D metabolism by inorganic phosphorus. *Arch Biochem Biophys* 154, 566-574
- Tenhouse, H. S. & Econs, M. J. (2001) Mendelian hypophosphatemias, 8th ed. edn. McGraw Hill Book Co., New York, NY. pp 5039-5067
- Tenhouse, H. S., Gauthier, C., Martel, J., Gesek, F. A., Coutermarsh, B. A. & Friedman, P. A. (1998) Na⁺-phosphate cotransport in mouse distal convoluted tubule cells: evidence for Glvr-1 and Ram-1 gene expression. *J Bone Miner Res* 13, 590-597
- Tenhouse, H. S., Martel, J., Rubin, J. & Harvey, N. (1994) Effect of phosphate supplementation on the expression of the mutant phenotype in murine X-linked hypophosphatemic rickets. *Bone* 15, 677-683
- Tenhouse, H. S., Werner, A., Biber, J., Ma, S., Martel, J., Roy, S. & Murer, H. (1994) Renal Na(+)-phosphate cotransport in murine X-linked hypophosphatemic rickets. Molecular characterization. *J Clin Invest* 93, 671-676
- TheADHRConsortium (2000) Autosomal dominant hypophosphataemic rickets is associated with mutations in FGF23. The ADHR Consortium. *Nat Genet* 26, 345-348
- TheHYPConsortium (1995) A gene (*PEX*) with homologies to endopeptidases is mutated in patients with X-linked hypophosphatemic rickets. *Nat Genet* 11, 130-136
- Thomas, G. (2002) Furin at the cutting edge: from protein traffic to embryogenesis and disease. *Nat Rev Mol Cell Biol* 3, 753-766
- Thomson, J. G. (1966) Calcifying collagenolysis (tumoural calcinosis). *Brit.J.Radio.*, 532-562
- Topaz, O., Shurman, D. L., Bergman, R., Indelman, M., Ratajczak, P., Mizrachi, M., Khamaysi, Z., Behar, D., Petronius, D., Friedman, V., Želikovic, I., Raimer, S., Metzker, A., Richard, G. & Sprecher, E. (2004) Mutations in GALNT3, encoding a protein involved in O-linked glycosylation, cause familial tumoral calcinosis. *Nat Genet* 36, 579-581
- Tsai, B., Ye, Y. & Rapoport, T. A. (2002) Retro-translocation of proteins from the endoplasmic reticulum into the cytosol. *Nat Rev Mol Cell Biol* 3, 246-255
- Turner, A. J., Isaac, R. E. & Coates, D. (2001) The neprilysin (NEP) family of zinc metalloendopeptidases: genomics and function. *Bioessays* 23, 261-269
- Turner, A. J. & Tanzawa, K. (1997) Mammalian membrane metallopeptidases: NEP, ECE, KELL, and PEX. *Faseb J* 11, 355-364
- Valdenaire, O., Richards, J. G., Faull, R. L. & Schweizer, A. (1999) XCE, a new member of the endothelin-converting enzyme and neutral endopeptidase family, is

- preferentially expressed in the CNS. *Brain Res Mol Brain Res* 64, 211-221
- Van den Steen, P., Rudd, P. M., Dwek, R. A. & Opdenakker, G. (1998) Concepts and principles of O-linked glycosylation. *Crit Rev Biochem Mol Biol* 33, 151-208
- Walling, M. W. (1977) Intestinal Ca and phosphate transport: differential responses to vitamin D3 metabolites. *Am J Physiol* 233, E488-494
- Wei, S., Feng, Y., Kalinina, E. & Fricker, L. D. (2003) Neuropeptide-processing carboxypeptidases. *Life Sci* 73, 655-662
- White, K. E., Cabral, J. M., Davis S. I., Fishburn T. Evans, W. E., Ichikawa, S., Fields J., Yu X., Shaw N. J., McLellan N. J., McKeown C., FitzPatrick D., Yu K., Ornitz D. M. & Econs, M. J. (2005) Mutations that cause osteoglophonic dysplasia define novel roles for FGFR1 in bone elongation. *Am J Hum Genet* 76, 361-367
- White, K. E., Carn, G., Lorenz-Depiereux, B., Benet-Pages, A., Strom, T. M. & Econs, M. J. (2001) Autosomal-dominant hypophosphatemic rickets (ADHR) mutations stabilize FGF-23. *Kidney Int* 60, 2079-2086
- White, K. E., Jonsson, K. B., Carn, G., Hampson, G., Spector, T. D., Mannstadt, M., Lorenz-Depiereux, B., Miyauchi, A., Yang, I. M., Ljunggren, O., Meitinger, T., Strom, T. M., Juppner, H. & Econs, M. J. (2001) The autosomal dominant hypophosphatemic rickets (ADHR) gene is a secreted polypeptide overexpressed by tumors that cause phosphate wasting. *J Clin Endocrinol Metab* 86, 497-500
- Wilber, J. F. & Slatopolsky, E. (1968) Hyperphosphatemia and tumoral calcinosis. *Ann Intern Med* 68, 1043-1049
- Wilkie, A. O., Patey, S. J., Kan, S. H., van den Ouweland, A. M. & Hamel, B. C. (2002) FGFs, their receptors, and human limb malformations: clinical and molecular correlations. *Am J Med Genet* 112, 266-278
- Xiao, Z. S., Crenshaw, M., Guo, R., Nesbitt, T., Drezner, M. K. & Quarles, L. D. (1998) Intrinsic mineralization defect in Hyp mouse osteoblasts. *Am J Physiol* 275, E700-708
- Yamashita, T., Konishi, M., Miyake, A., Inui, K. & Itoh, N. (2002) Fibroblast growth factor (FGF)-23 inhibits renal phosphate reabsorption by activation of the mitogen-activated protein kinase pathway. *J Biol Chem* 277, 28265-28270
- Yamashita, T., Yoshioka, M. & Itoh, N. (2000) Identification of a novel fibroblast growth factor, FGF-23, preferentially expressed in the ventrolateral thalamic nucleus of the brain. *Biochem Biophys Res Commun* 277, 494-498
- Yamazaki, Y., Okazaki, R., Shibata, M., Hasegawa, Y., Satoh, K., Tajima, T., Takeuchi, Y., Fujita, T., Nakahara, K., Yamashita, T. & Fukumoto, S. (2002) Increased circulatory level of biologically active full-length FGF-23 in patients with hypophosphatemic rickets/osteomalacia. *J Clin Endocrinol Metab* 87, 4957-4960
- Yoshizawa, T., Handa, Y., Uematsu, Y., Takeda, S., Sekine, K., Yoshihara, Y., Kawakami, T., Arioka, K., Sato, H., Uchiyama, Y., Masushige, S., Fukamizu, A., Matsumoto, T. & Kato, S. (1997) Mice lacking the vitamin D receptor exhibit impaired bone formation, uterine hypoplasia and growth retardation after weaning. *Nat Genet* 16, 391-396
- Zhou, A., Martin, S., Lipkind, G., LaMendola, J. & Steiner, D. F. (1998) Regulatory roles of the P domain of the subtilisin-like prohormone convertases. *J Biol Chem* 273, 11107-11114

The here presented doctoral thesis is based on the data and results obtained during my work at the laboratory of Prof. Dr. Thomas Meitinger at the “Institut für Humangenetik”, GSF-Forschungszentrum für Umwelt und Gesundheit, from January 2001 until December 2004.

ACKNOWLEDGMENTS

First of all I would like to express my sincere gratitude to my supervisor PD Dr. Tim-Matthias Strom for his continuous interest in my work, the many stimulating discussions we had during this time and for letting me benefit from his enormous scientific knowledge. Thank you also for the intensive corrections of this work.

I would like to thank Prof. Dr. Thomas Meitinger for the opportunity to work in his laboratory and for his critical and favourable comments on my thesis. I also want to thank Prof. Dr. Thomas Cremer for supporting this thesis at the “Ludwig-Maximilian Universität” of Munich.

My special thanks to Dr. Bettina Lorenz-Depiereux for her enormous enthusiasm and patience, her intensive theoretical and practical supervision during the experimental work, for proofreading the manuscript and her many helpful comments. It has been a great pleasure to work and learn all these years with her. I also want to thank Dr. Hans Zischka for his valuable discussions, good ideas and teaching me protein biochemistry.

I want to thank my lab mates Evelyn Botz, Janine Wagenstaller, Dr. Konstanze Hörtnagel, Dr. Monika Grabowsky, and Michael Kaulfersch for the fun and enjoyable moments we spent together. I also thank all other former and present members of the department for the nice working atmosphere.

I want to thank Ilse and Nikos Katechakis for their support and encouragement. Thanks also to my friend Gaed for his positive attitude in life and never-ending good mood.

My deepest thanks to my parents for encouraging me to learn at a young age and providing their love, care and support at every moment.

My last thanks to Alexis. To meet him was the first step towards this work.

Als meus pares i germana.

CURRICULUM VITAE

Personal data: Ana Benet Pagès
 Giselastr. 6
 D-82319 Starnberg
 +49 (0)8151/ 74 66 52
 05/ 07/ 1974 in Girona, Spain

Institut address: GSF Forschungszentrum
 Institut für Humangenetik
 Ingoldstädter Landstrasse 1
 D - 85764 Neuherberg
 +49 (0)89 3187 3320

School education:

1980 – 1988 primary school in Pineda de Mar, Spain
 1988 – 1991 secondary school at “Institut Vedruna”; Malgrat, Spain
 1991 – 1993 secondary school at “Institut Bisbe Sivilla”; Calella, Spain

University education:

1993 – 2000 studies in Biology, specialization in Genetics and Cellular
 Biology at the “Universitat Autònoma de Barcelona“ (UAB);
 Bellaterra, Spain
 07/ 2000 “Llicenciatura de Biologia“ (Diplom Biologie)

Professional experience:

Scientific collaborator at the following institutions:

1998 Department of Aquatic Ecology, “Centre d’Estudis Avancats de
 Blanes“ (CEAB); Blanes, Spain
 1998 – 1999 Department of Cytogenetics, “Hospital Sant Pau de
 Barcelona“; Barcelona, Spain
 05-12/ 2000 Department of Medical Genetics, “Kinderklinik und Poliklinik im
 Dr.Haunerschen Kinderspital, Ludwig Maximilian Universität“;
 Munich, Germany

PhD student:

2001 - 2004 Institute of Human Genetics, GSF (Forschungszentrum für
 Umwelt und Gesundheit), GmbH, Munich, Germany

SCIENTIFIC PUBLICATIONS

Articles:

K. E. White, G. Carn, B. Lorenz-Depiereux, **A. Benet-Pagès**, T. M. Strom, M. J. Econs (2001). Autosomal-dominant hypophosphatemic rickets (ADHR) mutations stabilize FGF-23. *Kidney International* 60, 2079-2086

K. A. Giehl, G. N. Eckstein, **A. Benet-Pagès**, A. Tosti, D. A. R. de Berker, T. Meitinger, B. Müller-Myhsok, T. M. Strom (2004). A Gene Locus Responsible for the Familial Hair Shaft Abnormality Pili Annulati Maps to Chromosome 12q24.32-24.33. *J Invest Dermatol* 123, 1073-1077

A. Benet-Pagès, B. Lorenz-Depiereux, H. Zischka, K.E. White, M. J. Econs, T. M. Strom (2004). FGF23 is processed by proprotein convertases but not by PHEX. *Bone* 35, 455-462

A. Benet-Pagès, P. Orlik, T. M. Strom, B. Lorenz-Depiereux (2005). An FGF23 missense mutation causes familial tumoral calcinosis with hyperphosphatemia. *Human Molecular Genetics* 14, 3:385-390

Reviews:

B. Lorenz-Depiereux, **A. Benet-Pagès**, Tim M Strom (2005). Molekulargenetik der hypophosphatämischen Rachitis. In: *Hyperphosphatämische Rachitis. Diagnose und Betreuung von Kindern mit spezifischen Kleinwuchsformen*. Eds: K. Mohnike, K. H. Klingebiel. AWB-Verlag, Berlin. In press.

Poster presentations:

B. Lorenz-Depiereux, **A. Benet-Pagès**, K. E. White, S. Hauck, M. Grabowski, G. Carn, M. Ueffing, M. J. Econs, T. Meitinger, T. M. Strom (2001). The autosomal dominant hypophosphatemic rickets (ADHR) gene is a secreted fibroblast growth factor (FGF23). *European Journal of Human Genetics* 9 Suppl. 1, P0772

D. Dunstheimer, M. Hauschild, M. Sindichakis, E. Hoffmann, **A. Benet-Pagès**, T. M. Strom, P. H. Heidemann (2003). Immundysregulation, Polyendokrinopathie, Enteropathie und Autoimmunhepatitis: Das IPEX-Syndrom. *Deutschen Gesellschaft für Endokrinologie, Kinderheilkunde* 151, 10:1123

A. Benet-Pagès, B. Lorenz-Depiereux, T. M. Strom (2003). Co-incubation provided no evidence that FGF23 is a substrate for PHEX. *European Journal of Human Genetics* 11 Suppl. 1, P559

K. A. Giehl, G. N. Eckstein, **A. Benet-Pagès**, A. Tosti, D. A. R. de Berker, T. Meitinger, B. Müller-Myhsok, T. M. Strom (2004). A Gene Locus Responsible for Pili Annulati Maps to Chromosome 12q24.32-24.33. *Journal of the German Society of Dermatology* 6 (Band 2), 504

Oral Presentations:

A. Benet-Pagès. FGF23 in phosphate metabolism. Guest speaker at the 9th Kyoto Symposium of the Japan Pediatric Endocrine Society. Kyoto, April 2005.

A. Benet-Pagès, P. Orlik, T.M. Strom, B. Lorenz-Depiereux. An FGF23 missense mutation causes familial tumoral calcinosis with hyperphosphatemia. European Society of Human Genetics, European Journal of Human Genetics 13 Suppl. 1, 64. Prague, May 2005.

ERKLÄRUNG

Hiermit versichere ich, dass die vorliegende Dissertation das Ergebnis eigenständigen Arbeit ist und dass ich dieses Manuskript persönlich verfasst habe. Zudem habe ich keine anderen als die angegebenen Quellen und Hilfsmittel verwendet.

Hiermit erkläre ich, dass ich mich anderweitig einer Doktorprüfung ohne Erfolg nicht unterzogen habe.

München, 23. April 2005

Anna Benet Pagès